

1m
(2)

NAVAL POSTGRADUATE SCHOOL

Monterey, California

AD-A241 894



DTIC

THESIS

STUDY OF TRANSITION PHENOMENA IN A
STRAIGHT CHANNEL WITH
40 TO 1 ASPECT RATIO WITH AND WITHOUT
IMPOSED PULSATIONS
PART TWO: REYNOLDS NUMBER SURVEYS

by

Bradley Joseph Smith

March 1991

Thesis Advisor
Co-Advisor

Phillip M. Ligrani
Chelakara S. Subramanian

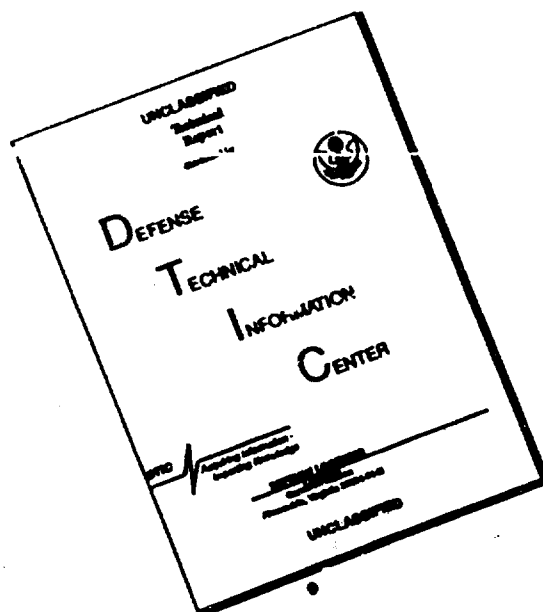
Approved for public release; distribution is unlimited.

91-14278



91 10 28 032

DISCLAIMER NOTICE



THIS DOCUMENT IS BEST
QUALITY AVAILABLE. THE COPY
FURNISHED TO DTIC CONTAINED
A SIGNIFICANT NUMBER OF
PAGES WHICH DO NOT
REPRODUCE LEGIBLY.

Unclassified

security classification of this page

REPORT DOCUMENTATION PAGE

1a Report Security Classification <u>Unclassified</u>			1b Restrictive Markings		
2a Security Classification Authority			3 Distribution Availability of Report		
2b Declassification Downgrading Schedule			Approved for public release; distribution is unlimited.		
4 Performing Organization Report Number(s)			5 Monitoring Organization Report Number(s)		
5a Name of Performing Organization Naval Postgraduate School		6b Office Symbol (if applicable) 34	7a Name of Monitoring Organization Naval Postgraduate School		
6c Address (city, state, and ZIP code) Monterey, CA 93943-5000			7b Address (city, state, and ZIP code) Monterey, CA 93943-5000		
8a Name of Funding Sponsoring Organization		8b Office Symbol (if applicable)	9 Procurement Instrument Identification Number		
8c Address (city, state, and ZIP code)			10 Source of Funding Numbers		
			Program Element No	Project No	Task No
			Work Unit Accession No		
11 Title (include security classification) STUDY OF TRANSITION PHENOMENA IN A STRAIGHT CHANNEL WITH 40 TO 1 ASPECT RATIO WITH AND WITHOUT IMPOSED PULSATIONS PART TWO: REYNOLDS NUMBER SURVEYS					
12 Personal Author(s) Bradley Joseph Smith					
13a Type of Report Master's Thesis		13b Time Covered From To		14 Date of Report (year, month, day) March 1991	
15 Page Count 112					
16 Supplementary Notation The views expressed in this thesis are those of the author and do not reflect the official policy or position of the Department of Defense or the U.S. Government.					
17 Cosati Codes			18 Subject Terms (continue on reverse if necessary and identify by block number)		
Field	Group	Subgroup	Imposed Pulsations, Transition from Laminar to Turbulent Flow, Phase-Averaged Velocity, Longitudinal Velocity Fluctuations, Intermittency		
19 Abstract (continue on reverse if necessary and identify by block number) A channel with rectangular cross-section, 40 to 1 aspect ratio (height is 0.0127 m) and 4.27 m test section length (336 channel lengths) is used to study the effects of imposed pulsations on laminar, transitional, and turbulent flow phenomena. Periodic velocity variations are produced in the test section using a single rotating vane located in the flow downstream of the test section. Survey data for Y/d of 0.50, 0.85, and 0.90 show how normalized average velocity and turbulence intensity data vary with Reynolds number for Reynolds numbers ranging from 1100 to 3400 at Stokes numbers of 4.08 and 5.79 and Strouhal numbers from 0.033 to 0.121. These conditions are produced from pulsations imposed at 1 Hz and 2 Hz to show how transition develops both with and without imposed pulsations. Intermittency variations increase from near zero to one as Reynolds number changes from 1450 to 2100 for $Y/d = 0.90, 0.85$, and 0.50 . Time-averaged magnitudes of the normalized longitudinal turbulence intensity increase significantly as Re changes from 1450 to 3100 at $Y/d = 0.90$. A maxima is reached near $Re = 2400$. Afterwards these data show a decrease and level off in the turbulent region. At $Y/d = 0.85$, the same trend in normalized longitudinal turbulence intensity appears with a maxima appearing near $Re = 2300$. For the center of the channel ($Y/d = 0.50$), the maxima appears near $Re = 2000$. The normalized longitudinal turbulence intensity level in the turbulent region increases with Y/d . Of particular interest are conditions where the normalized longitudinal turbulence intensity is greater near the center of the channel than near the walls. This occurs for Reynolds numbers of 1500 to 2500. Spectra show evidence of intermittency and drastic increases in fluctuating energy starting at $Re = 1500$ and continuing to $Re = 1700$.					
20 Distribution Availability of Abstract <input checked="" type="checkbox"/> unclassified unlimited <input type="checkbox"/> same as report <input type="checkbox"/> DTIC users			21 Abstract Security Classification Unclassified		
22a Name of Responsible Individual Phillip M. Ligrani			22b Telephone (include Area code) (408) 646-3382		22c Office Symbol ME/Li

DD FORM 1473,84 MAR

83 APR edition may be used until exhausted
All other editions are obsolete

security classification of this page

Unclassified

Approved for public release; distribution is unlimited.

Study of Transition Phenomena in a Straight Channel With
40 to 1 Aspect Ratio With and Without
Imposed Pulsations
Part Two: Reynolds Number Surveys

by

Bradley Joseph Smith
Lieutenant, United States Navy
B.S.Ch.E., Wayne State University, 1983

Submitted in partial fulfillment of the
requirements for the degree of

MASTER OF SCIENCE IN MECHANICAL ENGINEERING

from the

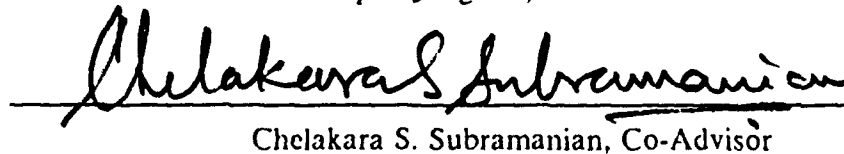
NAVAL POSTGRADUATE SCHOOL
March 1991

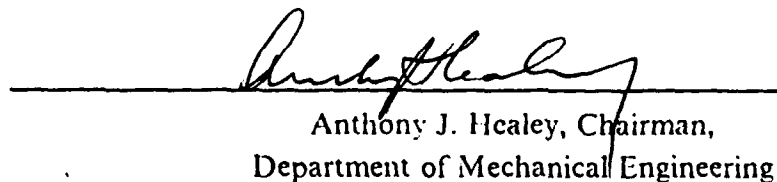
Author:


Bradley Joseph Smith

Approved by:


Phillip M. Ligrani, Thesis Advisor


Chelakara S. Subramanian, Co-Advisor


Anthony J. Healey, Chairman,
Department of Mechanical Engineering

ABSTRACT

A channel with rectangular cross-section, 40 to 1 aspect ratio (height is 0.0127 m) and 4.27 m test section length (336 channel lengths) is used to study the effects of imposed pulsations on laminar, transitional, and turbulent flow phenomena. Periodic velocity variations are produced in the test section using a single rotating vane located in the flow downstream of the test section. Survey data for Y/d of 0.50, 0.85, and 0.90 show how normalized average velocity and turbulence intensity data vary with Reynolds number for Reynolds numbers ranging from 1100 to 3400 at Stokes numbers of 4.08 and 5.79 and Strouhal numbers from 0.033 to 0.121. These conditions are produced from pulsations imposed at 1 Hz and 2 Hz to show how transition develops both with and without imposed pulsations. Intermittency variations increase from near zero to one as Reynolds number changes from 1450 to 2100 for $Y/d \approx 0.90$, 0.85, and 0.50. Time-averaged magnitudes of the normalized longitudinal turbulence intensity increase significantly as Re changes from 1450 to 3100 at $Y/d \approx 0.90$. A maxima is reached near $Re \approx 2400$. Afterwards these data show a decrease and level off in the turbulent region. At $Y/d = 0.85$, the same trend in normalized longitudinal turbulence intensity appears with a maxima appearing near $Re = 2300$. For the center of the channel ($Y/d = 0.50$), the maxima appears near $Re = 2000$. The normalized longitudinal turbulence intensity level in the turbulent region increases with Y/d . Of particular interest are conditions where the normalized longitudinal turbulence intensity is greater near the center of the channel than near the walls. This occurs for Reynolds numbers of 1500 to 2500. Spectra show evidence of intermittency and drastic increases in fluctuating energy starting at $Re = 1500$ and continuing to $Re = 1700$.



A-1	
-----	--

TABLE OF CONTENTS

I. INTRODUCTION	1
A. BACKGROUND	1
B. OBJECTIVES	3
C. THESIS ORGANIZATION	4
II. EXPERIMENTAL FACILITIES	5
A. CHANNEL	5
B. UNSTEADINESS DEVICE	6
C. FLOW MEASUREMENT INSTRUMENTS	7
1. Hot-wire Anemometer	7
2. Hot-wire Bridge, Signal Conditioner, High Speed Data Acquisition System and Data Storage	7
3. Phase-Averaging	8
III. EXPERIMENTAL PROCEDURES	9
A. HOT-WIRE CALIBRATION	9
B. DATA PROCESSING	9
1. Bulk Velocity	9
2. Instantaneous Velocity and Phase Averaging	9
C. SPECTRAL MEASUREMENTS	10
IV. DISCUSSION OF RESULTS	11
A. CHANNEL FLOW DEVELOPMENT LENGTHS	11
B. REYNOLDS NUMBER SURVEY OF IMPOSED PULSATION EFFECTS	11
1. Local Mean Streamwise Velocity	11
2. Longitudinal Turbulence Intensity	11
3. Normalized Phase-Averaged Velocity Magnitudes	12
4. Intermittency	12
5. Spectral Measurements	14
6. Phase Average Velocity and Turbulence Intensity Traces	14

V. SUMMARY AND CONCLUSIONS	15
APPENDIX A. SOFTWARE DIRECTORY	16
APPENDIX B. FIGURES	19
LIST OF REFERENCES	96
INITIAL DISTRIBUTION LIST	99

LIST OF FIGURES

Figure 1. Straight Channel Schematic	20
Figure 2. Unsteadiness Device	21
Figure 3. Phase Angle and Mean Velocity Variation with Vane Position	22
Figure 4. Flow Measurement Equipment	23
Figure 5. Bulk Velocity vs Orifice Differential Pressure	24
Figure 6. Channel Pressure Distribution	25
Figure 7. Inlet Turbulence Intensity Conditions	26
Figure 8. V_{avg} vs Re ($Y/d = 0.50$)	27
Figure 9. V_{avg} vs Re ($Y/d = 0.85$)	28
Figure 10. V_{avg} vs Re ($Y/d = 0.90$)	29
Figure 11. V_{avg}/V_{blk} vs Re ($Y/d = 0.50$)	30
Figure 12. V_{avg}/V_{blk} vs Re ($Y/d = 0.85$)	31
Figure 13. V_{avg}/V_{blk} vs Re ($Y/d = 0.90$)	32
Figure 14. V_{avg}/V_{cl} vs Re ($Y/d = 0.85$)	33
Figure 15. V_{avg}/V_{cl} vs Re ($Y/d = 0.90$)	34
Figure 16. V_{rms} vs Re ($Y/d = 0.50$)	35
Figure 17. V_{rms} vs Re ($Y/d = 0.85$)	36
Figure 18. V_{rms} vs Re ($Y/d = 0.90$)	37
Figure 19. V_{rms}/V_{cl} vs Re ($Y/d = 0.50$)	38
Figure 20. V_{rms}/V_{cl} vs Re ($Y/d = 0.85$)	39
Figure 21. V_{rms}/V_{cl} vs Re ($Y/d = 0.90$)	40
Figure 22. V_{rms}/V_{avg} vs Re ($Y/d = 0.50$)	41
Figure 23. V_{rms}/V_{avg} vs Re ($Y/d = 0.85$)	42
Figure 24. V_{rms}/V_{avg} vs Re ($Y/d = 0.90$)	43
Figure 25. $\Delta U_{hat}/V_{blk}$ vs Re (1 Hz)	44
Figure 26. $\Delta U_{hat}/V_{blk}$ vs Re (2 Hz)	45
Figure 27. Intermittency vs Re (1 Hz, 2 Hz)	46
Figure 28. Threshold and Second Time Derivatives vs V_{blk} ($Y/d = 0.50$)	47
Figure 29. Threshold Factor vs V_{blk}	48
Figure 30. Corrected Intermittency vs Re (2 Hz)	49
Figure 31. Typical Dynamic Signal Analyzer Settings	50

Figure 32. Spectral Frequency Response (0 Hz)	51
Figure 33. Spectral Frequency Response (1 Hz)	52
Figure 34. Spectral Frequency Response (2 Hz)	53
Figure 35. Spectral Frequency Response (3 Hz)	54
Figure 36. Spectral Frequency Response (4 Hz)	55
Figure 37. Average and RMS Velocity Traces ($Y/d=0.85$, $Re=1100$, 0 Hz)	56
Figure 38. Average and RMS Velocity Traces ($Y/d=0.85$, $Re=1250$, 0 Hz)	57
Figure 39. Average and RMS Velocity Traces ($Y/d=0.85$, $Re=1350$, 0 Hz)	58
Figure 40. Average and RMS Velocity Traces ($Y/d=0.85$, $Re=1440$, 0 Hz)	59
Figure 41. Average and RMS Velocity Traces ($Y/d=0.85$, $Re=1550$, 0 Hz)	60
Figure 42. Average and RMS Velocity Traces ($Y/d=0.85$, $Re=1710$, 0 Hz)	61
Figure 43. Average and RMS Velocity Traces ($Y/d=0.85$, $Re=1850$, 0 Hz)	62
Figure 44. Average and RMS Velocity Traces ($Y/d=0.85$, $Re=1920$, 0 Hz)	63
Figure 45. Average and RMS Velocity Traces ($Y/d=0.85$, $Re=2000$, 0 Hz)	64
Figure 46. Average and RMS Velocity Traces ($Y/d=0.85$, $Re=2040$, 0 Hz)	65
Figure 47. Average and RMS Velocity Traces ($Y/d=0.85$, $Re=2090$, 0 Hz)	66
Figure 48. Average and RMS Velocity Traces ($Y/d=0.85$, $Re=2200$, 0 Hz)	67
Figure 49. Average and RMS Velocity Traces ($Y/d=0.85$, $Re=2300$, 0 Hz)	68
Figure 50. Average and RMS Velocity Traces ($Y/d=0.85$, $Re=2350$, 0 Hz)	69
Figure 51. Average and RMS Velocity Traces ($Y/d=0.85$, $Re=2400$, 0 Hz)	70
Figure 52. Average and RMS Velocity Traces ($Y/d=0.85$, $Re=2450$, 0 Hz)	71
Figure 53. Average and RMS Velocity Traces ($Y/d=0.85$, $Re=2500$, 0 Hz)	72
Figure 54. Average and RMS Velocity Traces ($Y/d=0.85$, $Re=2800$, 0 Hz)	73
Figure 55. Average and RMS Velocity Traces ($Y/d=0.85$, $Re=3100$, 0 Hz)	74
Figure 56. Average and RMS Velocity Traces ($Y/d=0.85$, $Re=3400$, 0 Hz)	75
Figure 57. Average and RMS Velocity Traces ($Y/d=0.85$, $Re=1100$, 2 Hz)	76
Figure 58. Average and RMS Velocity Traces ($Y/d=0.85$, $Re=1250$, 2 Hz)	77
Figure 59. Average and RMS Velocity Traces ($Y/d=0.85$, $Re=1350$, 2 Hz)	78
Figure 60. Average and RMS Velocity Traces ($Y/d=0.85$, $Re=1440$, 2 Hz)	79
Figure 61. Average and RMS Velocity Traces ($Y/d=0.85$, $Re=1550$, 2 Hz)	80
Figure 62. Average and RMS Velocity Traces ($Y/d=0.85$, $Re=1710$, 2 Hz)	81
Figure 63. Average and RMS Velocity Traces ($Y/d=0.85$, $Re=1850$, 2 Hz)	82
Figure 64. Average and RMS Velocity Traces ($Y/d=0.85$, $Re=1920$, 2 Hz)	83
Figure 65. Average and RMS Velocity Traces ($Y/d=0.85$, $Re=2000$, 2 Hz)	84
Figure 66. Average and RMS Velocity Traces ($Y/d=0.85$, $Re=2040$, 2 Hz)	85

Figure 67. Average and RMS Velocity Traces ($Y/d = 0.85$, $Re = 2090$, 2 Hz)	86
Figure 68. Average and RMS Velocity Traces ($Y/d = 0.85$, $Re = 2200$, 2 Hz)	87
Figure 69. Average and RMS Velocity Traces ($Y/d = 0.85$, $Re = 2300$, 2 Hz)	88
Figure 70. Average and RMS Velocity Traces ($Y/d = 0.85$, $Re = 2350$, 2 Hz)	89
Figure 71. Average and RMS Velocity Traces ($Y/d = 0.85$, $Re = 2400$, 2 Hz)	90
Figure 72. Average and RMS Velocity Traces ($Y/d = 0.85$, $Re = 2450$, 2 Hz)	91
Figure 73. Average and RMS Velocity Traces ($Y/d = 0.85$, $Re = 2500$, 2 Hz)	92
Figure 74. Average and RMS Velocity Traces ($Y/d = 0.85$, $Re = 2800$, 2 Hz)	93
Figure 75. Average and RMS Velocity Traces ($Y/d = 0.85$, $Re = 3100$, 2 Hz)	94
Figure 76. Average and RMS Velocity Traces ($Y/d = 0.85$, $Re = 3400$, 2 Hz)	95

LIST OF SYMBOLS

d	channel height
f_{osc}	frequency of imposed pulsation
n_{cycl}	number of imposed pulsation cycles
Re	Reynolds number, $V_{bulk}d/\nu$
Str	Strouhal number, $2\pi f_{osc}d/V_{bulk}$
δ_s	Stokes layer thickness, $\sqrt{\frac{\nu}{2\pi f_{osc}}}$
U	instantaneous longitudinal velocity
V_{bulk}	bulk mean velocity
V_{cl}	centerline velocity ($Y/d = 0.50$)
V_{avg}, \bar{u}	mean streamwise velocity
V_{rms}	rms velocity, $\sqrt{\overline{u'^2}}$
\hat{u}	phase-averaged streamwise velocity
\tilde{u}	periodic streamwise velocity component from imposed pulsations
u'	instantaneous streamwise fluctuating velocity
x	longitudinal coordinate, measured from nozzle exit
y, Y	normal coordinate, measured from the bottom wall

z	spanwise coordinate, measured from the channel centerline
D	difference
Ω	Stokes number, $d/2t_u$
ν	kinematic viscosity (m^2/s)
γ	turbulence intermittency

ACKNOWLEDGEMENTS

This work is sponsored by the Office of Naval Research and the Naval Postgraduate School. Dr. Spiro Lekoudis is the program monitor.

The author wishes to acknowledge and thank Professors Ligrani and Subramanian for their guidance in conducting the research presented and in drafting this document, and Lieutenant Morrow for his cooperation and support throughout the course of the experimental study.

I. INTRODUCTION

A. BACKGROUND

Flow pulsations and unsteadiness are present in many practical engineering flow situations. Most flows of technological interest also undergo transition from a laminar to turbulent state. Transition is by itself extremely complex; however, with flow pulsations and unsteadiness, accurate prediction of the location and extent of transition and accompanying changes of important flow properties is even farther beyond present computational modeling abilities. Consequently, experiments are necessary to elucidate flow behavior. According to Shemer [Ref. 1], such experiments should be "restricted to the simplest and most well-defined conditions" to "obtain a clear physical description of a fluid dynamical process."

The present study employs a straight channel to investigate a situation consistent with Shemer's suggestion. This flow is also studied because little experimental information is available for transitioning flow in straight channels with imposed pulsations. Some experimental results are published for pipe flows as well as limited analytic and numeric results for channel flows; however, the author knows of no other experiments, other than the continuing current work, performed to study the stability or transition of plane channel flow with imposed pulsations.

Here, pulsations are induced with a single rotating vane located downstream of the flow test section. The device is similar to the rotating profiled sleeves employed by Tu and Ramaprian [Ref. 2], Ramaprian and Tu [Ref. 3] and Stettler and Hussain [Ref. 4] to study the influences of sinusoidal pulsations on pipe flows. Their sleeves are used in water and operate simply by altering the exit flow area. Other studies of influences of imposed pulsations on pipe flows use reciprocating pistons in cylinders to produce pulsations [Refs. 5,6,7, 8,9,10, 11]. Simpson et al [Ref. 12] use a rotating blade damper system at the inlet of their wind tunnel, upstream of screens and honeycomb, in order to study the effects of pulsations on turbulent boundary layer flows. By changing the motion of the five individual damper blades, sinusoidal perturbations to the flow are produced with amplitudes amounting to 11-93 % of the maximum velocity over frequencies from 0.6-2 Hz.

Of the experimental studies of transitional flows in pipes, Merkli and Thomann [Ref. 5], Sergeev [Ref. 6], Hino and Sawamoto [Ref. 7], Hino et al [Ref. 8], Gerrard [Ref. 9],

Gilbrech and Combs [Ref. 10], Sarpkaya [Ref. 11], Ramaprian and Tu [Ref. 3], Shemer [Ref. 1] and Stettler and Hussain [Ref. 4] also examine the effects of imposed pulsations. Of these studies, [Refs. 5-8] investigate the instability of sinusoidally modulated pipe flow with zero mean flow. Gerrard [Ref. 9] conducts his experiments at transition Reynolds number of 3770. He relates variations of turbulent flow over individual flow pulsations to magnitudes of vorticity diffusion. Gerrard also suggests that, with high pulsation frequency, viscous effects are confined to a very thin Stokes layer near the wall where the fluid is retarded. Gilbrech and Combs [Ref. 10] and Sarpkaya [Ref. 11] examine the effects of amplitude and frequency of imposed pulsations on the growth rate of artificially introduced plugs. Both investigators indicate that pulsations increase the critical Reynolds number as long as they are not so large as to cause local flow reversals. Ramaprian and Tu [Ref. 3] study transitional pipe flow at a mean Reynolds number of 2100. They indicate that flow pulsations at frequencies ranging from 0.05 to 1.75 Hz increase the critical Reynolds number only when the turbulent intermittency is small. With higher intermittency levels, the authors suggest that imposed pulsations affect the flow only when the pulsation frequency is near the characteristic frequency of the turbulence. Shemer's [Ref. 1] work focuses on large pulsation amplitudes at a single low frequency. For a mean Reynolds number of about 4000 and a pulsation frequency of 0.37 Hz, he concludes that transition is governed primarily by the instantaneous Reynolds number. Stettler and Hussain [Ref. 4] present results for Stokes numbers as high as 70. The authors provide a three-dimensional map of stability-transition regimes, and also indicate that transition in pipes is associated with plugs of turbulence which can grow or shrink in size.

Numerical and analytical investigations of the influences of imposed pulsations on flow in a plane channel are described by Grosch and Salwen [Ref. 13], Herbert [Ref. 14], Hall [Ref. 15], von Kerczek [Ref. 16] and Singer, et al [Refs. 17,18]. In addition to these studies, Tozzi [Ref. 19] provides results of a numerical investigation of the influences of imposed pulsations on flow in a pipe, and Davies [Ref. 20] provides a review of much work done on the stability of time periodic flows. Of the above mentioned analytic studies of plane channel flow, Grosch and Salwen [Ref. 13] solve a set of linearized equations by integrating through one period of pulsation. They conclude that flows with small amplitudes of imposed pulsations are more stable than steady flows, where the degree of stabilization depends upon interactions between shear waves generated by the imposed pulsation and flow disturbances. A modified version of Grosch and Salwen's energy analysis is described by Herbert [Ref. 14]. Hall [Ref. 15] reports results

obtained with high frequency pulsations and concludes that such pulsations are slightly destabilizing irrespective of amplitude. von Kerczek [Ref. 16] modulates the pressure gradient in a perturbation analysis, and shows that the oscillating flow is more stable than the steady flow for frequencies of imposed pulsations greater than about one tenth of the frequency of the steady flow neutral disturbance. However, at both very low and very high frequencies of imposed pulsations, the flow is slightly unstable. Singer et al [Refs. 17,18] describe results from a direct Navier-Stokes simulation of flow in a plane channel with imposed pulsations and indicate that imposed sinusoidal pulsations provide a stabilizing effect at all but very low frequencies. Significant variations in the amplitudes of Tollmein-Schlichting waves are also noted which depend upon the Strouhal number and the amplitude of the pulsations, as well as on initial amplitudes of the Tollmein-Schlichting waves. Tozzi's [Ref. 19] study of pipe flow shows that imposed pulsations are stabilizing up to very high amplitudes of imposed pulsation.

B. OBJECTIVES

This study provides experimental data which show the influences of imposed pulsations on laminar, transitional, and turbulent flows in a rectangular cross-section channel with 40 to 1 aspect ratio and L/d of 336 ($d = 0.0127\text{m}$). The imposed pulsation device employed is based on existing designs, but here is applied to channel flow with air. Mean streamwise velocity and longitudinal turbulent intensity velocity data as a function of Reynolds number for various pulsation frequencies are given for three locations across the channel height. The current study is complementary to the work of Morrow [Ref. 21] and is an extension of work by Koth [Ref. 22], Coumes [Ref. 23], and Longest [Ref. 24]. These previous studies found imposed pulsations at 1 and 2 Hz to have a greater destabilizing effect on the longitudinal velocity fluctuations in the Stokes layer at some Reynolds numbers than observed in the present study. The present results are given for Strouhal numbers from 0.039 to 0.121, and Reynolds numbers ranging from 1100 to 3400 (V_{bh} from 1.3 to 4.1 m/s), where each is based on bulk mean velocity and channel height. To produce these conditions, pulsations are imposed on the flow at frequencies of 1 Hz and 2 Hz. These imposed pulsation frequencies correspond to kinematic viscosity based Stokes numbers of 4.08 and 5.79, respectively.

C. THESIS ORGANIZATION

In the chapters that follow, the experimental facilities, including the channel, unsteadiness device and data acquisition system, are detailed in Chapter II. The experimental procedures for calibration of the hot-wire probe, channel validation, flow measurement and spectral analysis are described in Chapter III. Results are discussed in Chapter IV. A summary of results and conclusions appear in Chapter V.

II. EXPERIMENTAL FACILITIES

A. CHANNEL

The straight channel was specifically designed for the present study and is located in the laboratories of the Department of Mechanical Engineering of the Naval Postgraduate School. Figure 1 is a schematic of the channel, and the coordinate system employed. x is the longitudinal coordinate measured from the downstream edge of the nozzle, y is the normal coordinate measured from the bottom wall, and z is the transverse coordinate, measured from the spanwise centerline of the channel.

The test section of the channel is 4.27 m long, 1.27 cm high and 50.8 cm wide (inside dimensions). This gives an internal aspect ratio of 40 to 1. The top and bottom walls are 6.35 mm thick lexan supported by ribs and cross beams along their length. The side walls are removable for access to the inside of the channel. Inlet flow is managed with a honeycomb, screens and a 20:1 contraction ratio nozzle. Two layers of cheese cloth are also placed at the inlet to remove dust and dirt from the entering air. At the test section exit are three 10.16 cm long frames. Screens are between the flanges of the frames and honeycomb is placed just upstream of the last screen. The unsteadiness device is housed in the middle frame. A two-dimensional diffuser (45.72 cm long, 3 degree total angle), located downstream of the honeycomb section, connects the straight section to the exit plenum. This plenum provides a uniform volume of low pressure air at the diffuser exit. The plenum is a cube with inside dimensions of 60.96 cm along each side and is connected to the suction side of a 5 hp blower via piping of 5.08 cm inside diameter. Flow through the channel is metered by a 3.81 cm orifice plate assembly located near the plenum exit. The channel is rigidly mounted on steel frames with supporting ribs along its length. With this mounting arrangement, no measurable deflection of the channel walls occurs with either steady or pulsating flow. Vibration damping systems are employed on the mounting frame and test section to further reduce vibrations due to mechanical sources. Additionally, all results are obtained at night with no other activity in the laboratory to minimize disturbances from acoustic sources.

Channel bulk flow velocities (V_{bh}) of 15 m/s are possible; however, the present study uses a range of V_{bh} from 1.3 to 4.1 m/s. The channel is designed so transition will occur after laminar flow has developed fully. The measured turbulence intensity of the flow at the nozzle exit (Figure 7) is 0.12 to 0.14 percent for Reynolds numbers less than 2100

with no imposed pulsations, as well as with pulsations imposed at 1, 2, 3, and 4 Hz. As Re increases to 3600, inlet intensities both with and without imposed pulsations are slightly higher (0.17 to 0.24 percent).

B. UNSTEADINESS DEVICE

Periodic variations of the flow rate can be induced in the test sections of the wind tunnels, channel flows and pipe flows by introducing a periodic blockage at the inlet or exit of flow passages. The most important requirement of such an unsteady device is the ability to produce controlled deterministic and periodic unsteadiness without adding other disturbances. In an open circuit induction channel, the unsteady device is best located just downstream of the test section, thereby eliminating convection of wakes and other flow disturbances into the test section.

A single rotating vane is used to impose pulsations in the present study, as shown in Figure 2. A single vane makes this possible since the interior height of the channel is relatively small (1.27 cm). The vane is a 3.2 mm thick brass strip with rounded edges, and is supported at the ends by a 3.2 mm diameter shaft with bushings fitted to the side walls of the frame. Three intermediate spanwise struts increase the rigidity of the vane as it rotates. One of the shafts extends to accommodate a 48 tooth spur gear driven by a 12 tooth spur pinion mounted on the shaft of a Superior Electric, M092-FD310 Stepper Motor. The motor is driven by a Modulynx MITAS PMS085-D050 Drive controlled by a Modulynx MITAS PMS085-C2AR Drive Controller. This arrangement allows the motor shaft to be positioned at 1/200th increments of one motor shaft revolution. The 1 to 4 gearing ratio, coupled with two cycles of imposed flow pulsations per vane rotation, gives one motor revolution corresponding to one half of one cycle of an imposed flow pulsation. The imposed pulsation frequency is set by programming the Drive Controller for a particular motor speed which then sets the vane rotation rate. The amplitude of the imposed pulsations is altered by changing the width of the vane. A vane width of 8.7 mm is employed in the present study.

When the vane rotation rate is small enough, the vane produces a quasi-steady flow and the flow behaves as if the vane were fixed at each position and allowed to reach steady state behavior. The variation of the mean velocity under such circumstances is approximately sinusoidal, as illustrated in Figure 3. This waveform results because, momentarily, mass flow rates (and resulting velocities in the straight test section) are roughly proportional to the flow passage area provided by the vane as it rotates. In Figure 3, flow resistance is maximum and velocity in the straight section is minimum

when the vane is normal to the flow with position 2. With vane position 4, the flow resistance is minimum and the velocity is maximum.

Actual flow around the rotating vane is quite complex. Velocity and pressure variations are affected not only by the varying flow resistance from the vane, but also by other fluid dynamic effects such as dynamic flow separation and flow inertia. At large vane speeds, the vane rotations will likely result in a local swirl with blockage like a solid cylinder and minimal bulk flow periodicity. Imposed oscillatory flow behavior is thus different and difficult to predict compared to quasi-steady flow. The assessment of the performance of the rotating vane as it produces imposed velocity pulsations in the test section is given by Ligrani, et al [Ref. 25].

C. FLOW MEASUREMENT INSTRUMENTS

Figure 4 presents a schematic of the flow measurement equipment.

1. Hot-wire Anemometer

A DANTEC 55P51 hot-wire probe, with sensor diameter of $5\mu\text{m}$ and sensor length of 1.25 mm, is used for instantaneous velocity measurements. The probe is mounted with the wire horizontal and normal to the flow direction. The probe position is controlled by a rotatable lever arm which can adjust through a range of Y/d of 0.05 to 0.95. The lever arm is calibrated for probe positioning with an accuracy of approximately 0.5 mm with respect to the y coordinate. For all measurements presented, the probe is located 3.74 m from beginning of the test section and 97.6 mm left of spanwise center. These are equivalent to $x'/d = 294.5$ and $z'/d = 7.7$.

2. Hot-wire Bridge, Signal Conditioner, High Speed Data Acquisition System and Data Storage

A DISA 55M10 constant temperature bridge is used to operate the hot-wire probe at an overheat ratio of 1.8. When connected to this bridge with the same settings used for measurements, the hot-wire is calibrated in the potential flow of a wind tunnel. During measurement, the DC voltage from hot-wire bridge is measured using a Hewlett-Packard 3466A digital multimeter.

A DANTEC Model 56N20 signal conditioner is used to amplify and filter the voltage from the bridge. During measurements, an amplifier gain of 10 is used, the low-pass filter is set to 10kHz and the high pass filter is set at 0.1 Hz to remove high frequency noise signal as well as the DC signal. The output of the signal conditioner is fed to a Hewlett-Packard 6944 Multiprogrammer with a buffered high speed A/D conversion system. The Multiprogrammer cards are driven using Hewlett-Packard

CAT 14752A software on a Hewlett-Packard 9000 series Model 310 computer. Digitized instantaneous voltages are stored on 3.5 inch diskettes for further processing. The heading to each data set includes the time, date, bulk velocity, pulsation frequency, and average voltage from the digital multimeter.

3. Phase-Averaging

The motor used to drive the vane generates voltage pulses sequentially in each of the four field windings used to step the motor. Fifty pulses are available to each field winding for each revolution of the motor shaft, giving a total of 200 pulses per revolution. The pulses from one of the four field windings are used to trigger the data acquisition and are precisely synchronized with the vane rotation. Thus, for a given vane imposed pulsation frequency, f_{osc} , the data sampling rate (TR) is given by:

$$\begin{aligned} \text{TR}(\text{samples/sec}) &= \\ f_{osc} \times (\text{pulses/motor shaft rev.}) \times (\text{motor shaft rev./imposed pulsations}) \\ &= f_{osc} \times 50 \times 2 \\ &= 100 \times f_{osc} \end{aligned}$$

With this approach, 100 samples of data are obtained, spaced uniformly, over each period of flow pulsation, providing a phase resolution of 1/100 of the imposed pulsation cycle.

Data are acquired for 640 sequential flow pulsations so that the memory buffer of the multiprogrammer (64 kbytes) is completely filled. Afterwards, data are stored in the computer memory, where they are packed into 640 arrays of 100 samples each. Data are then stored on a disk for later processing. Because non-uniform width voltage pulses may be generated by the motor drive as the motor is started and stopped, the first 6000 points are ignored as data are processed, and all acquisitions are completed well before the vane motor is stopped. When no pulsations are imposed on the flow, data acquisition is triggered using a signal from a square wave function generator set to the same frequency as employed with imposed pulsations.

III. EXPERIMENTAL PROCEDURES

A. HOT-WIRE CALIBRATION

The hot-wire is calibrated in the freestream of the wind tunnel located in the laboratories of the Mechanical Engineering Department of the Naval Postgraduate School. During calibration, the hot-wire probe is mounted normal to the flow in potential freestream flow and connected to the hot-wire bridge discussed previously. Output from the hot-wire bridge is read on a Keithly 169 Digital Multimeter. Freestream velocity in the wind tunnel is measured utilizing a Kiel pressure probe, a wall static pressure tap, and a Validyne PS 309 Digital Manometer. Voltage and differential pressure readings are taken for a range of pressure drops corresponding to velocities between 1.0 and 4.0 m/s. Following the calibration, the hot-wire is installed in the straight channel.

B. DATA PROCESSING

1. Bulk Velocity

The bulk flow velocity is determined from the pressure drop across the orifice plate located in the outlet piping which connects the outlet plenum and the blower. The channel Reynolds number and channel Strouhal number are then determined using this bulk flow velocity. The pressure drop is measured using a Validyne Model PS 309 Digital Manometer. Figure 5 shows the relationship of bulk velocity to pressure drop.

2. Instantaneous Velocity and Phase Averaging

Instantaneous voltages are converted into instantaneous velocities using a look-up table that accounts for hot-wire calibration coefficients, amplifier gains and mean voltage levels. With imposed periodic flow, instantaneous velocities are given by $U = \bar{u} + \tilde{u} + u'$, where \bar{u} is the time-averaged velocity, \tilde{u} is the periodic velocity, and u' is the fluctuating component.

In the present study, \tilde{u} and \bar{u} are combined as the phase-averaged velocity (\hat{u}), such that $U = \hat{u} + u'$, following Ramaprian and Tu [Ref. 3]. Thus for a steady flow with no periodic velocity, \hat{u} is then equal to \bar{u} . \hat{u} is then determined from phase-averaging instantaneous velocity results using the equation given by :

$$\hat{u}(n) \big|_{n=1}^{100} = \frac{1}{ncycl} \sum_{m=1}^{ncycl} U(m,n) \big|_{n=1}^{100}$$

Here, m and n correspond, respectively, to the number of cycles and locations across each phase where data are sampled. Typically 580 cycles are ensemble averaged to obtain a phase-averaged velocity trace.

C. SPECTRAL MEASUREMENTS

Spectra of analog voltages from the hot-wire bridge are determined using a Hewlett-Packard Model 3562A Dynamic Signal Analyzer (DSA). Spectral coordinates are $\log ((\text{volts})^2/\text{frequency (Hz)})$ versus frequency (Hz), where frequency varies from 0 to 200 Hz. Typical settings of other parameters are shown in Figure 31. With this arrangement, five sequential spectra are ensemble averaged to produce final results obtained for Reynolds numbers between 1400 and 1700.

IV. DISCUSSION OF RESULTS

A. CHANNEL FLOW DEVELOPMENT LENGTHS

Streamwise pressure distributions are shown in Figure 6 for $Re = 1100$, 2010 , and 3600 . Streamwise pressure gradients are constant and invariant with streamwise distance for $x/d > 55$, $x/d > 105$, and $x/d > 170$ for Reynolds numbers of 1100 , 2010 , and 3600 , respectively. Such behavior evidences fully developed flow, which, if present, gives normalized velocity profiles which are self-similar with respect to streamwise distance. These results are in close agreement with empirical values for duct flow given by Han [Ref. 26]. Schlichting [Ref. 27], using laminar theory, gives x/d development lengths of 44 for $Re = 1100$ and 146 for $Re = 3600$.

B. REYNOLDS NUMBER SURVEY OF IMPOSED PULSATION EFFECTS

Reynolds number surveys of mean streamwise velocity and longitudinal velocity fluctuations are presented for Y/d values of 0.50 , 0.85 , and 0.90 both with and without imposed pulsations. These surveys are based on the same profile data presented by Morrow [Ref. 21] at $x/d = 294.5$ and $z/d = 7.7$.

1. Local Mean Streamwise Velocity

Figure 8 through Figure 10 show the dimensional local mean streamwise velocity as a function of Reynolds number for Y/d of 0.50 , 0.85 , and 0.90 . Additional Reynolds number surveys are given in Figure 11 through Figure 13, which show local mean streamwise velocity normalized with respect to bulk velocity, while in Figure 14 and Figure 15, data are normalized with respect to centerline velocity. In each figure, except Figure 11, velocity increases with Reynolds number in the laminar and transitional regimes with less dependence on Reynolds number in the turbulent region. Such increases are largest at $Y/d = 0.50$. In each regime, at a particular Re , dimensional and normalized velocities decrease with increasing Y/d , as expected. In each of the figures, data in the transition region from Reynolds numbers of about 2100 to 2500 show some experimental scatter.

2. Longitudinal Turbulence Intensity

Dimensional longitudinal turbulence intensity data are shown in Figure 16 through Figure 18. The turbulence intensity data are normalized with respect to centerline velocity in Figure 19 through Figure 21 and with respect to local average

velocity in Figure 22 through Figure 24. Turbulence intensity data for all three locations increase with Reynolds number in the transition region ($Re = 1450$ to 2500) with less dependence on Reynolds number in the turbulent regime when Re becomes greater than 2500 . Local maxima appear from $Re = 2000$ to $Re = 2400$ in each figure which increase in magnitude with Y/d . In Figure 19 through Figure 21, normalized turbulence intensity data show similar qualitative behavior.

Imposed pulsations at 1 Hz have negligible effect on magnitudes of turbulence intensity survey, however with 2 Hz pulsations, intensities with imposed pulsations at $Y/d = 0.50$ are lower than values without pulsations for Reynolds numbers from 2400 to 2500 (Figure 22). These variations are not seen at either of the other Y/d locations studied. They are believed to result because of destabilization at 2 Hz resulting in earlier onset of fully turbulent flow with less local intensity.

3. Normalized Phase-Averaged Velocity Magnitudes

Figure 25 and Figure 26 show variations in peak-to-peak amplitudes of phase-averaged velocities normalized with respect to bulk mean velocity ($\Delta \hat{u}/V_{bulk}$) as a function of Reynolds number. In each of these figures, the data without pulsations is presented for comparison with imposed pulsation data. The 1 Hz survey (Figure 25) shows little effect of imposed pulsation on $\Delta \hat{u}/V_{bulk}$, whereas the 2 Hz survey (Figure 26) shows an increase in $\Delta \hat{u}/V_{bulk}$ with Reynolds number with local maxima apparent near $Re = 2000$ and $Re = 2450$ for all three Y/d locations. The maxima near $Re = 2450$ is greatest in magnitude. Smaller maxima near $Re = 2000$ and $Re = 2450$ are also visible in the 1 Hz surveys.

4. Intermittency

Figure 27 shows turbulence intermittency as a function of Reynolds number for each channel Y/d location of interest at imposed pulsation frequencies of 0 , 1 , and 2 Hz. The intermittency values (γ) are calculated from instantaneous second derivatives of streamwise velocity with respect to time. The second time derivative is calculated numerically using the finite difference method. This value is then compared to a threshold value in an on-off temporal identification function, ID , defined such that :

$$ID = 1, \text{ if } \frac{\partial^2 U}{\partial t^2} > \text{Thr (flow turbulent)}$$

and :

$$ID = 0, \text{ otherwise (flow non-turbulent).}$$

Intermittency is then the percent of the time that the flow is fully turbulent. The intermittency threshold, Thr, is given by :

$$\text{Thr} = \{105 - (64.66 \times (V_{bh} - 1.89))\}$$

This approach produces results as seen in Figure 27. Values for 2 Hz pulsations range from 0.5 to 0.8 at low Reynolds numbers (in the laminar region) depending on channel location. These values cannot be believed since one expects γ to be nearly zero when flow is fully laminar.

In order to provide more reasonable intermittency results, another method for computing the turbulence threshold is employed. Since similar intermittency trends are evident for each Y,d position, the new threshold is determined at the centerline and then taken to be valid for the other positions. To do this, average second time derivatives of velocity ($\frac{\partial^2 U}{\partial t^2}$) for the 0 and 2 Hz cases are determined. Figure 28 shows the second time derivative for each case (0 and 2 Hz) multiplied by a factor of 0.01 as a function of bulk mean velocity (and consequently Reynolds number). The threshold algorithm as described above is also presented in this figure. To determine the threshold factor, results for the 0 Hz case shown in Figure 27 are considered to be valid. The value of the original threshold algorithm at a given bulk velocity is divided by the average second time derivative of velocity to give the new threshold factor, T.F. T. F. values as a function of bulk velocity are then shown in Figure 29. A curve is then fit, as shown, to express the threshold factor as a function of the bulk mean velocity. This curve is given by :

$$\text{T.F.} = 2.5414V_{bh}^2 - 13.331V_{bh} + 17.412$$

thus :

$$\text{Thr} = \text{T.F.} \times \frac{\overline{\partial^2 U}}{\partial t^2}$$

With this approach, "corrected" intermittency survey results are shown in Figure 30 for pulsations at 0 and 2 Hz. In this figure, data for both the 0 and 2 Hz cases show intermittency varying from 0 to 1 as Reynolds number increases from 1550 to 2050.

5. Spectral Measurements

Spectral measurements are presented in Figure 32 through Figure 36 for $Y/d = 0.90$ at Reynolds numbers from 1400 to 1700 and pulsation frequencies of 0, 1, 2, 3, and 4 Hz. Figure 31 shows the dynamic signal analyzer (DSA) settings for spectral measurement. At $Re = 1550$, with no imposed pulsations, spectra show "humps" similar to ones resulting from spectra of time traces having Dirac delta functions. These correspond to intermittent turbulent events. As the flow is subjected to pulsation, the transitional or critical Reynolds number decreases, displaying increasing overall spectral energy levels near $Re = 1500$.

6. Phase Average Velocity and Turbulence Intensity Traces

Figure 37 through Figure 76 show phase-averaged velocity and turbulence intensity traces for $Y/d = 0.85$ at 0 and 2 Hz produced as discussed in Appendix A. Phase-averaged traces for 2 Hz pulsations (Figure 57 to Figure 76) show sinusoidal behavior at low Reynolds numbers which become distorted as Reynolds number increases. As the bulk mean velocity and local average velocity increase with Re , the imposed pulsations show smaller percent-wise variations on instantaneous velocity traces. Increased turbulence levels are more apparent on instantaneous velocity traces and phase-averaged traces are increasingly distorted.

V. SUMMARY AND CONCLUSIONS

This study examines laminar, transitional, and turbulent flows in a 40 to 1 aspect ratio straight channel at Reynolds numbers from 1100 to 3400. The study also investigates the influences of pulsations imposed on the flows at frequencies of 1, 2, 3, and 4 Hz. Data are presented for Y/d locations of 0.50 (centerline), 0.85, and 0.90. Stokes numbers are 4.08 and 5.79, and Strouhal numbers vary from 0.039 to 0.122.

Local average velocity surveys, both dimensional and normalized, are largely unaffected by imposed pulsations. Longitudinal turbulence intensity levels for the three locations show increases with Reynolds number from $Re = 1100$ to $Re = 2200$, and then show decreases with Reynolds number from 2200 to 2500. Afterwards, smaller variations with Re are apparent as the flow becomes fully turbulent at $Re > 2500$. Longitudinal turbulence intensity values which are higher at the channel centerline than near the wall evidence a center mode of transition for Re from 1200 to 1500 (Zang and Krist [Ref. 28]). Maximum turbulence intensity values observed near $Re = 2200$ increase with Y/d , as does the turbulence intensity in the fully turbulent region.

For Reynolds numbers from 2350 to 2450, imposed pulsations at a Stokes number of 5.79 (2 Hz) result in decreased normalized turbulence intensity values compared to values seen at 0 and 1 Hz. This is believed to occur because pulsations destabilize the flow, an effect not seen for 1 Hz pulsations, perhaps because of their lower amplitudes.

Spectral measurements show overall energy level increases to occur between Re of 1500 and 1550, depending on pulsation frequency. Spectra show evidence of intermittency at Re of 1550 for imposed pulsations at 0, 1, 2, 3, and 4 Hz. Intermittency values for no imposed pulsations and for 2 Hz imposed pulsations increase from 0 to 1 as Re increases from 1450 to 2100.

Phase-averaged velocity traces show sinusoidal behavior over low Re below 1750. As the Reynolds number increases, sinusoidal traces become more distorted at Re of 1850 to 2200 in the transition regime, and at higher turbulent Re when turbulence intensity levels increase. Amplitudes (peak-to-peak) of phase-averaged traces show important variations with Re . With 2 Hz imposed pulsations, local maxima are evident near Re of 2000, 2200, and 2450.

APPENDIX A. SOFTWARE DIRECTORY

DEAN15 : Determines channel mass flow rate, bulk velocity and Reynolds number from orifice plate pressure drop. The program requires ambient temperature and pressure inputs which can be entered manually or via a data acquisition system connected to thermocouples and/or pressure transducers. Once ambient conditions are established, air density is calculated and orifice pressure drop is entered manually. Originally designed for curved channel applications, this version has been specifically modified for straight channel use.

HWCAL : Determines the constants for the King's Law calibration of the hot-wire. The program also provides a polynomial fit of the calibration data. The version used is written for the IBM 310 mainframe computer.

HOTWIREPAV : Reads the data stored in the A/D buffer of the high speed data acquisition system and stores the information on micro diskettes. Manual inputs are : triggering frequency, hot-wire DC voltage (ungained), oscillation frequency (flow blockage), bulk velocity, Reynolds number, and date and time of run.

DATAP : Calculates instantaneous and phase-averaged velocities. Initially a look up table is created. Effective velocities are calculated from the effective voltage values and stored for follow-on calculations. The hot-wire calibration constants obtained from HWCAL, and the amplifier gain are incorporated into these calculations. The velocity calibration is given by :

$$U_{eff} = k(E_{eff}^2 - E_0^2)^{1/N}$$

where k is the proportionality constant, E_{eff} is the effective voltage, and E_0 is the reference voltage at no flow. N is a constant (0.45) for moderate Reynolds numbers. Once the look up table is created, the program reads the instantaneous voltage values from the data file and converts them to instantaneous velocities. A plot of the instantaneous velocity versus time can be generated for any of 580 cycles (the first 60 cycles are discarded to allow for flow stabilization as the unsteady device is started).

Next the program phase averages the 580 cycles, and velocity versus phase angle (of the flow blockage) plots are available. Two plots are available from the averaged values : \hat{u} versus phase angle and $\sqrt{\hat{u}'^2} / \bar{u}$ versus phase angle. \hat{u} is the phase averaged

velocity, $\sqrt{\bar{u'^2}}$ is the phase averaged root mean squared (rms) velocity, and \bar{u} is the average velocity. In the case where there is no imposed unsteadiness, the phase averaged velocity, \bar{u} , is equal to the time averaged velocity, \bar{u} .

INTRMTCY : Takes data recorded by HOTWIREPAV and computes the intermittency. It uses the second time derivative of the instantaneous velocity, which is calculated numerically using the finite difference method. This value is then compared to a threshold value in an on-off temporal identification function, ID, defined such that :

$$\begin{aligned} \text{ID} &= 1, \text{ if } \frac{\partial^2 U}{\partial t^2} > \text{Thr, and} \\ \text{ID} &= 0, \text{ otherwise.} \end{aligned}$$

The threshold factor, Thr, is determined for different Reynolds numbers using the correlation :

$$\text{Thr} = \{105 - (64.66 \times (V_{blk} - 1.89))\}$$

If the Thr value falls less than 20 then its value is reset to 20. The values of ID are then phase averaged and time averaged for the traces and mean intermittency value, γ . This approach produces results which are reasonable for all but the 2 Hz imposed pulsation case.

In order to provide more reasonable results for intermittency, the method for computing the turbulence threshold is modified. Since the intermittency surveys show a similar trend for each Y/d position, the modification approach for the threshold is done at the centerline and taken to be valid for the other positions. The new threshold algorithm requires investigation of the average second time derivative of velocity ($\frac{\partial^2 U}{\partial t^2}$) for the 0 and 2 Hz case. The goal is to obtain a "threshold factor" to multiply the second time derivative since the intermittency is a function of the magnitude of the second time derivative as well as the bulk Reynolds number.

The approach for determining the threshold factor assumes the results for the 0 Hz case to be valid. The value of the original threshold algorithm at a given bulk velocity is divided by the average second time derivative of velocity. This is the threshold factor, T.F. A curve is then fit to express the threshold factor as a function of the bulk mean velocity. Now :

$$\text{Thr} = \text{T.F.} \times \frac{\partial^2 U}{\partial t^2}$$

where :

$$T.F. = 2.5414V_{blk}^2 - 13.331V_{blk} + 17.412$$

Since the threshold modification approach produces reasonable results for the 0 Hz case, which had previously been believable, it is assumed that the modification of Thr will have no significant effect on the 1 Hz case.

APPENDIX B. FIGURES

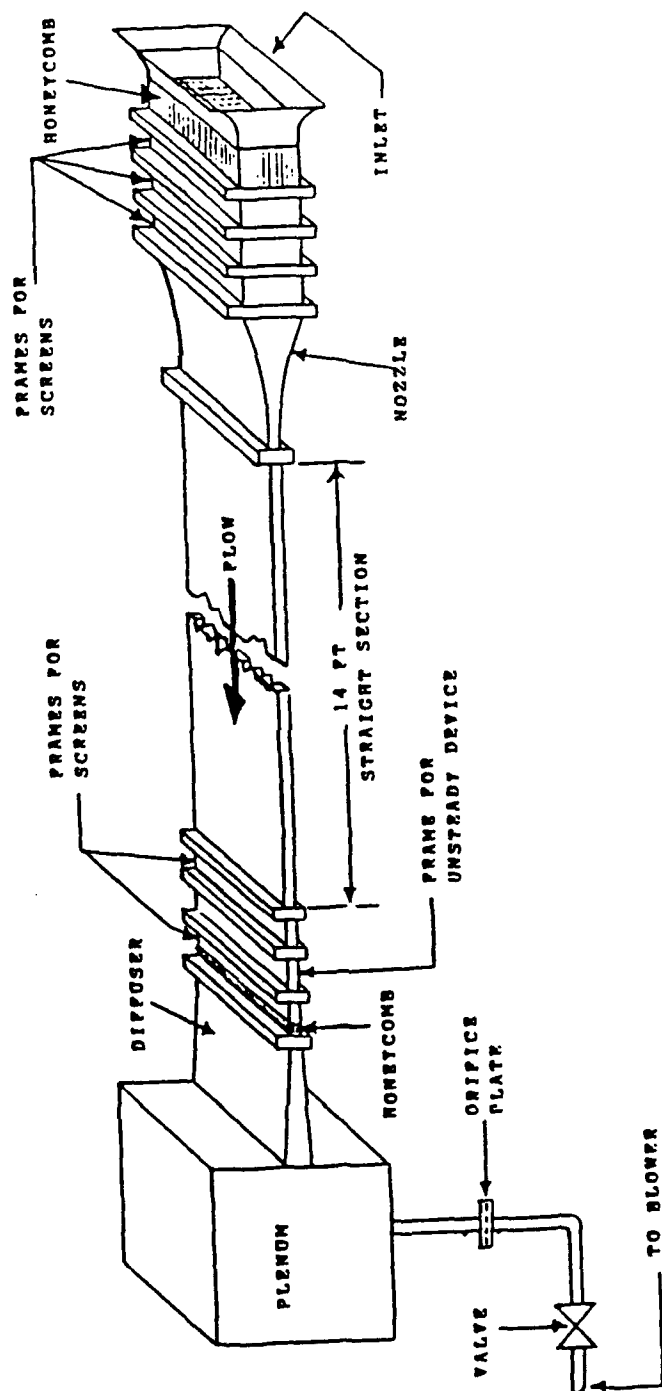


Figure 1. Straight Channel Schematic

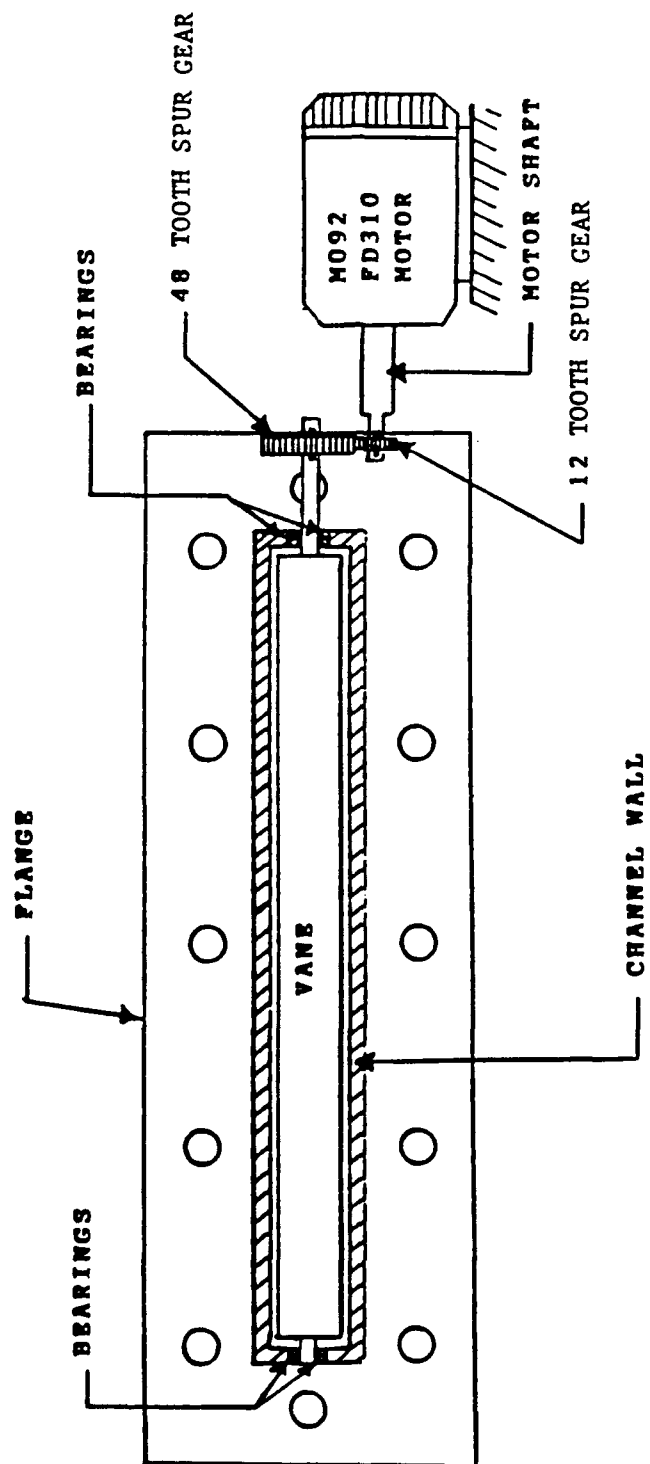


Figure 2. Unsteadiness Device

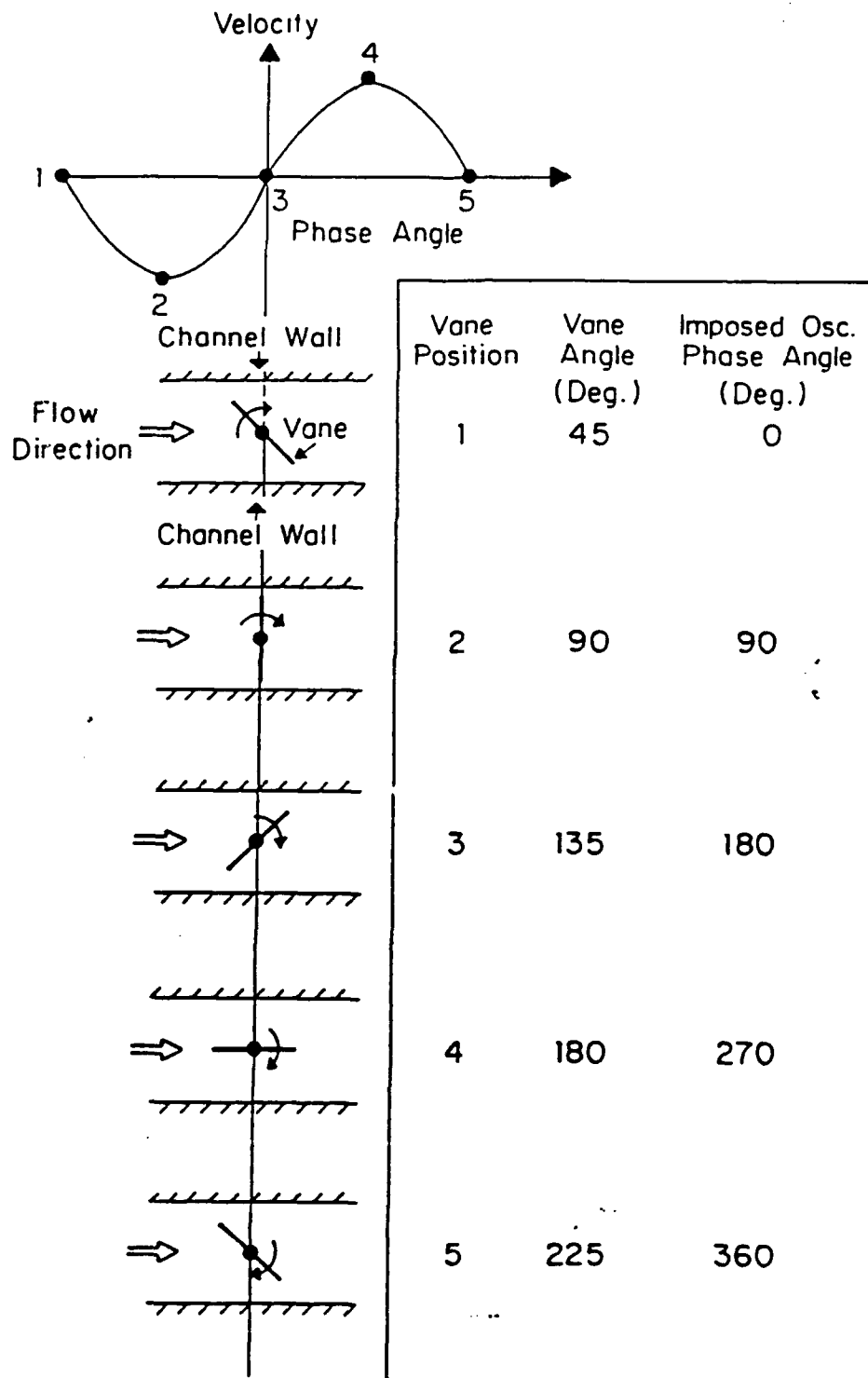


Figure 3. Phase Angle and Mean Velocity Variation with Vane Position

SCHEMATIC OF FLOW MEASUREMENT EQUIPMENT

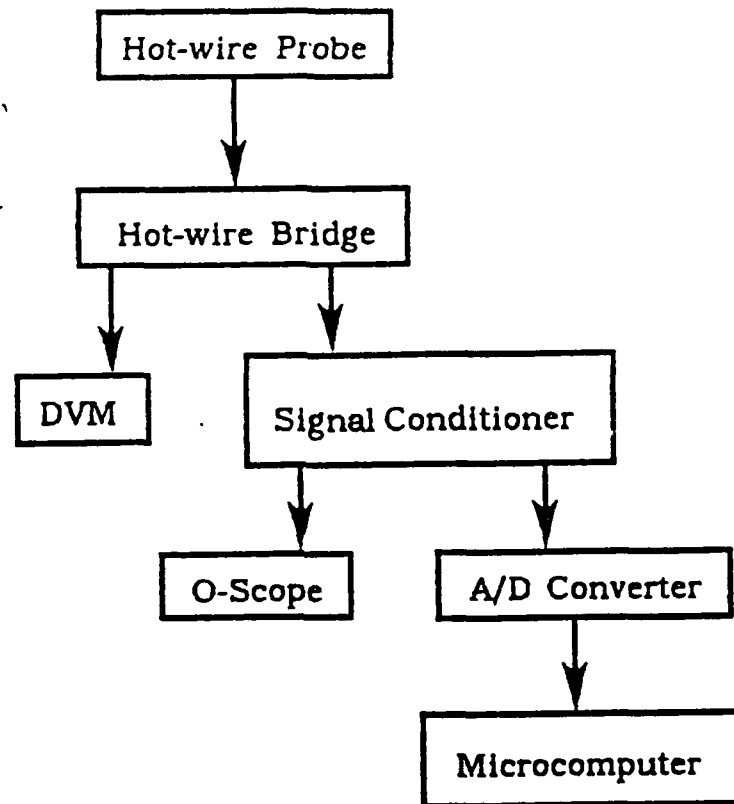


Figure 4. Flow Measurement Equipment

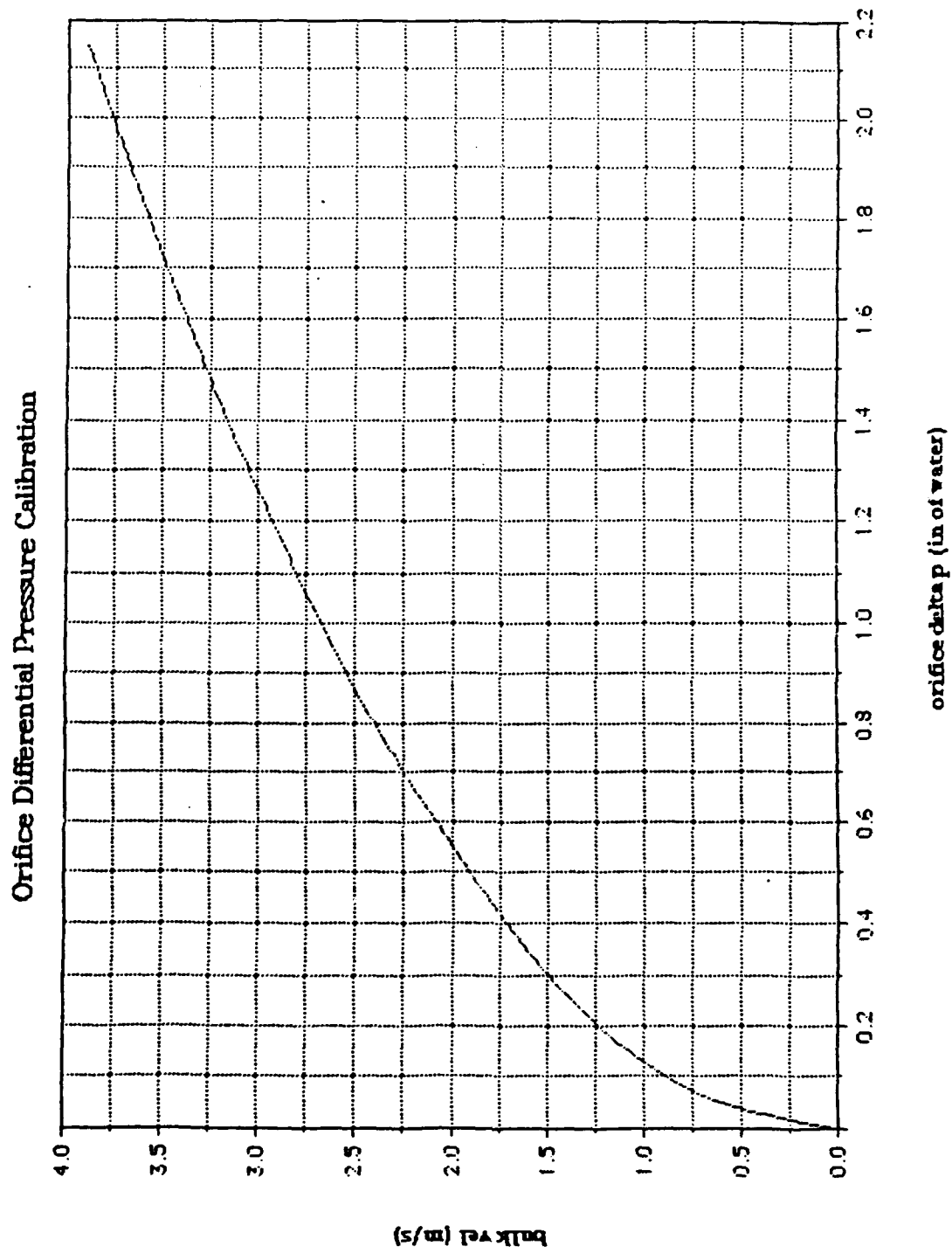


Figure 5. Bulk Velocity vs Orifice Differential Pressure

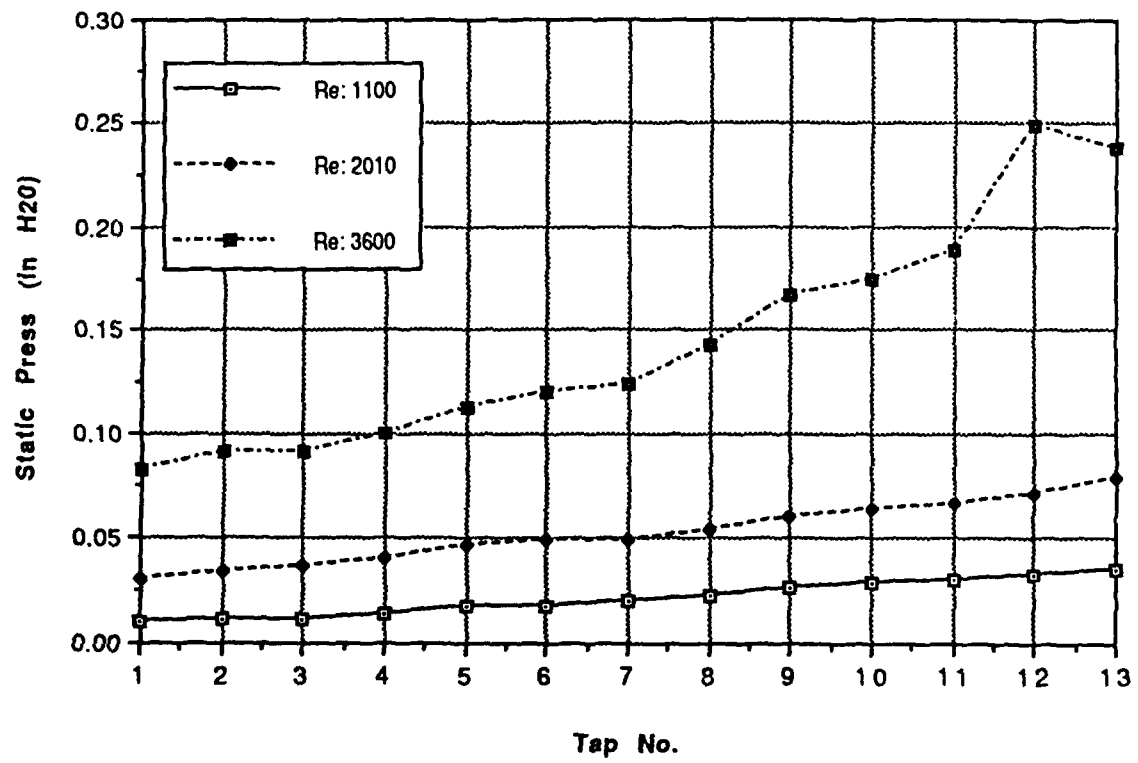


Figure 6. Channel Pressure Distribution

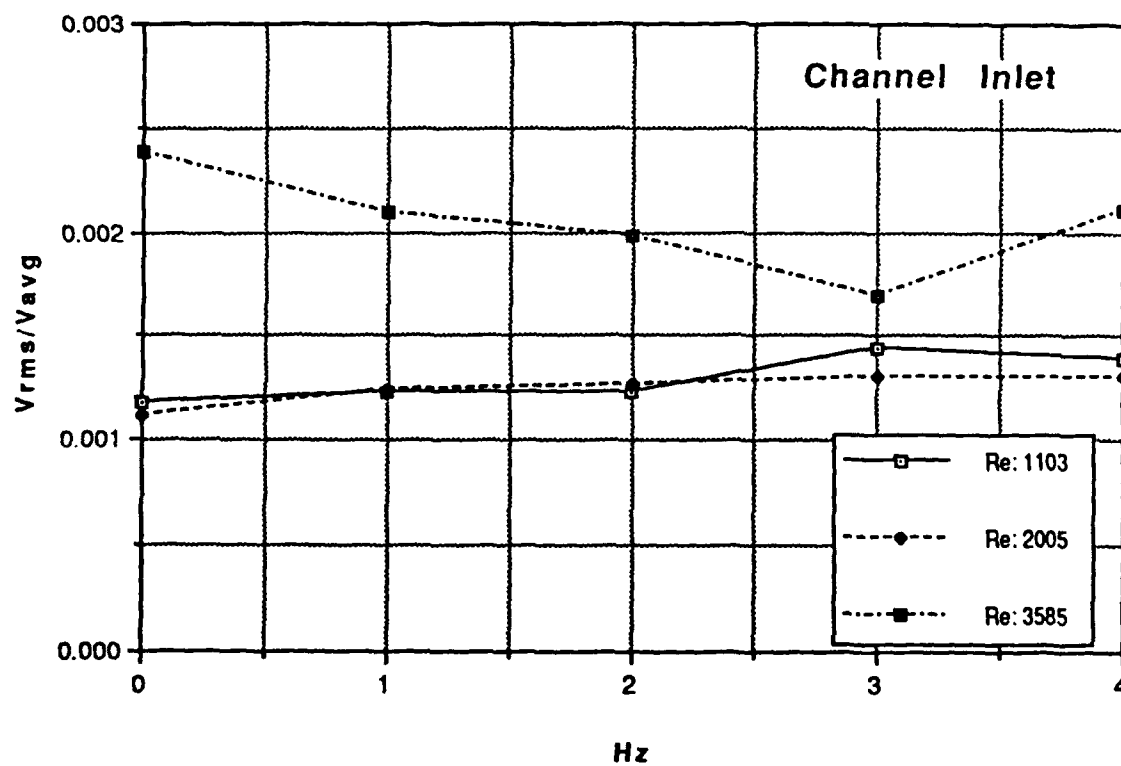


Figure 7. Inlet Turbulence Intensity Conditions

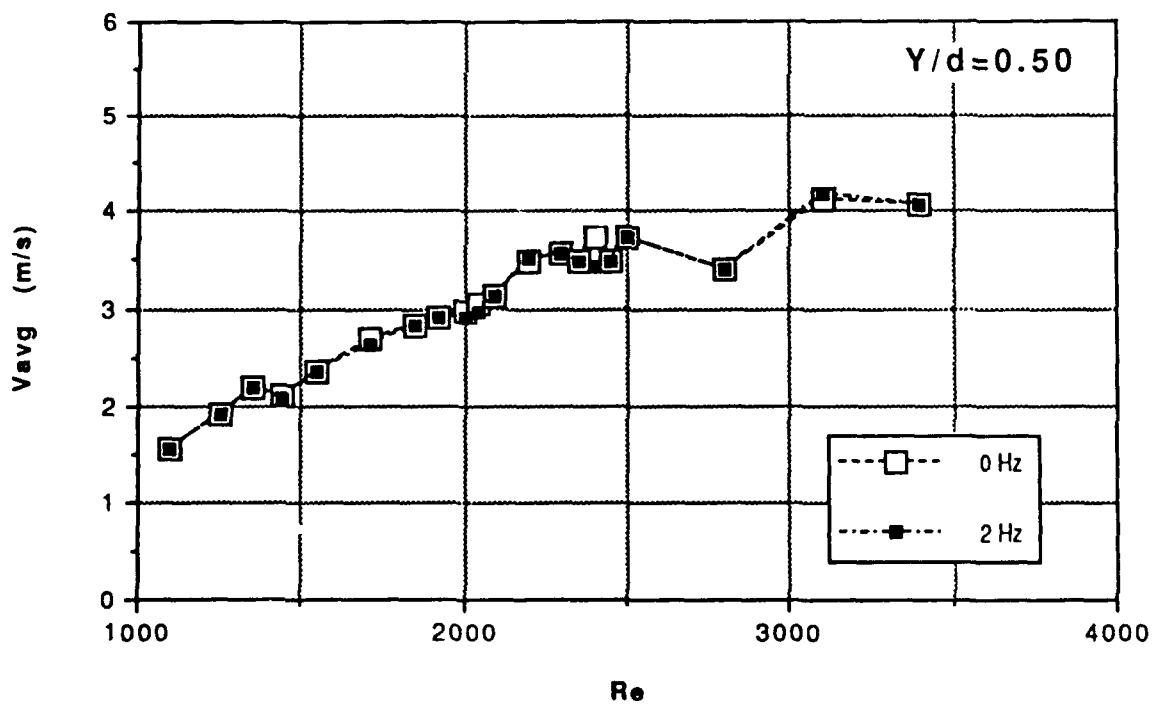
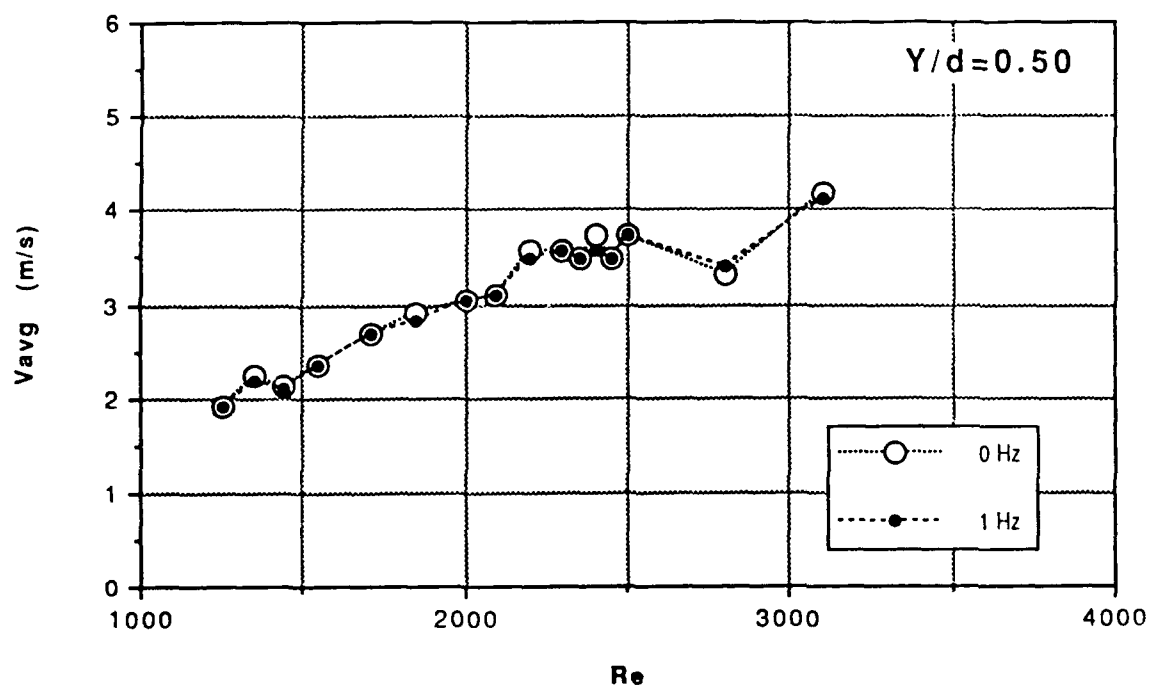


Figure 8. V_{avg} vs Re ($Y/d = 0.50$)

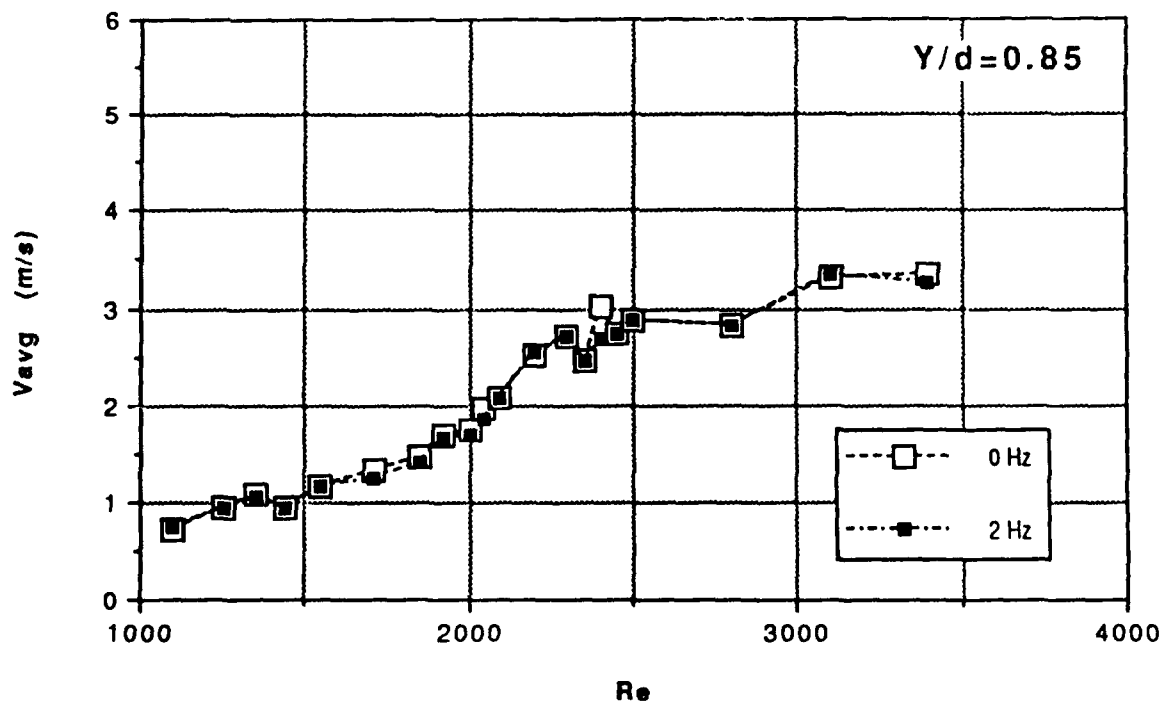
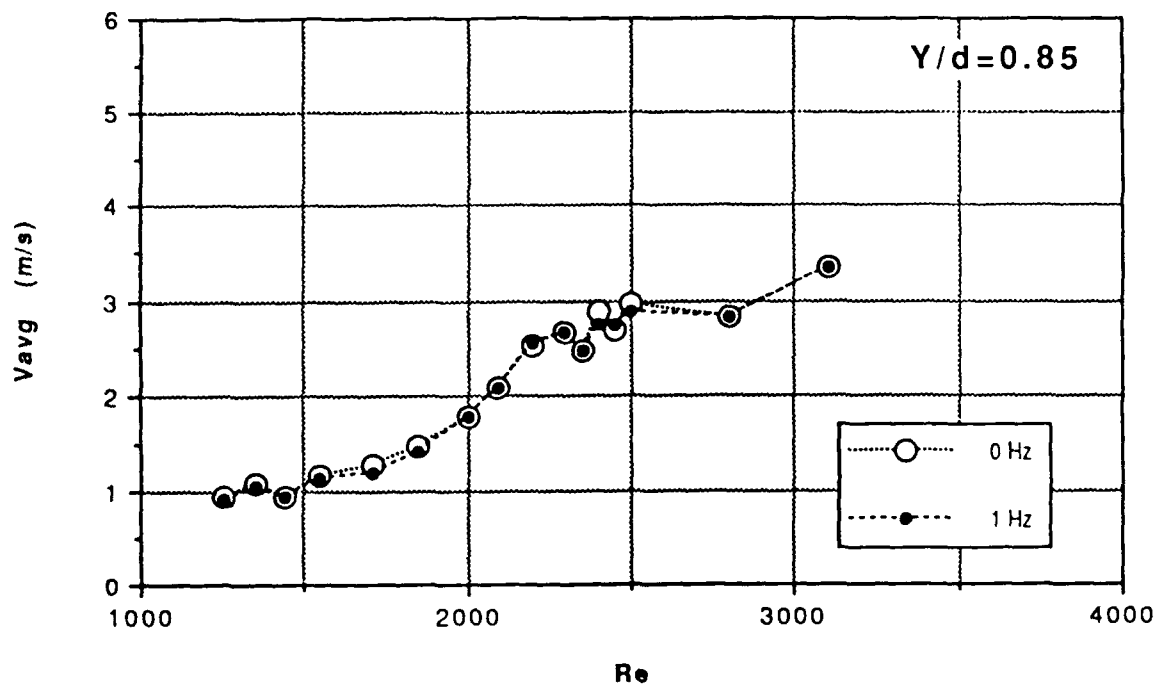


Figure 9. V_{avg} vs Re ($Y/d = 0.85$)

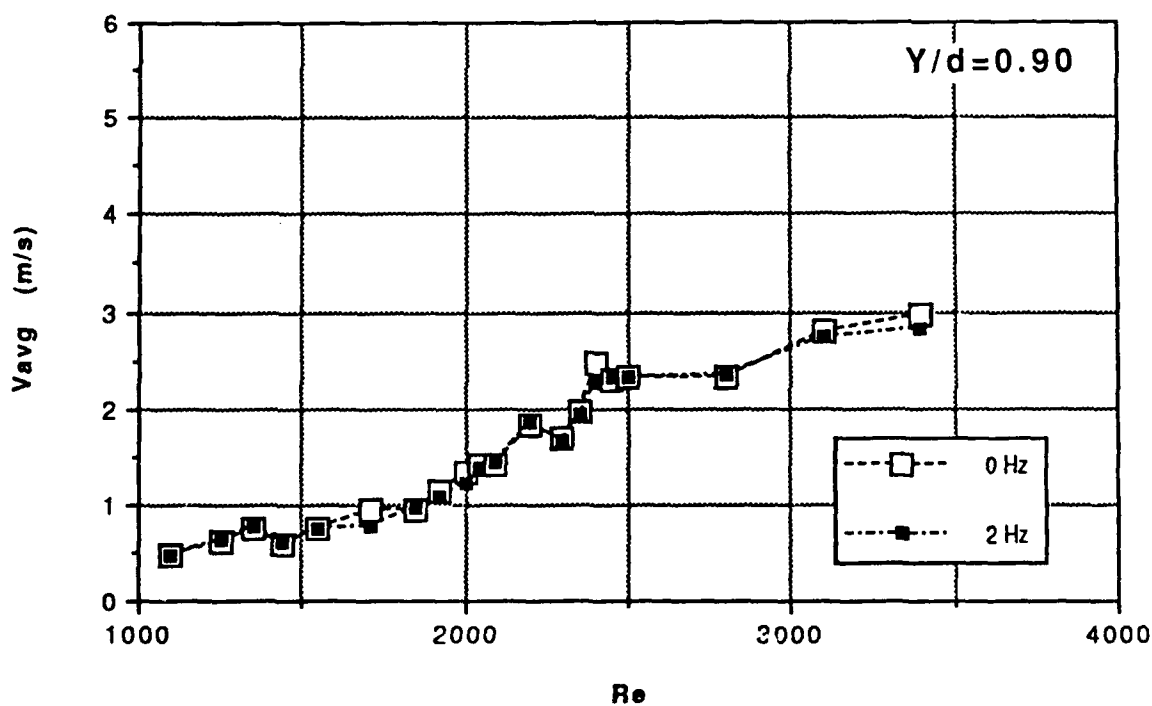
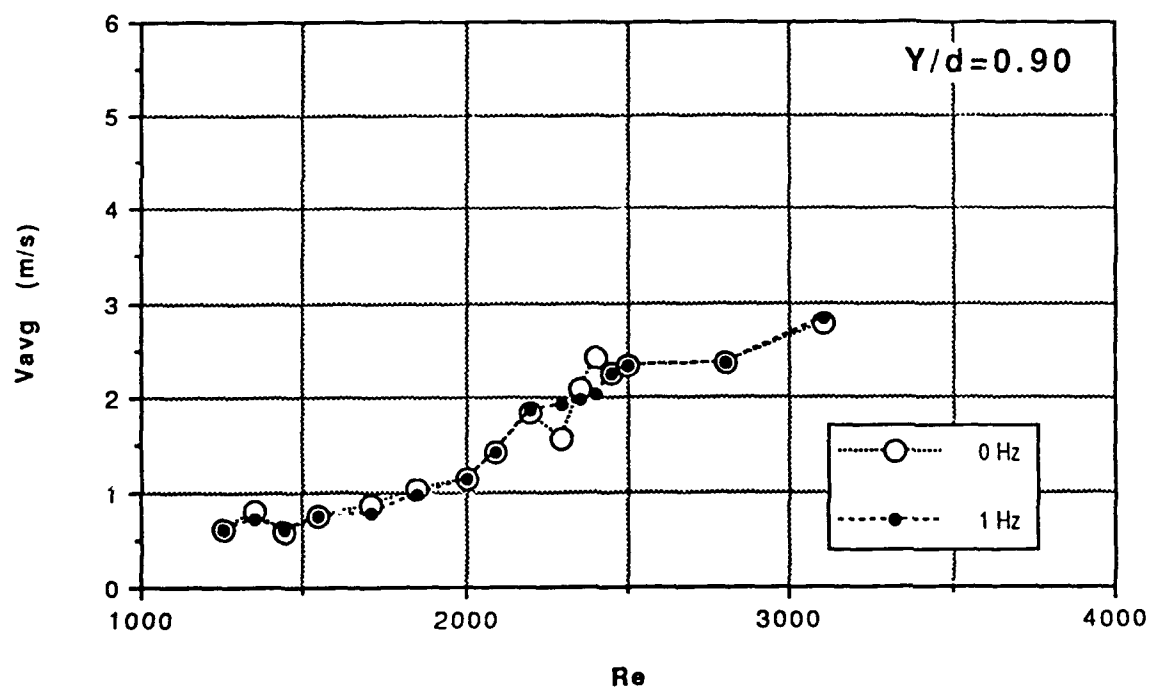


Figure 10. Vavg vs Re (Y/d = 0.90)

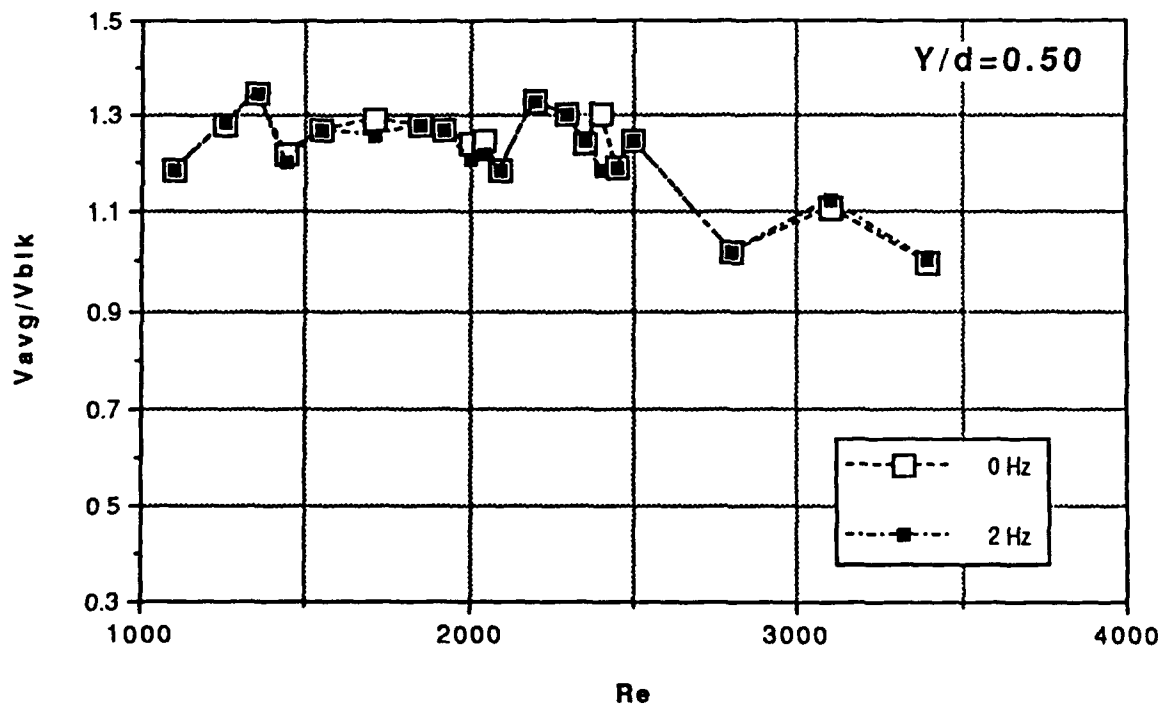
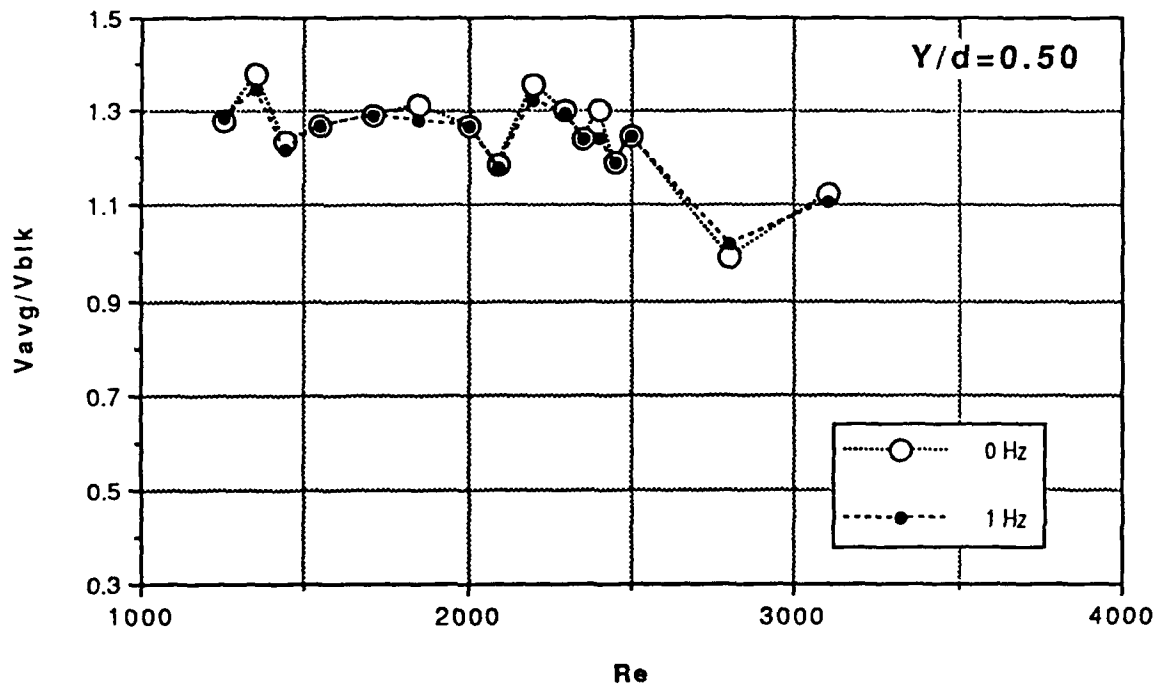


Figure 11. V_{avg}/V_{blk} vs Re ($Y/d = 0.50$)

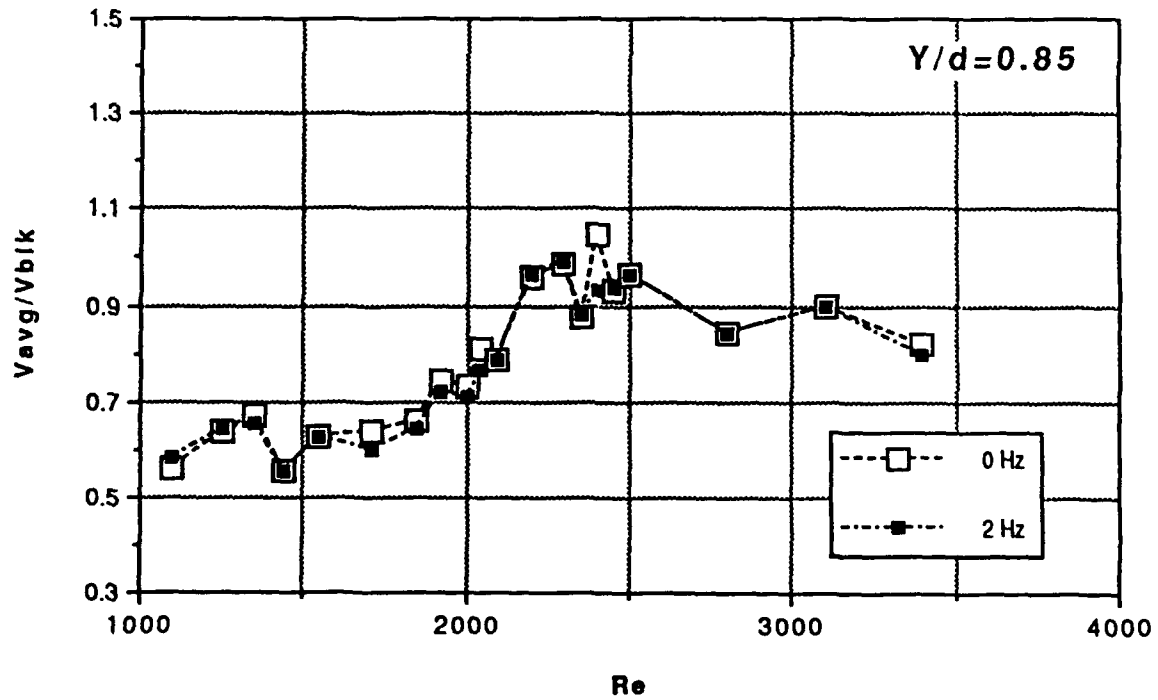
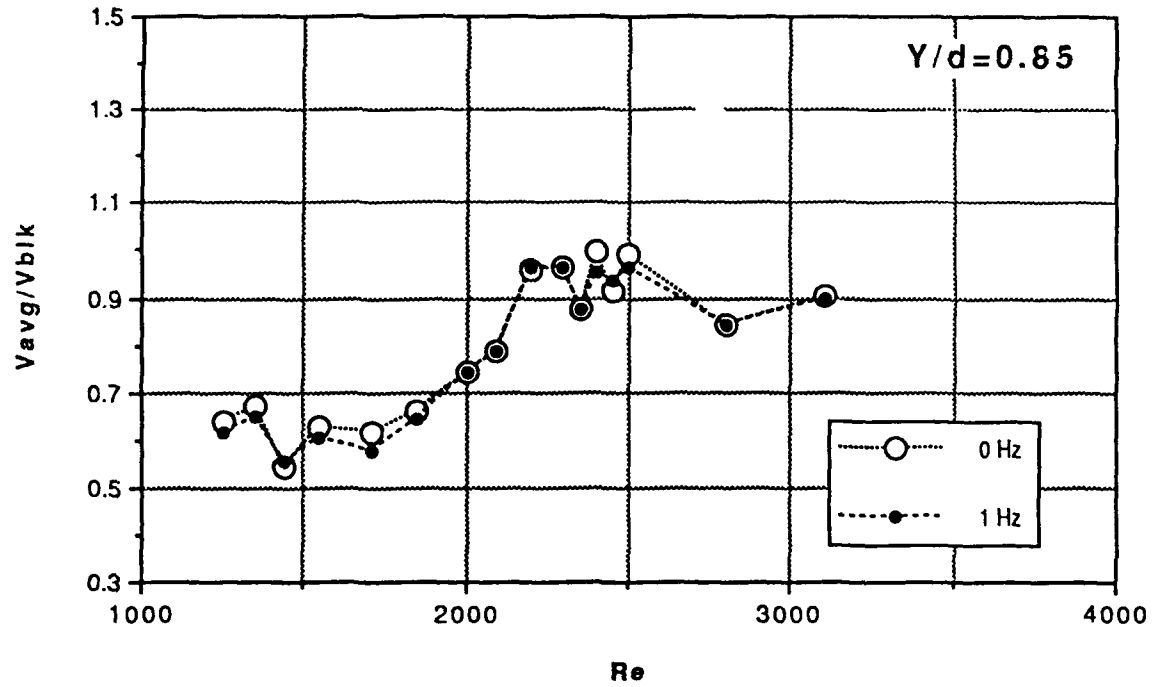


Figure 12. V_{avg}/V_{blk} vs Re ($Y/d = 0.85$)

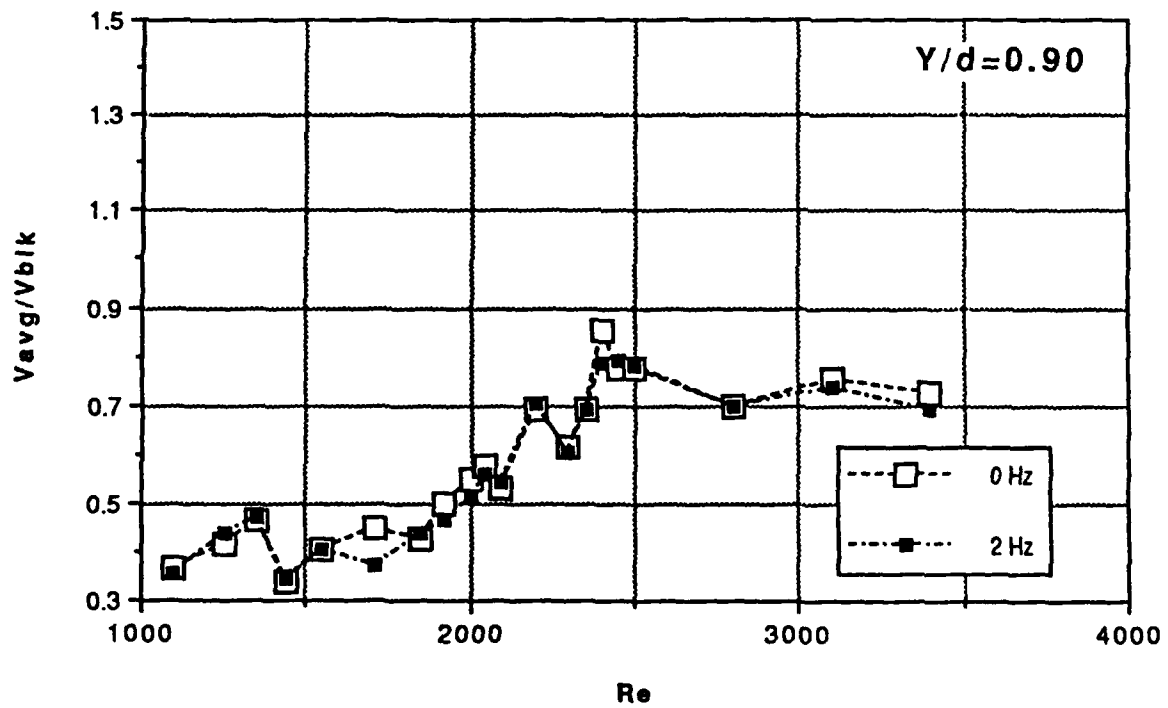
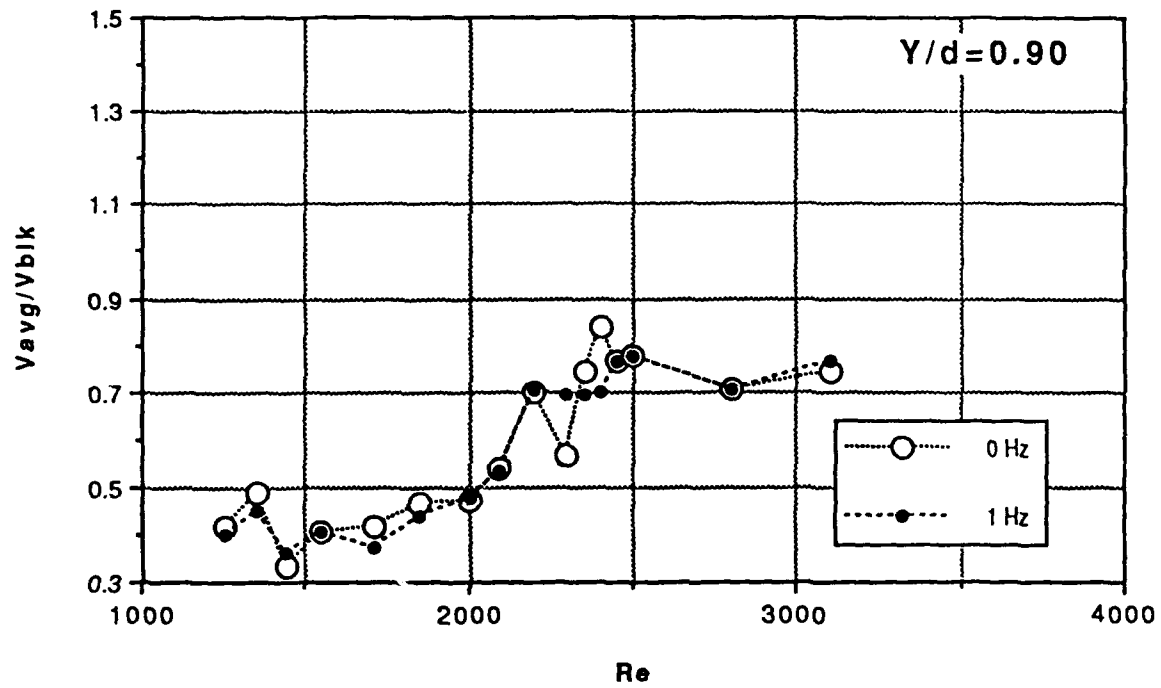


Figure 13. V_{avg}/V_{blk} vs Re ($Y/d = 0.90$)

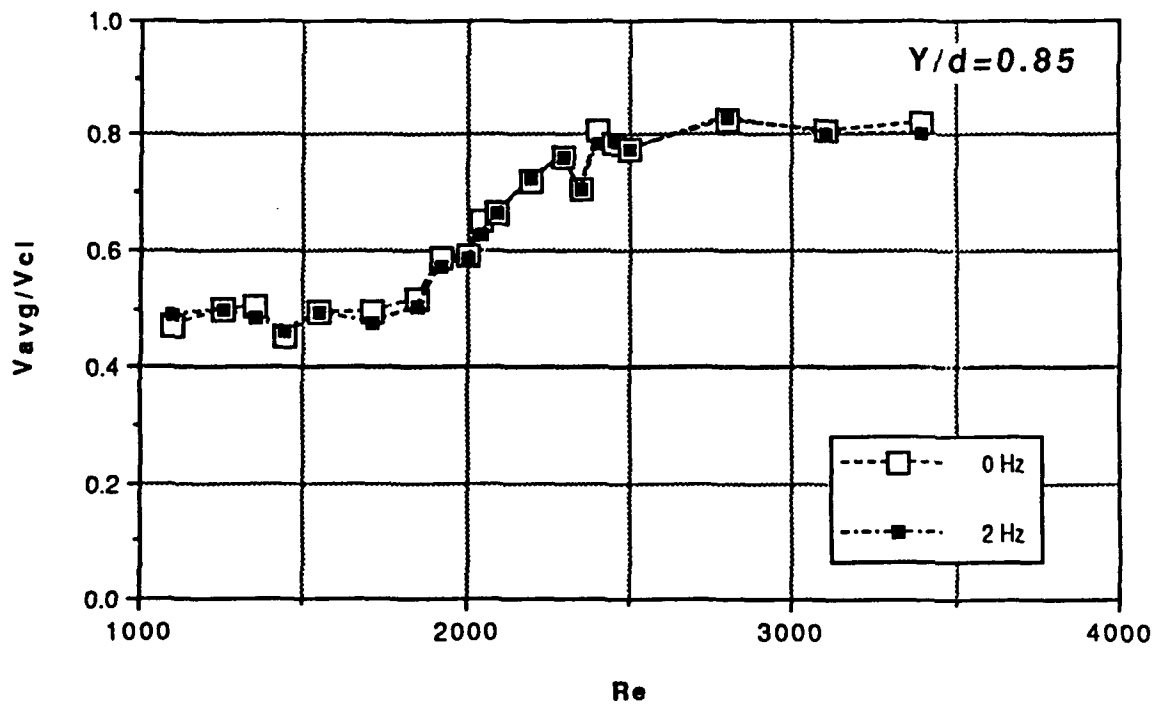
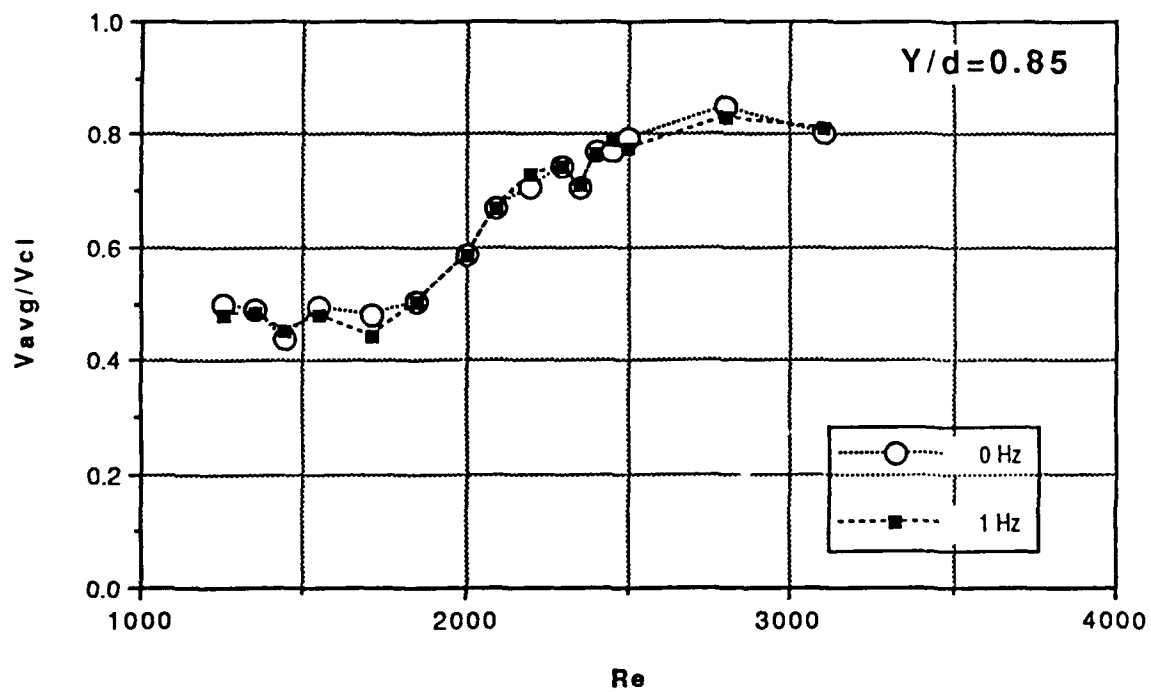


Figure 14. V_{avg}/V_{cl} vs Re ($Y/d = 0.85$)

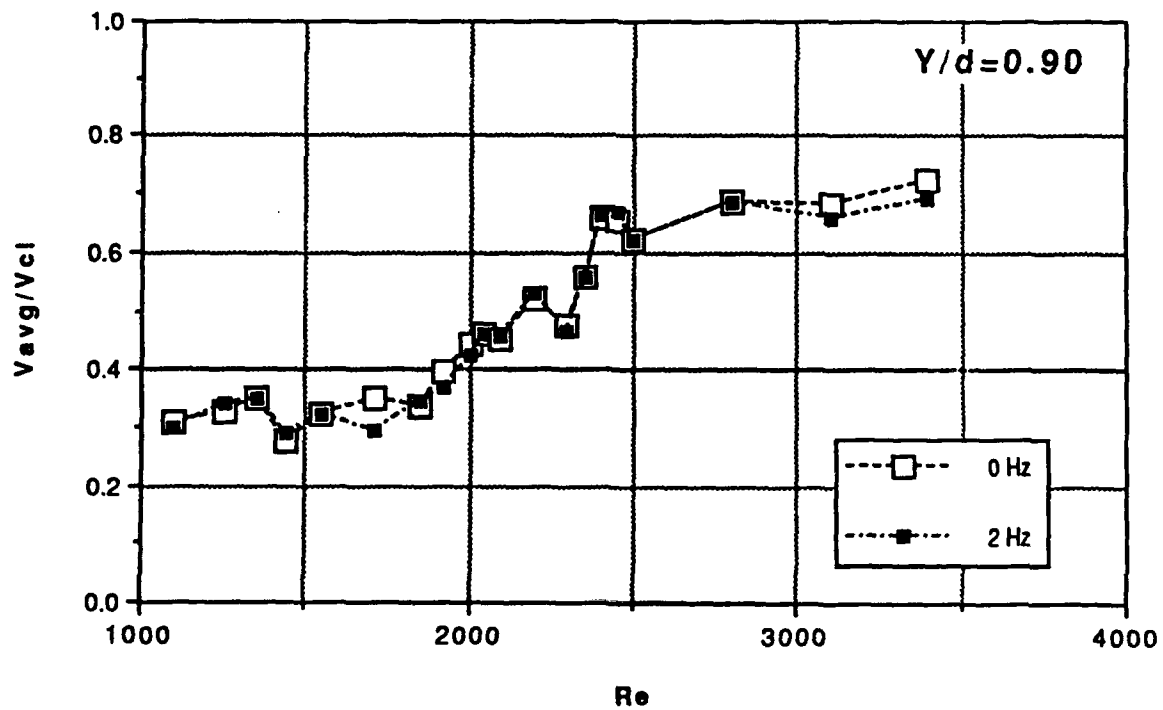
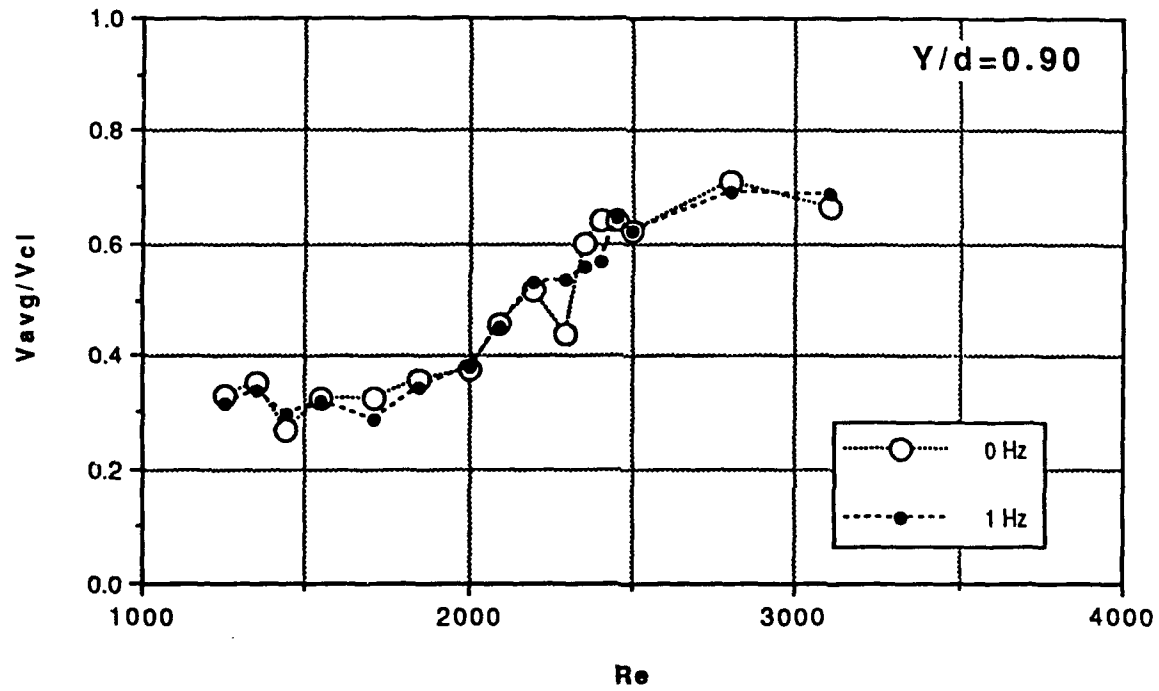


Figure 15. V_{avg}/V_{cl} vs Re ($Y/d=0.90$)

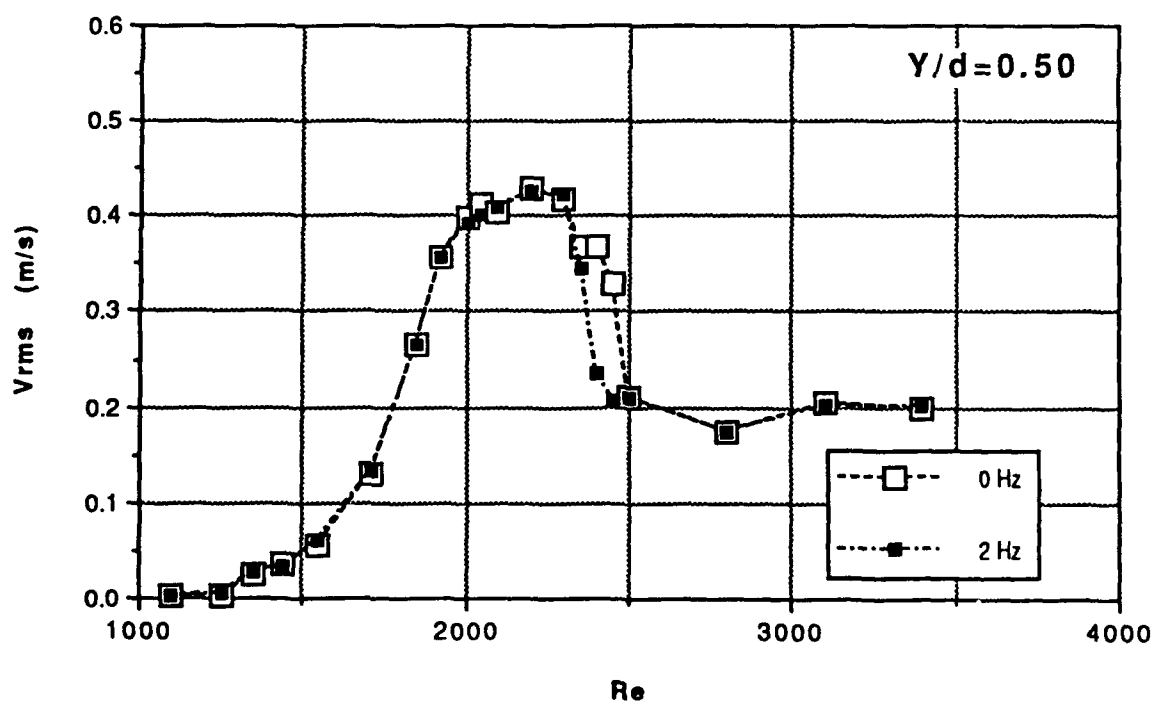
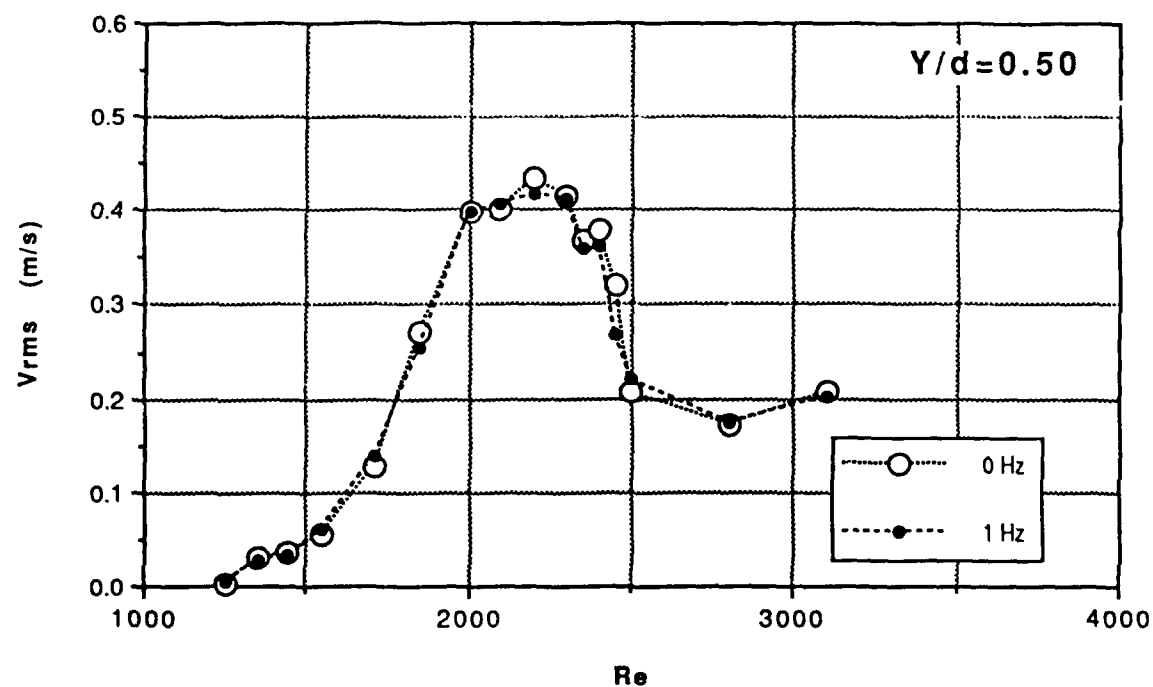


Figure 16. V_{rms} vs Re ($Y/d = 0.50$)

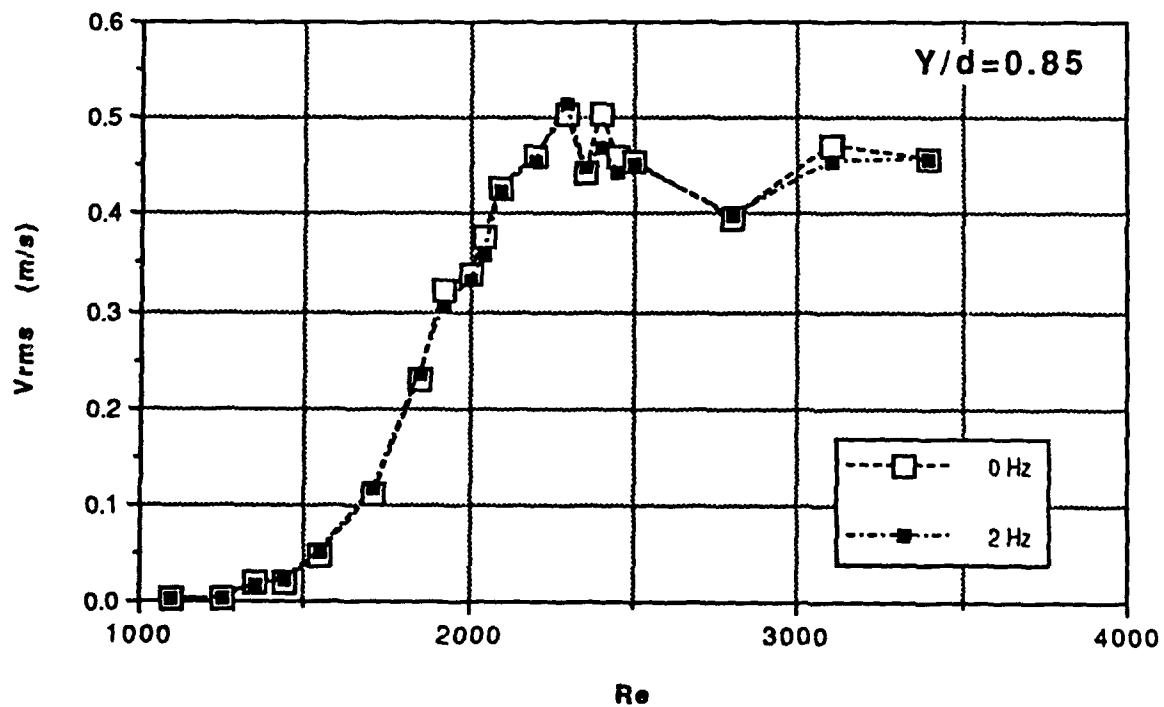
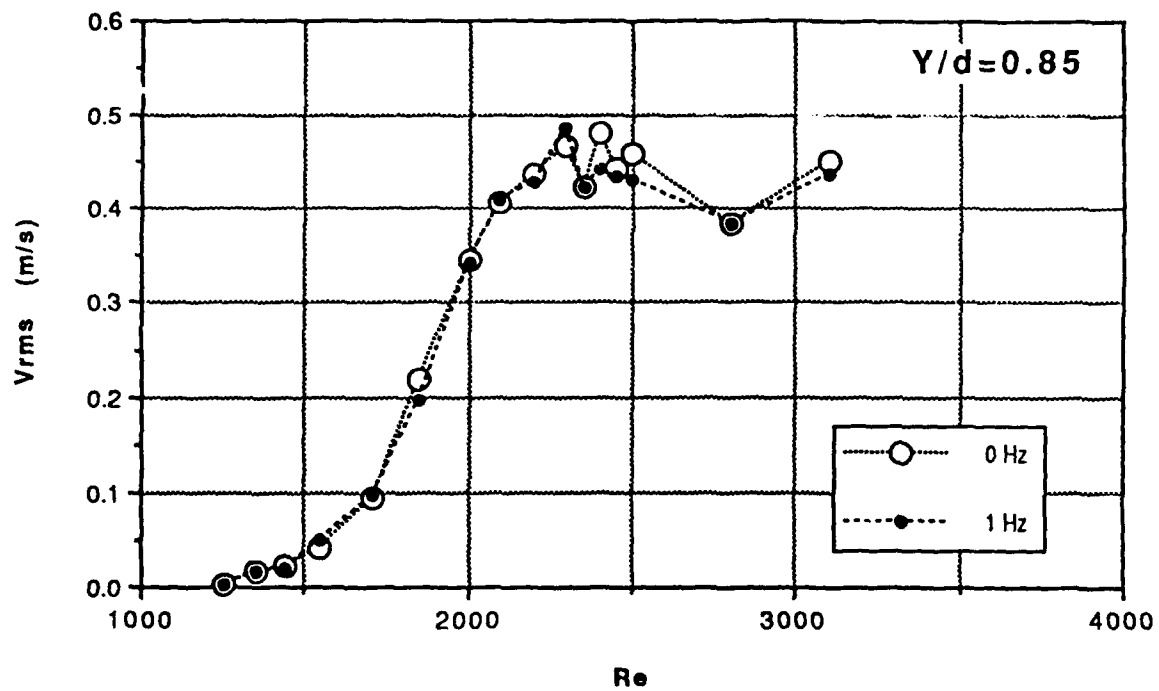


Figure 17. V_{rms} vs Re ($Y/d = 0.85$)

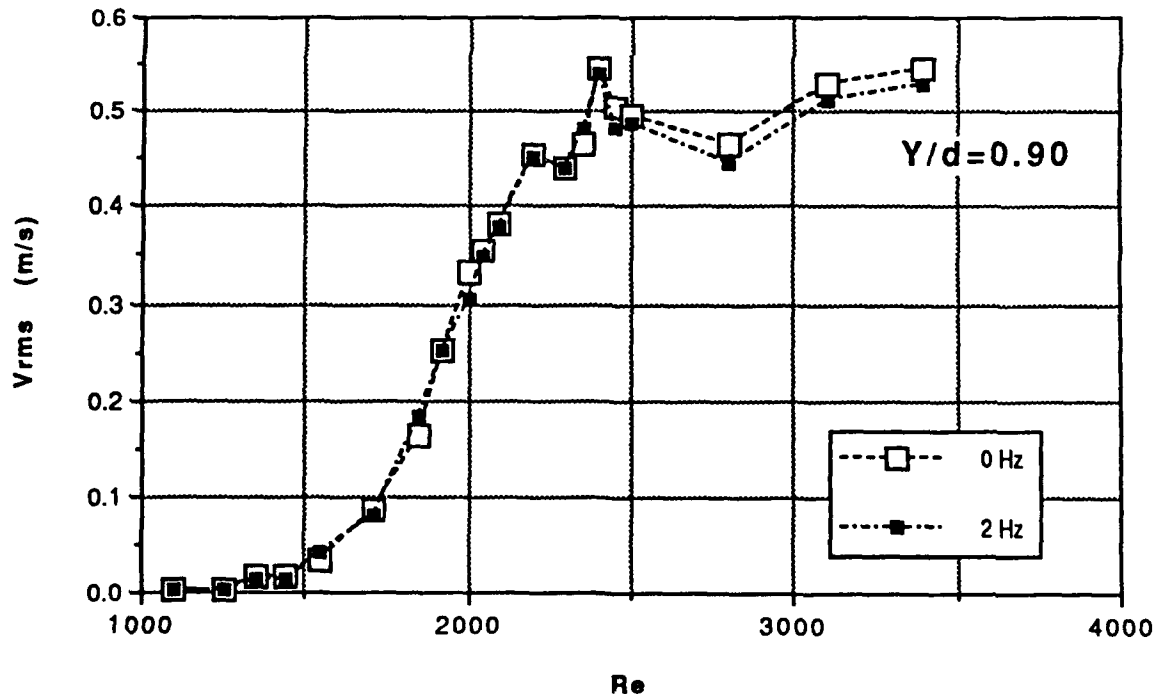
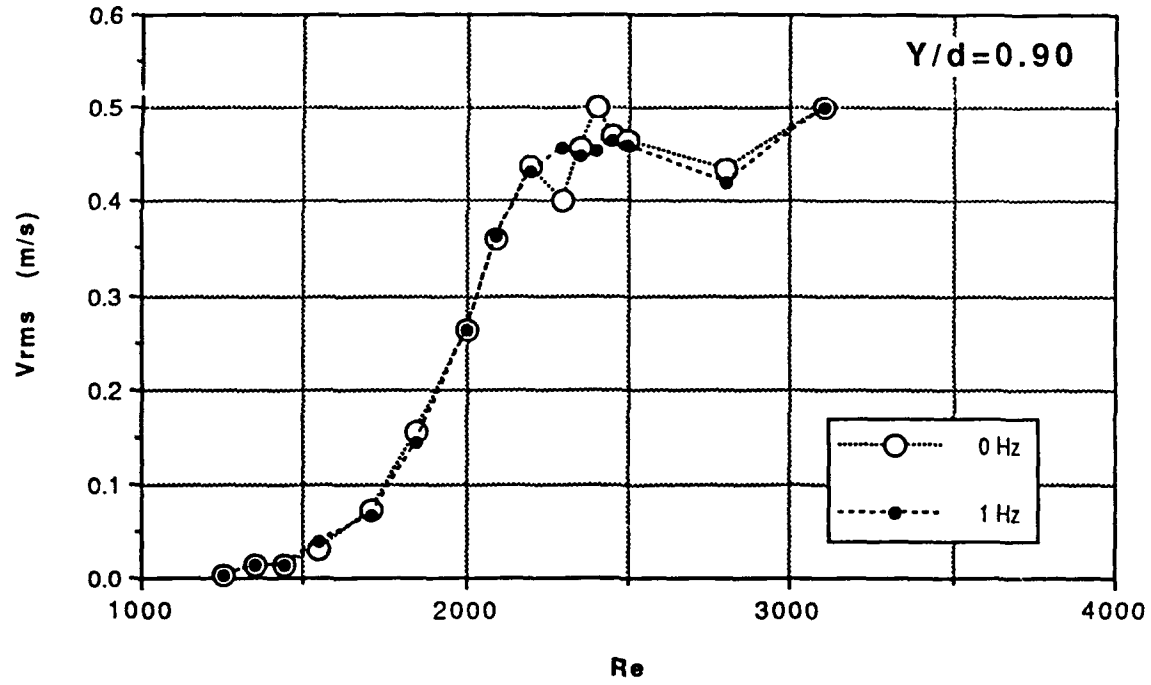


Figure 18. V_{rms} vs Re ($Y/d=0.90$)

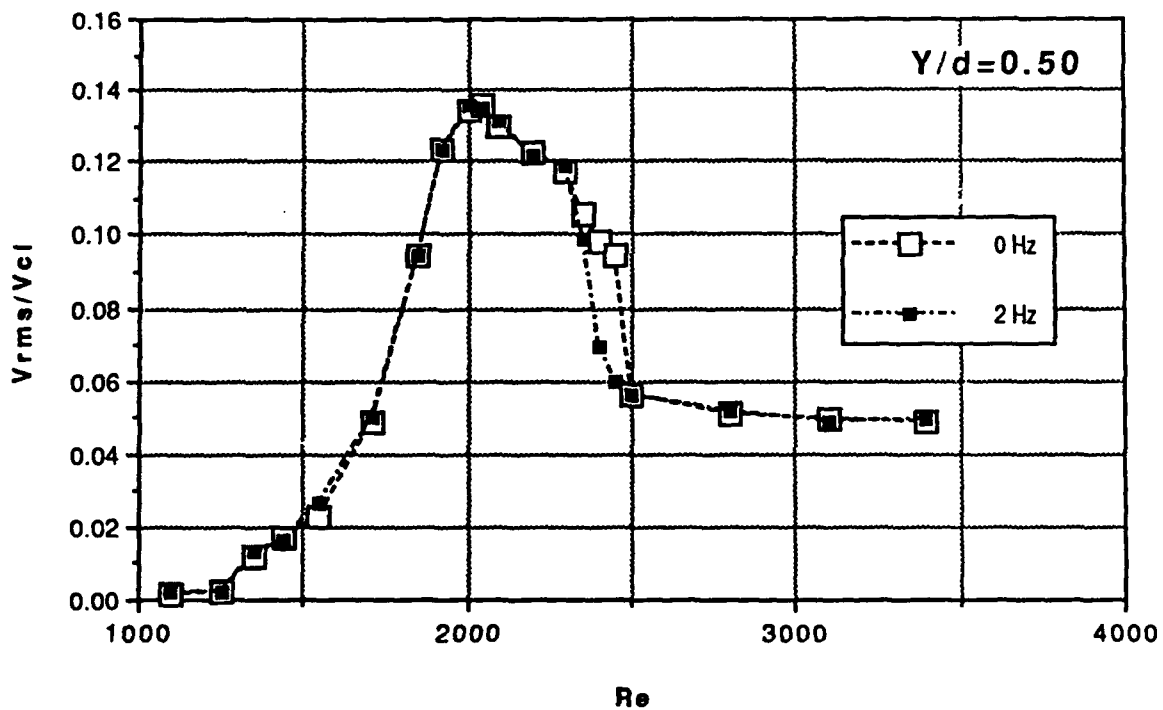
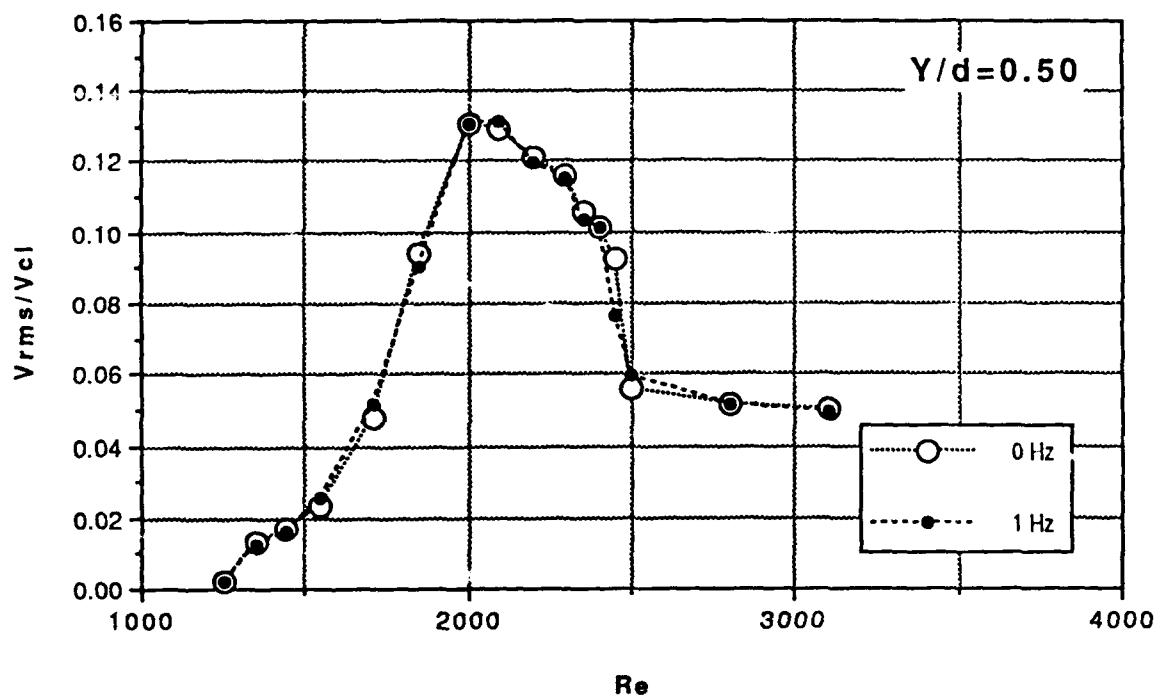


Figure 19. V_{rms}/V_{cl} vs Re ($Y/d=0.50$)

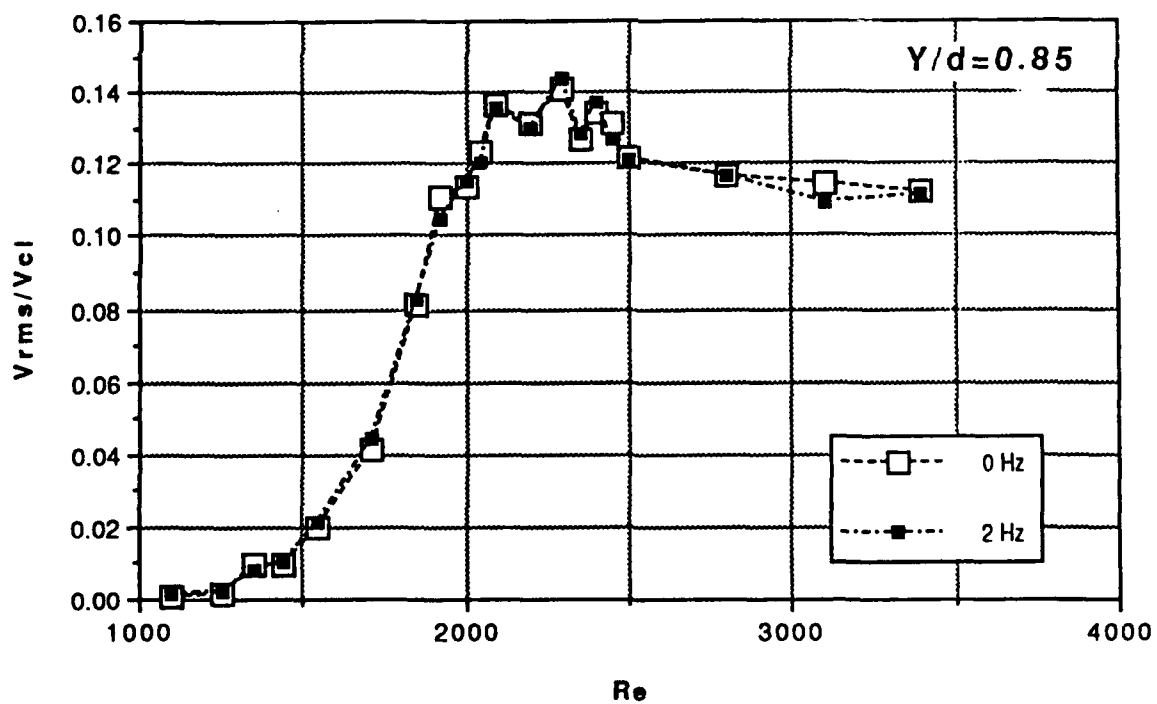
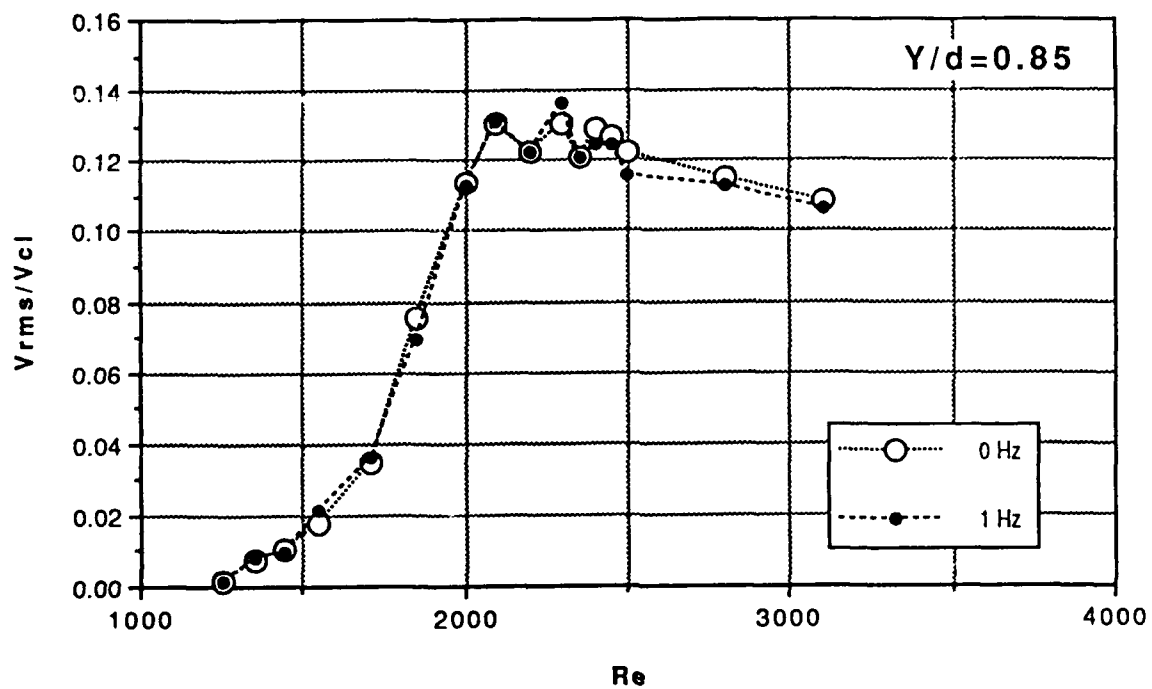


Figure 20. V_{rms}/V_{cl} vs Re ($Y/d=0.85$)

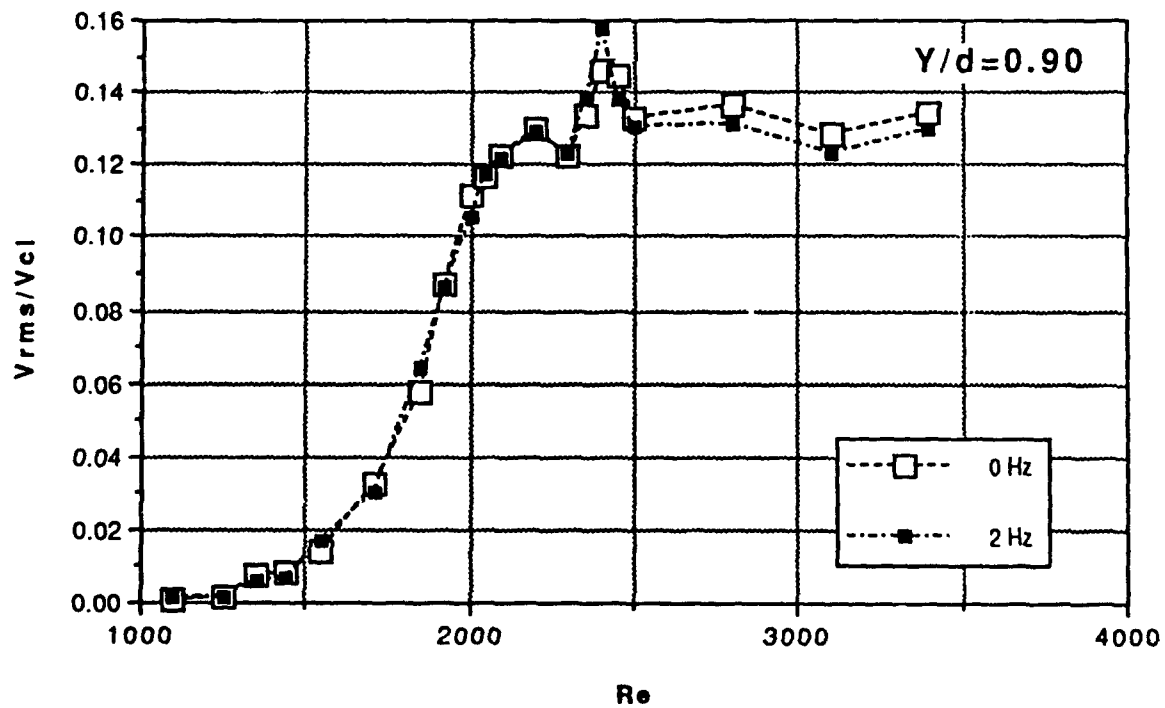
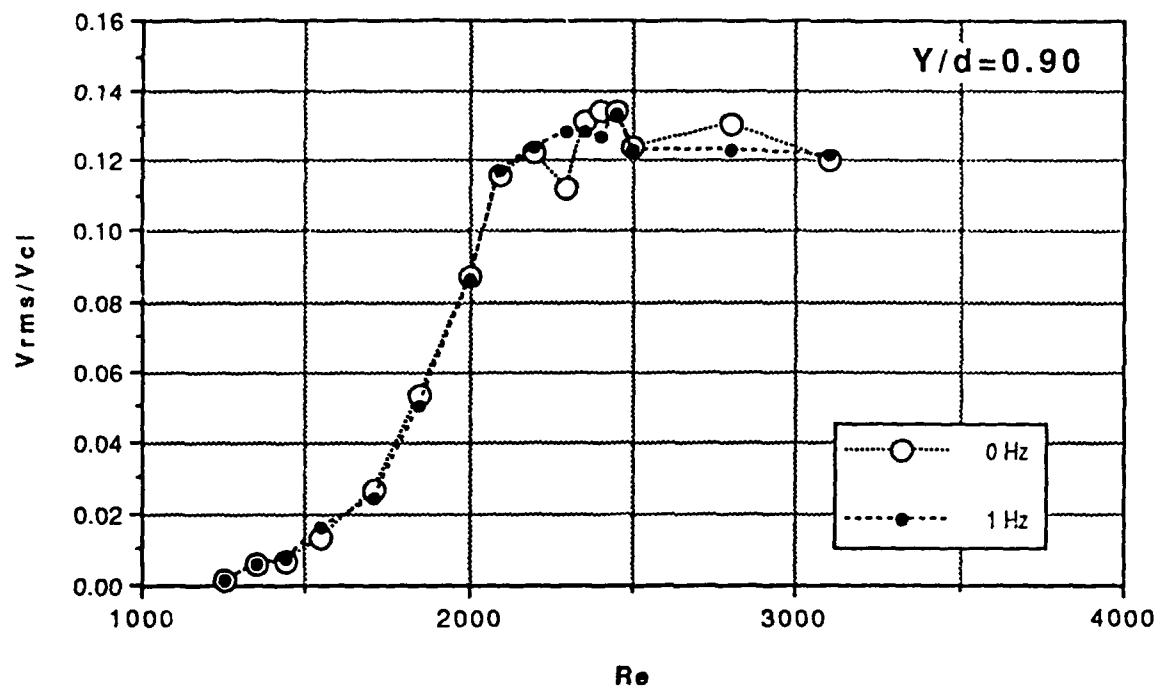


Figure 21. V_{rms}/V_{cl} vs Re ($Y/d = 0.90$)

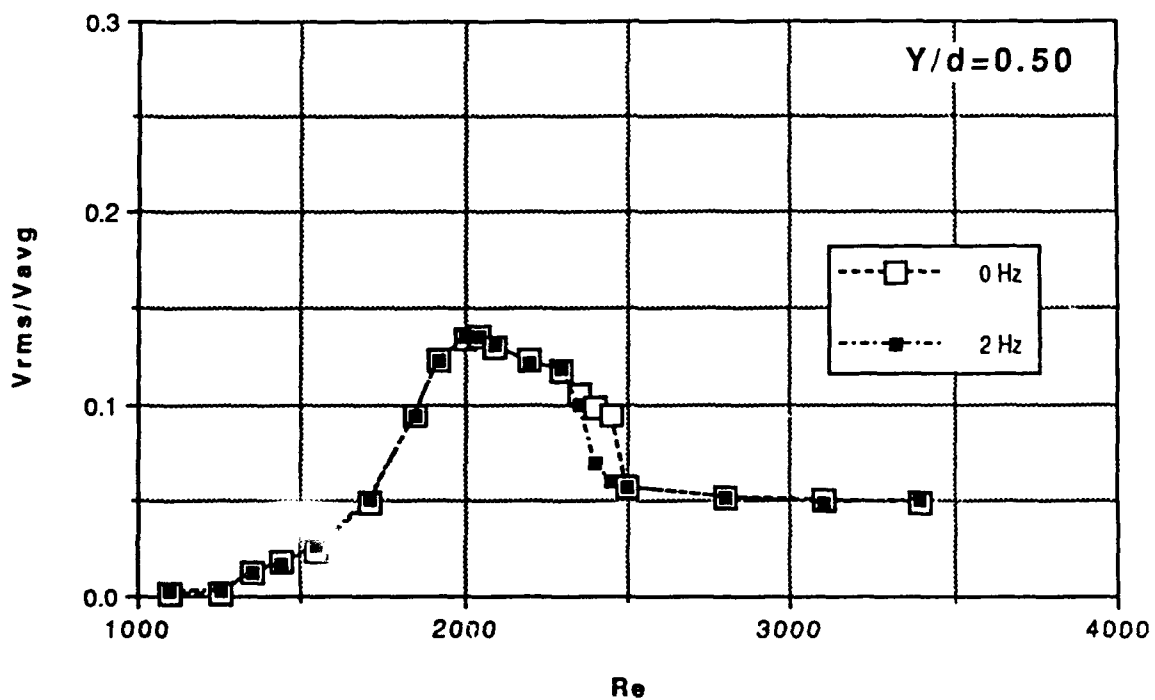
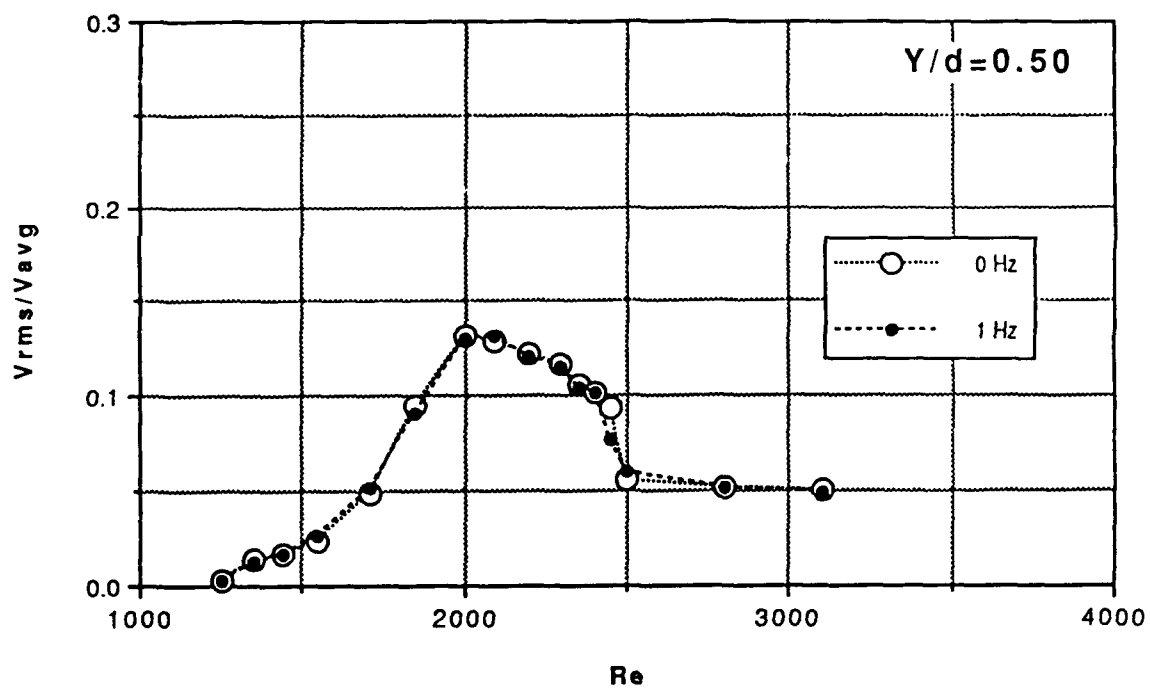


Figure 22. V_{rms}/V_{avg} vs Re ($Y/d = 0.50$)

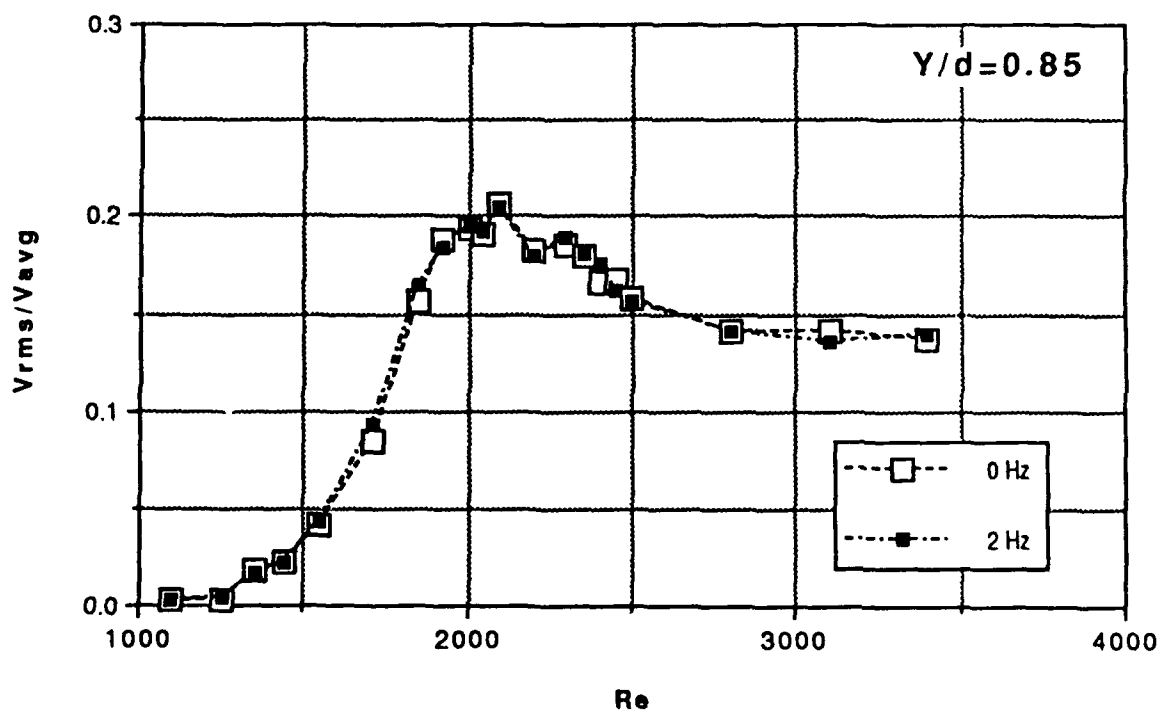
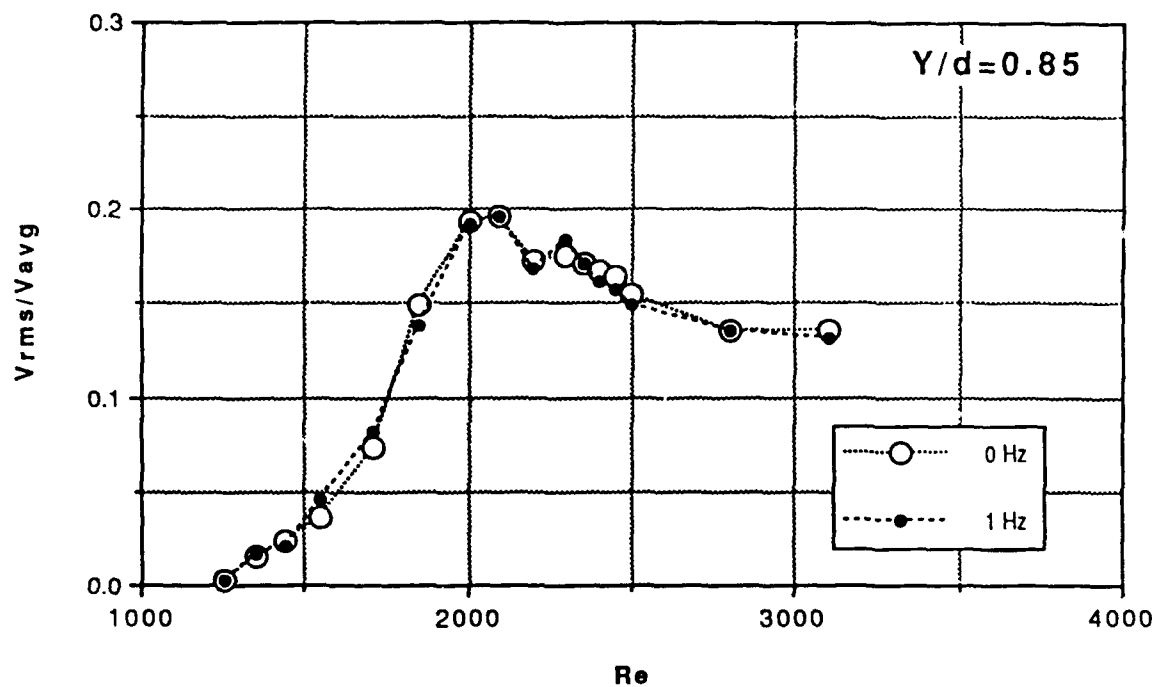


Figure 23. V_{rms}/V_{avg} vs Re ($Y/d = 0.85$)

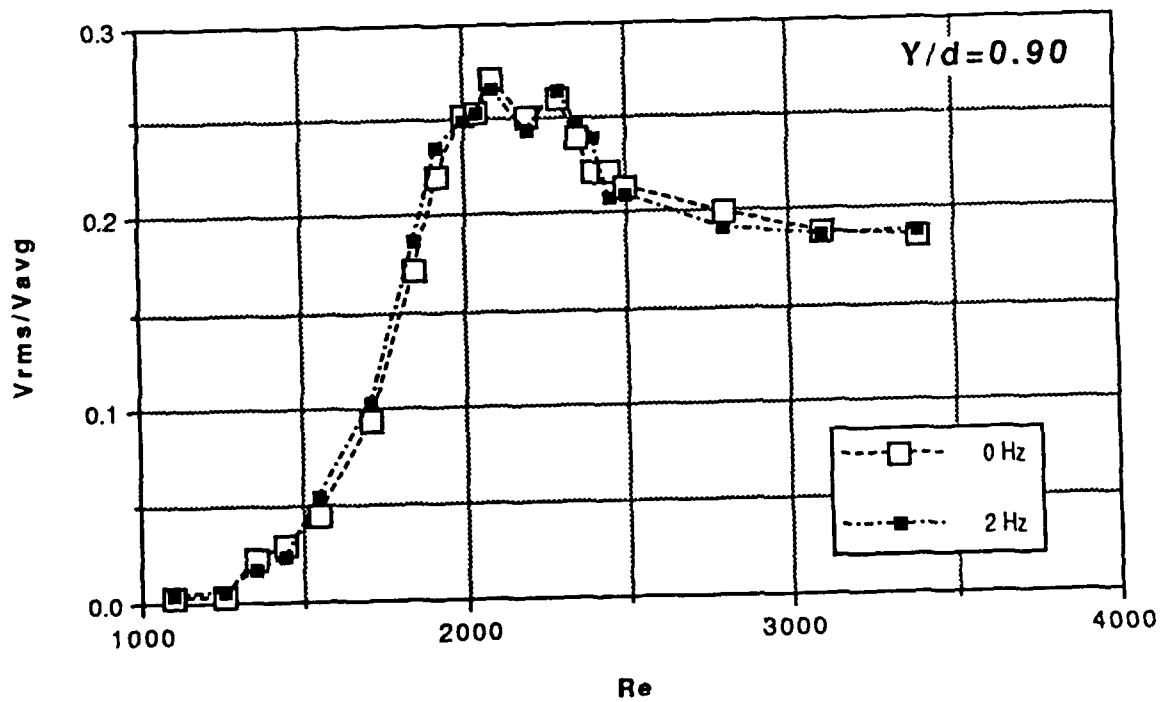
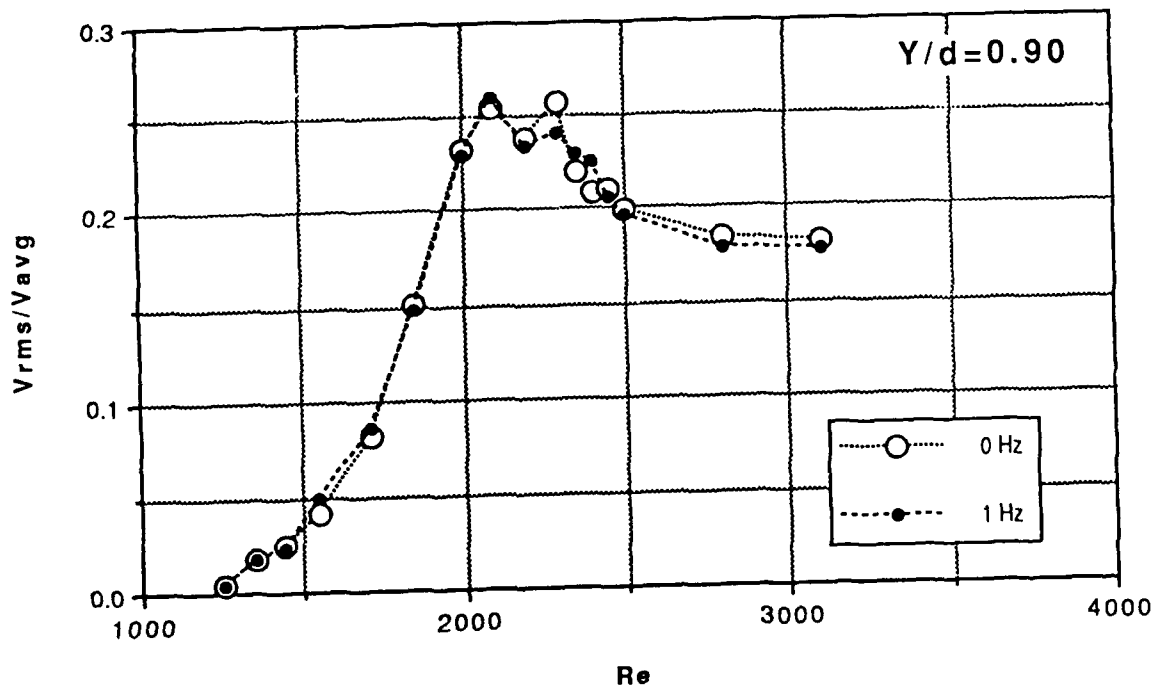


Figure 24. V_{rms}/V_{avg} vs Re ($Y/d = 0.90$)

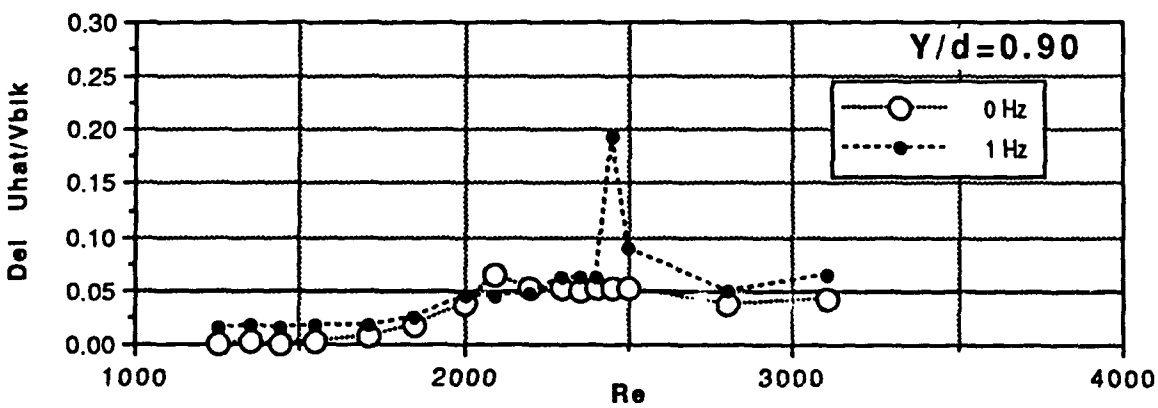
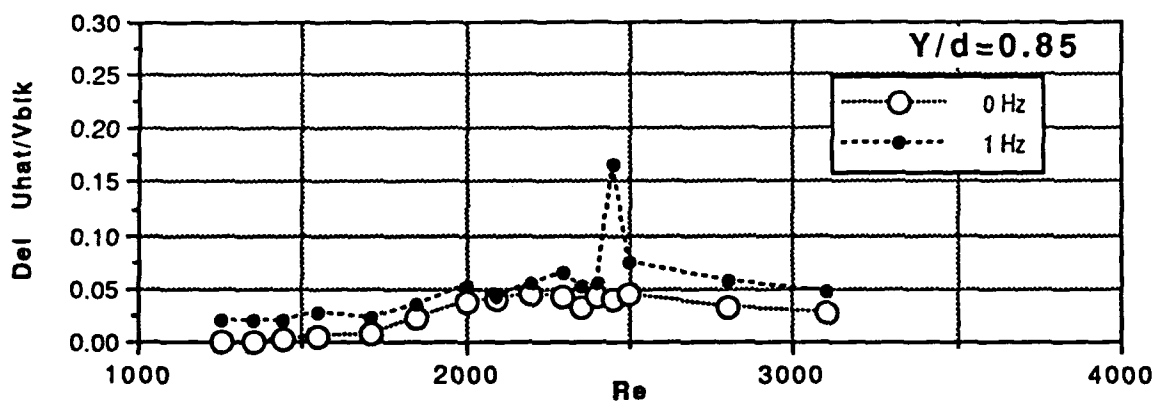
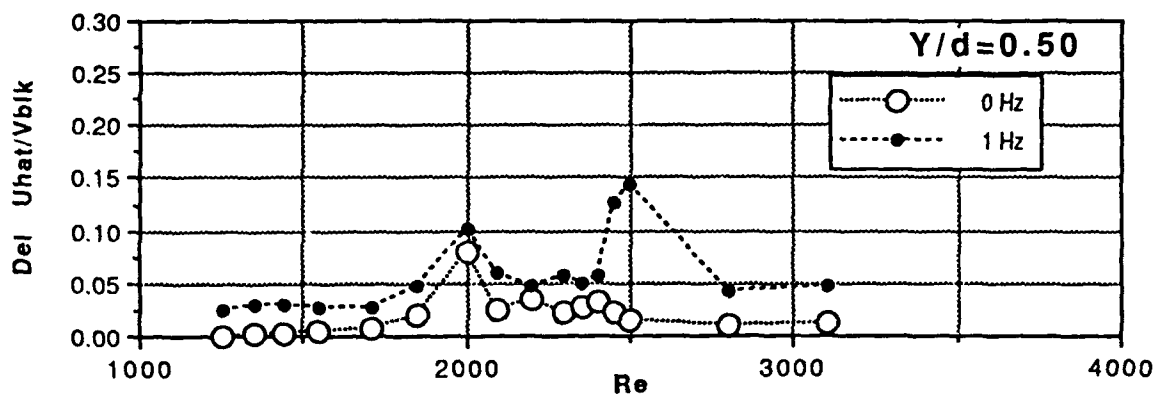


Figure 25. Delta $\hat{U}hat/V_{blk}$ vs Re (1 Hz)

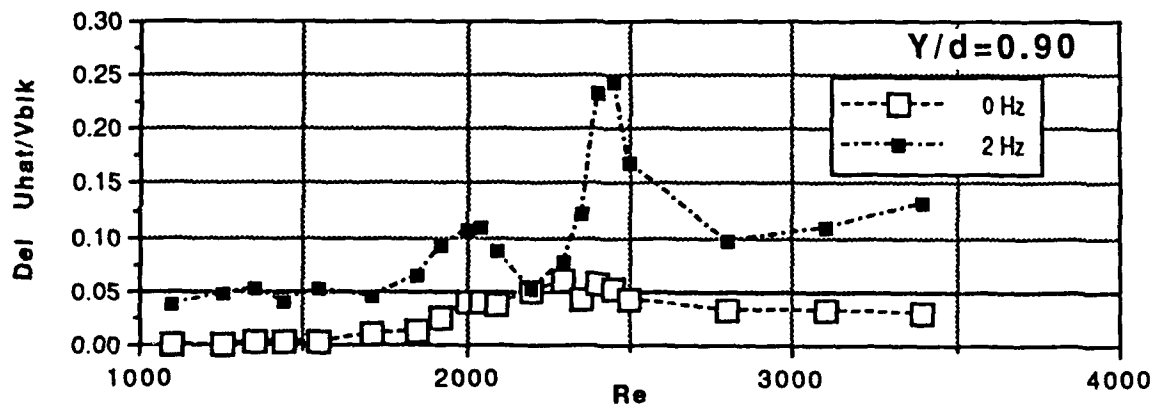
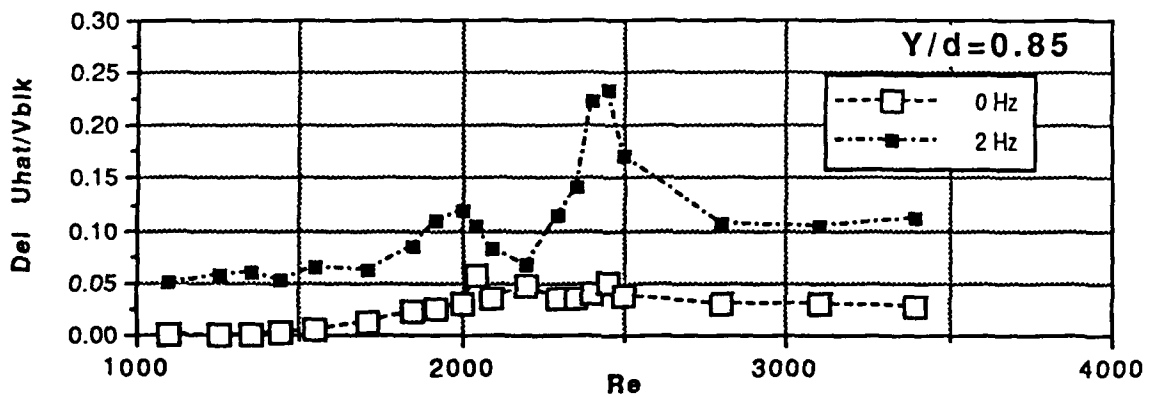
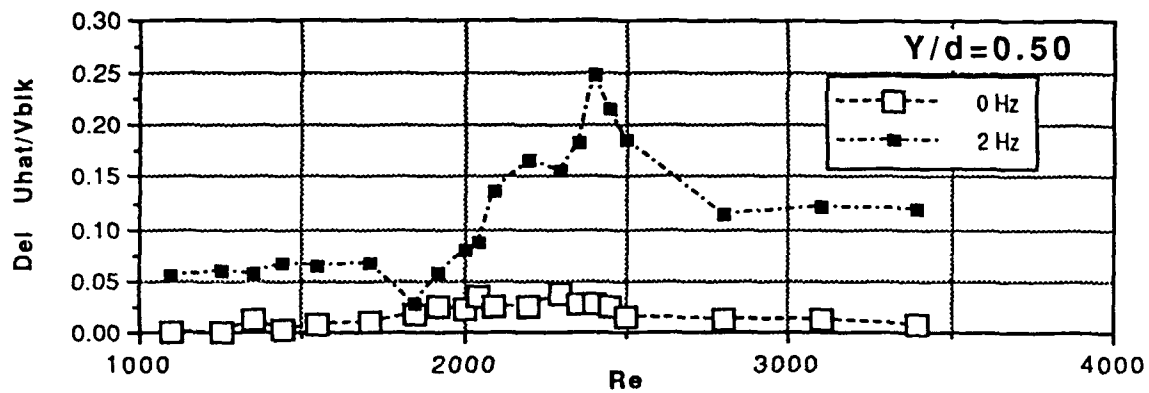


Figure 26. Delta \hat{U}/V_{blk} vs Re (2 Hz)

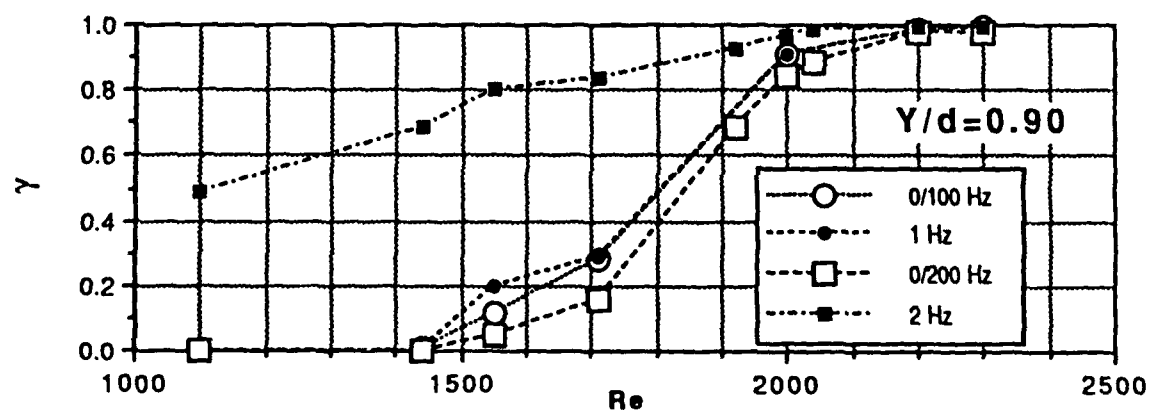
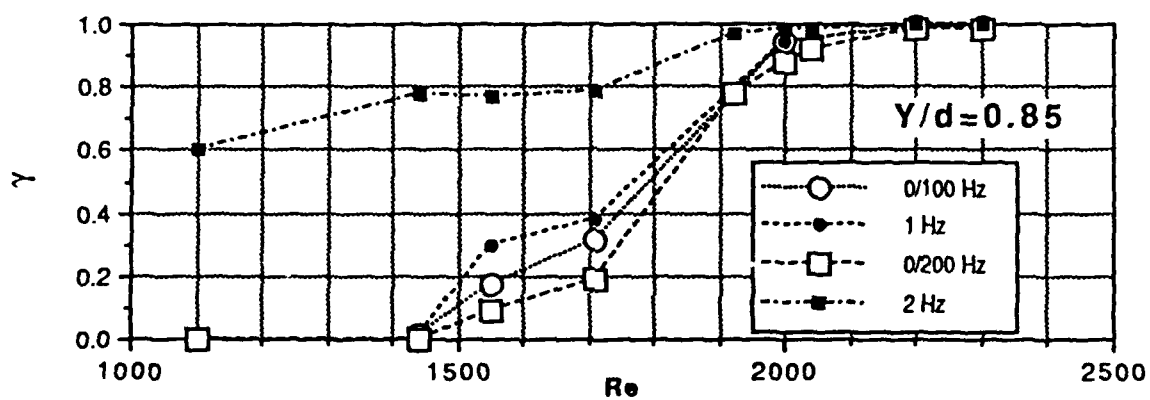
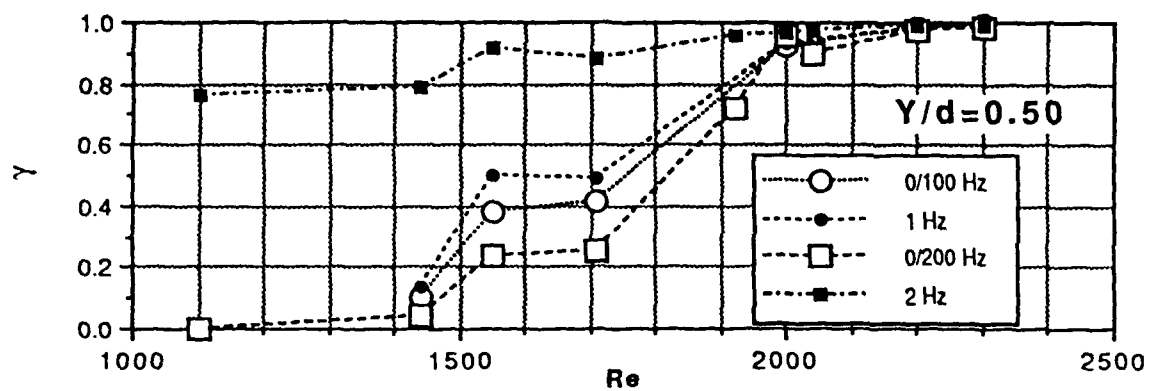


Figure 27. Intermittency vs Re (1 Hz, 2 Hz)

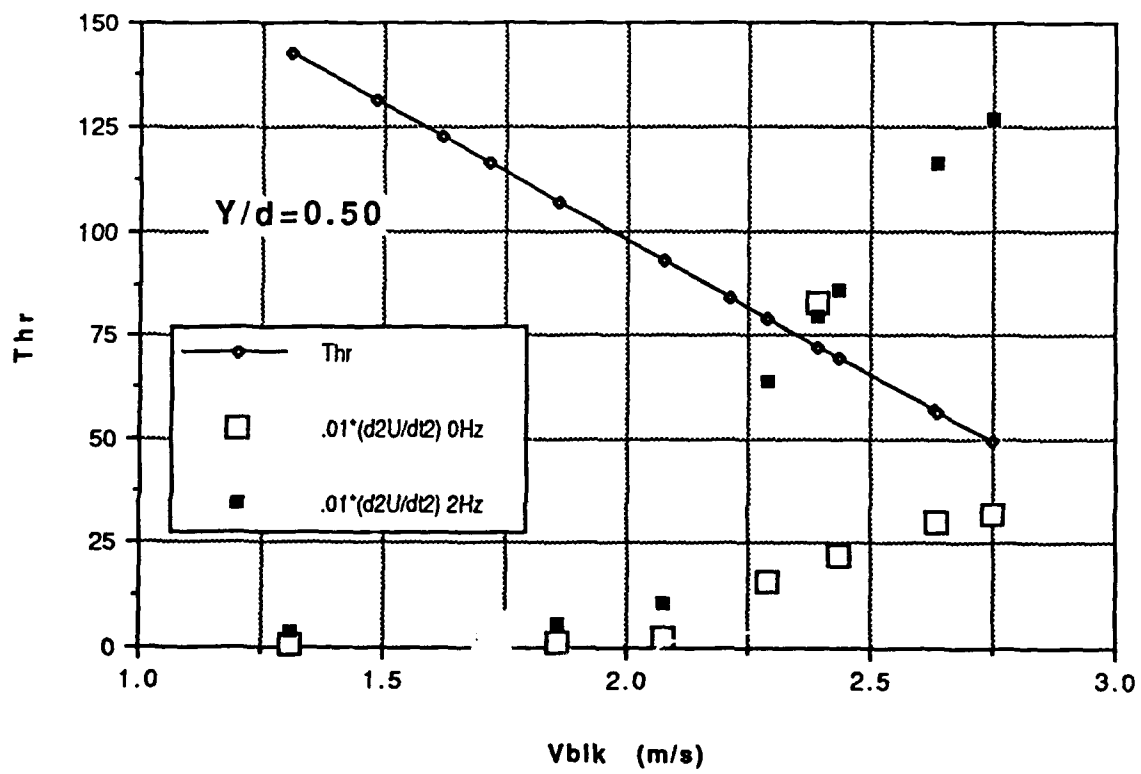


Figure 28. Threshold and Second Time Derivatives vs Vblk ($Y/d = 0.50$)

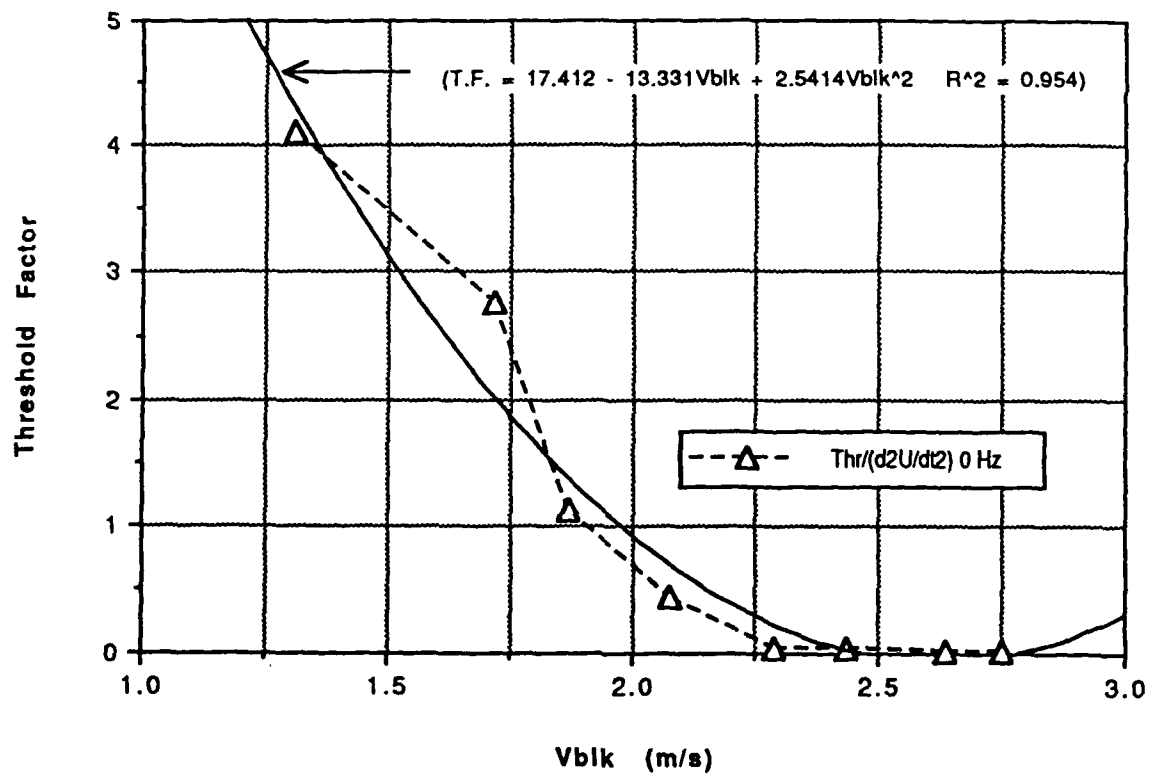


Figure 29. Threshold Factor vs Vblk

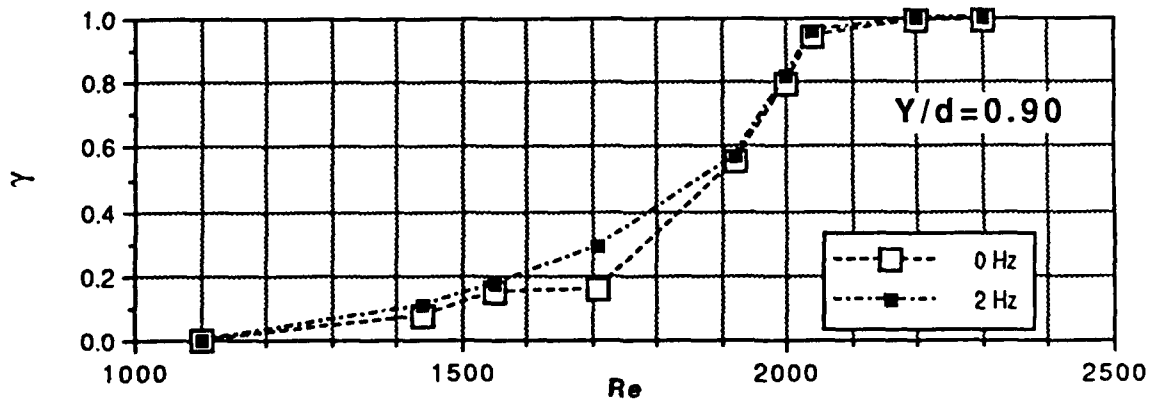
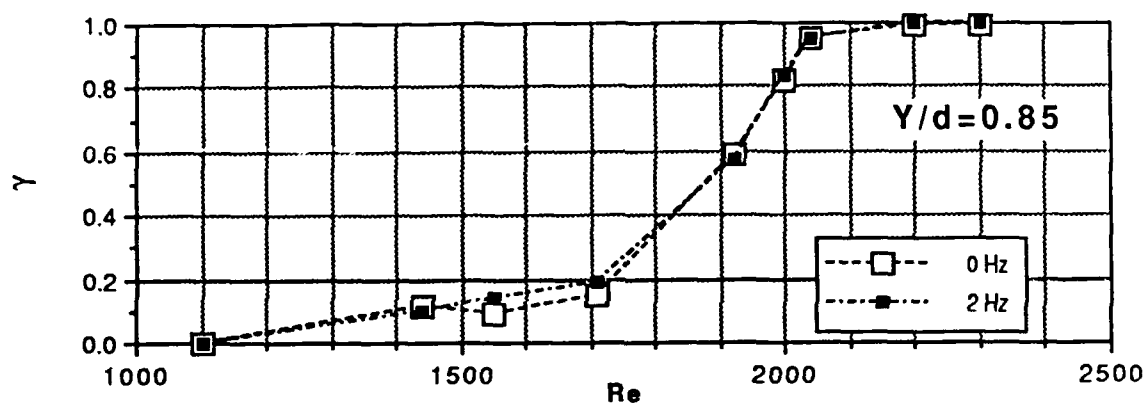
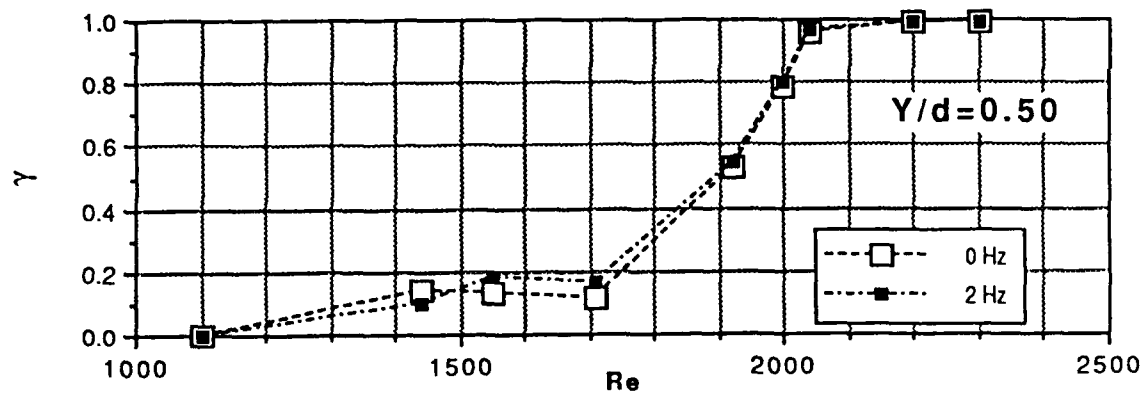


Figure 30. Corrected Intermittency vs Re (2 Hz)

Linear Resolution

MEASURE:	CHAN 1 Power Spec	CHAN 2 Off	
WINDOW:	CHAN 1 Hanning	CHAN 2 Hanning	
AVERAGE:	TYPE # AVGS	OVERLAP	TIME AVG
	Stable 5	0%	On
FREQ:	CENTER 100 Hz	SPAN 200 Hz	BW 375mHz
	REC LGTH Δt		
	4.0 S 1.95mS		
TRIGGER:	TYPE LEVEL	SLOPE	PREVIEW
	Freerun 0.0 Vpk	Pos	Off
INPUT:	RANGE ENG UNITS	COUPLING	DELAY
CH 1	AutoRng↑ 1.0 V/EU	DC (Flt)	0.0 S
CH 2	AutoRng↑ 1.0 V/EU	DC (Flt)	0.0 S
SOURCE:	TYPE	LEVEL	OFFSET
	Rndm Noise	0.0 Vpk	0.0 Vpk

Figure 31. Typical Dynamic Signal Analyzer Settings

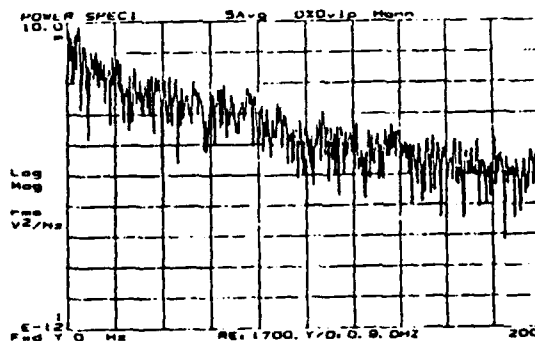
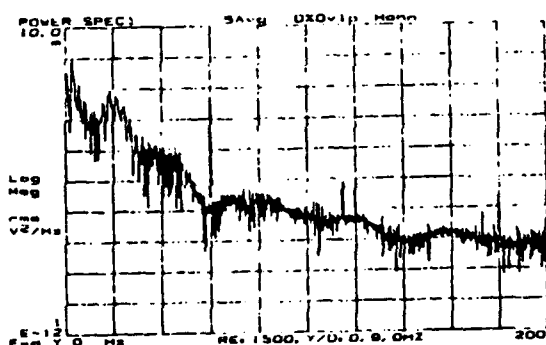
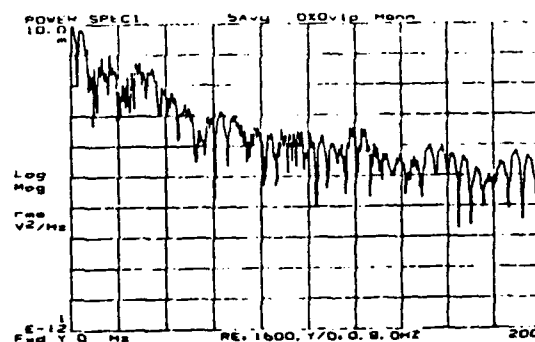
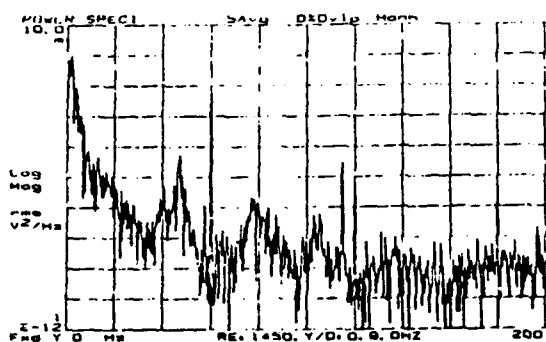
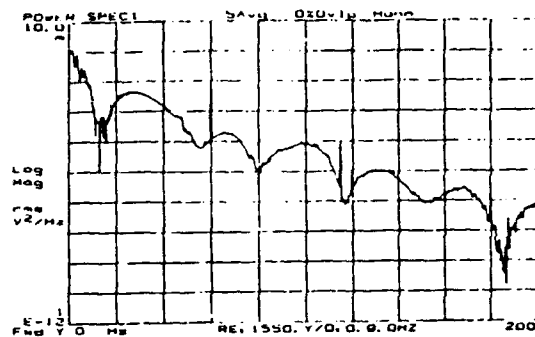
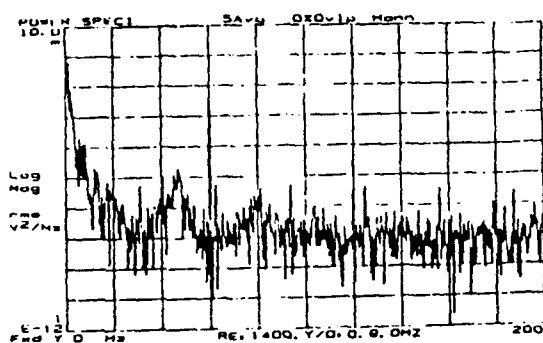


Figure 32. Spectral Frequency Response (0 Hz)

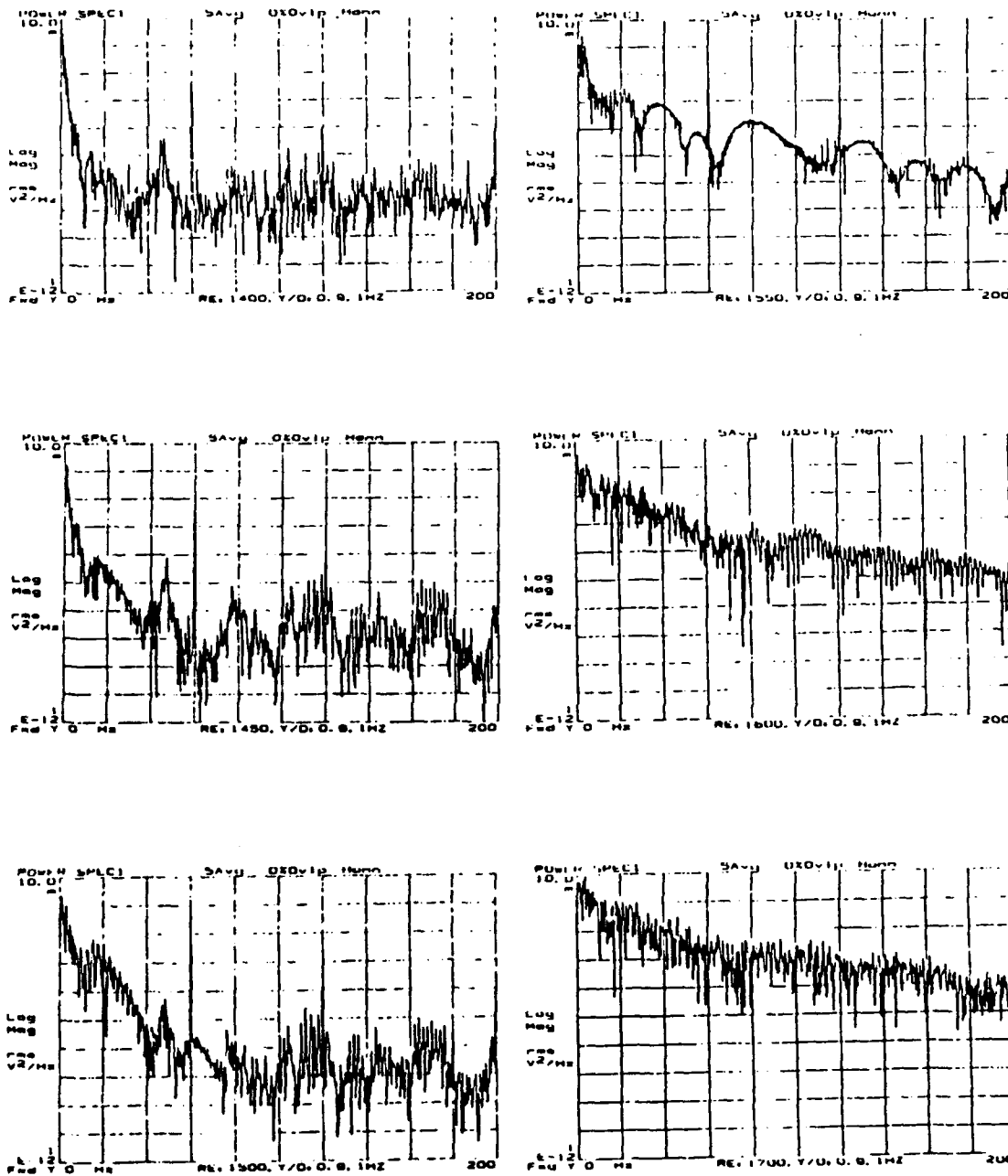


Figure 33. Spectral Frequency Response (1 Hz)

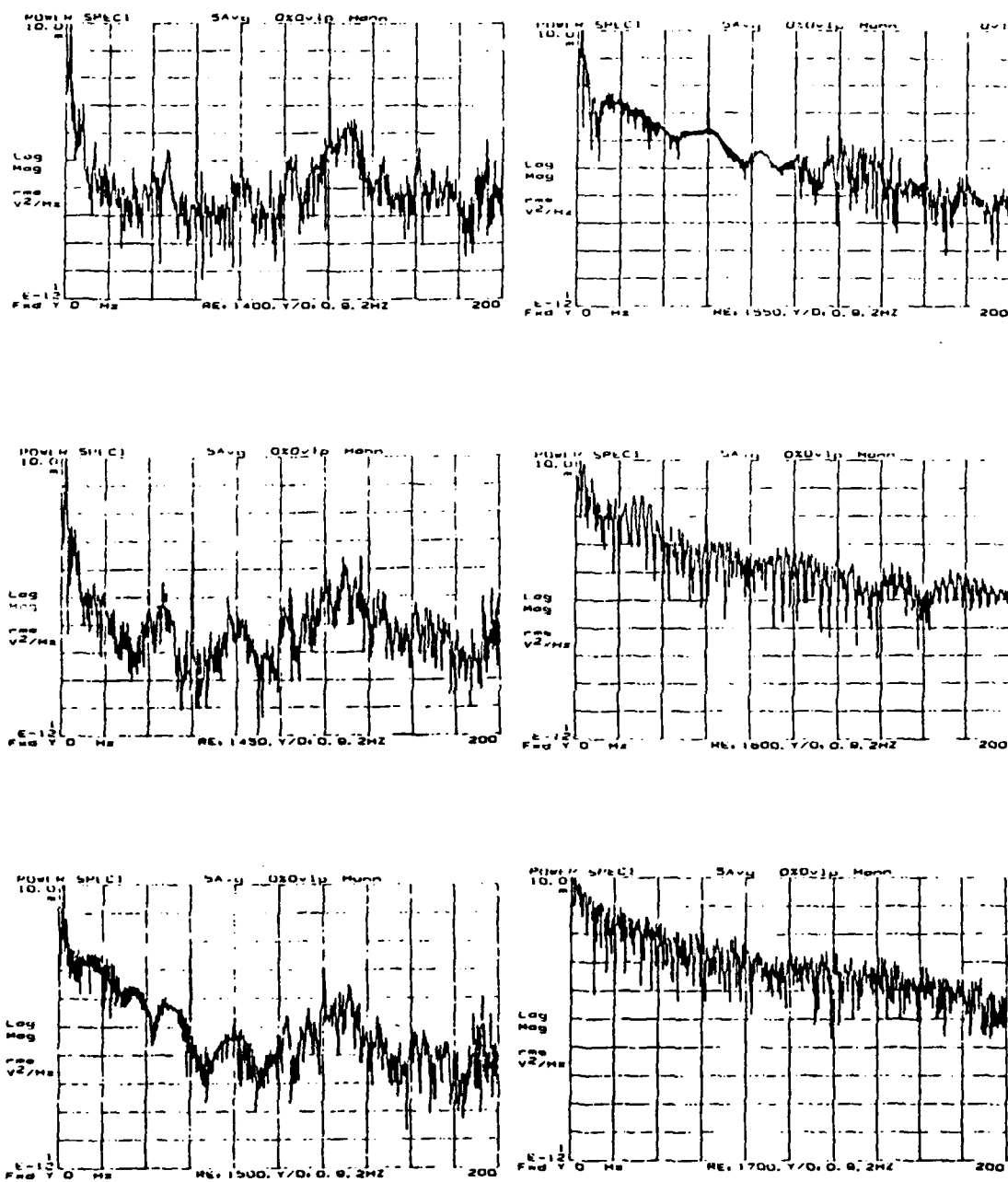


Figure 34. Spectral Frequency Response (2 Hz)

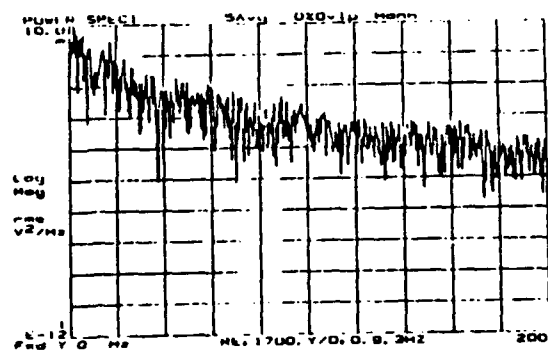
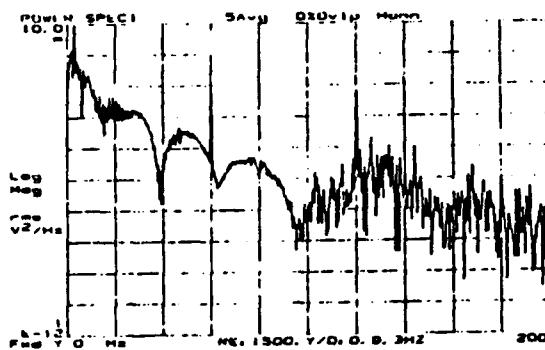
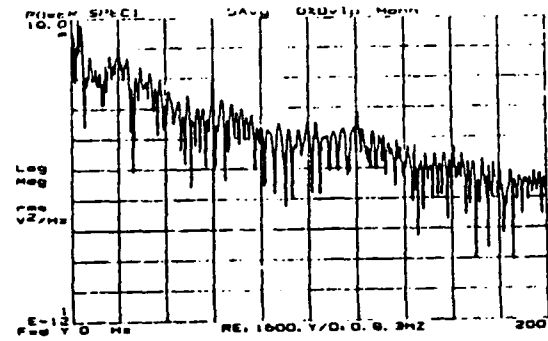
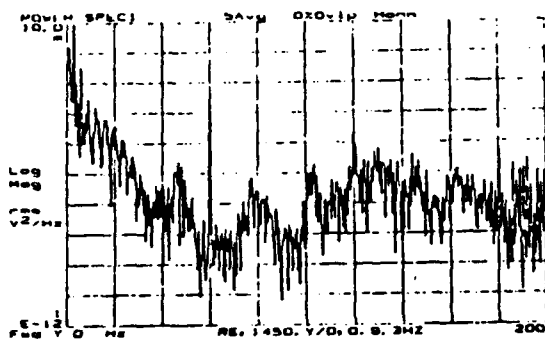
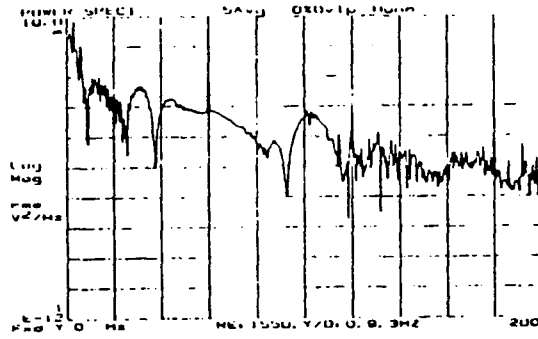
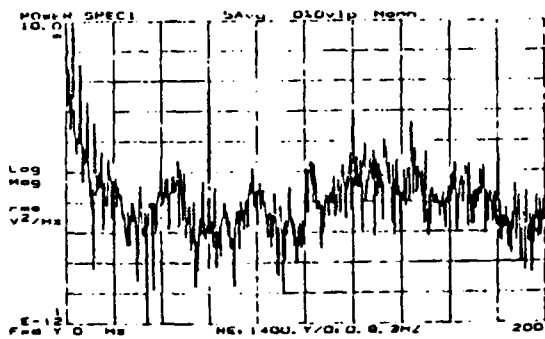


Figure 35. Spectral Frequency Response (3 Hz)

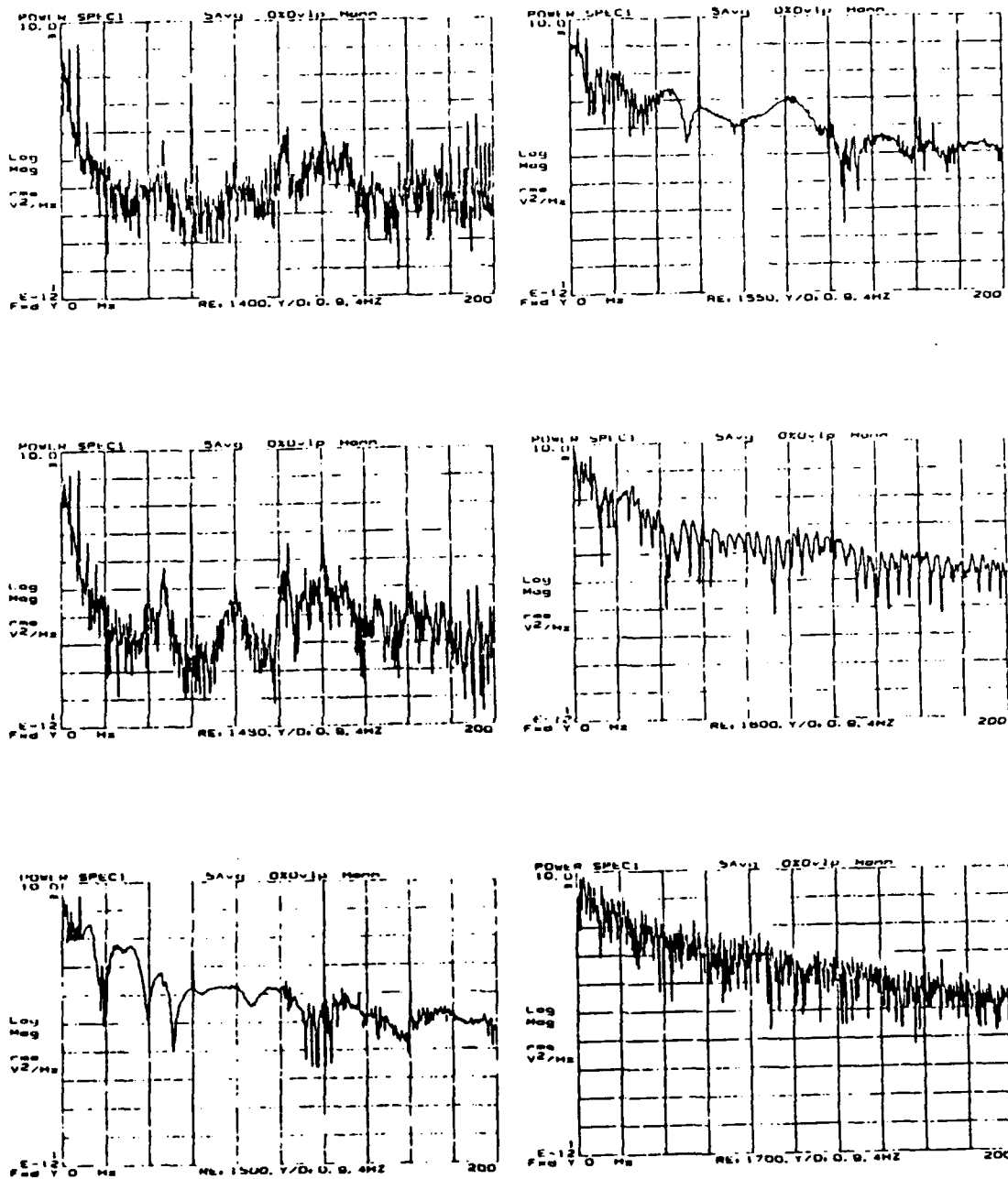
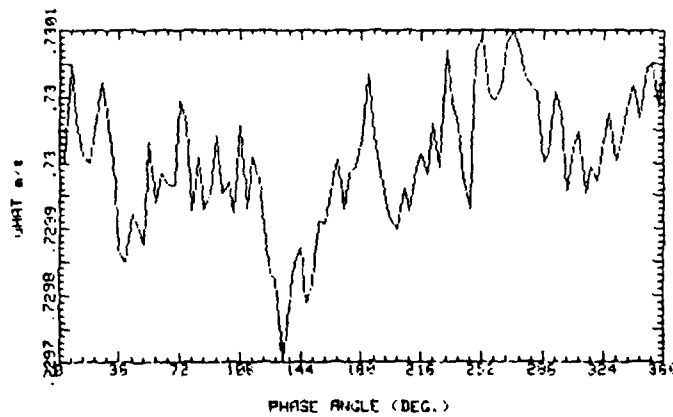
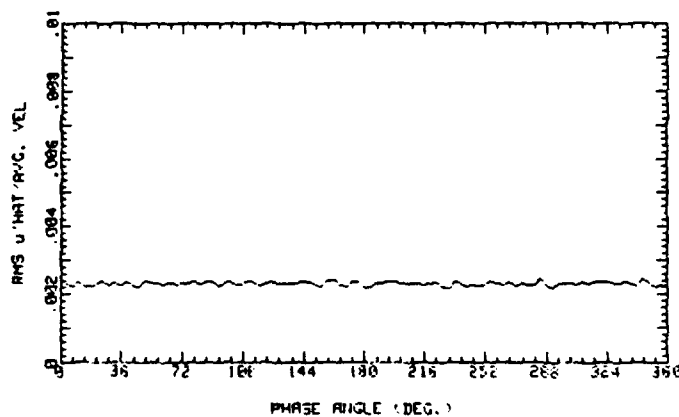


Figure 36. Spectral Frequency Response (4 Hz)

85_1150_0 111090.1557
 AVG. VEL .73m/s RMS VEL .001686m/s
 OSC. FREQ. 0Hz STR. # 0
 BULK VEL. 1.309m/s REY. # 1150



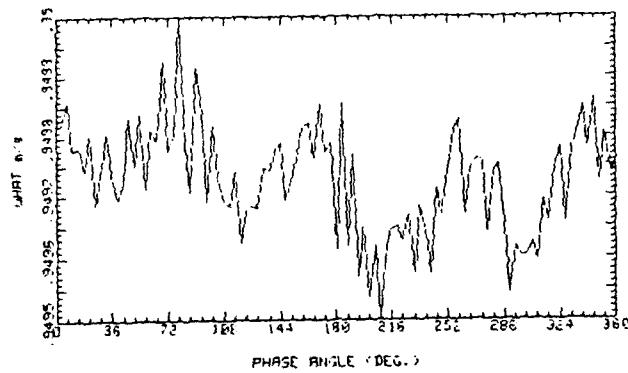
85_1150_0 111090.1557
 AVG. VEL .73m/s RMS VEL .001686m/s
 OSC. FREQ. 0Hz STR. # 0
 BULK VEL. 1.309m/s REY. # 1150



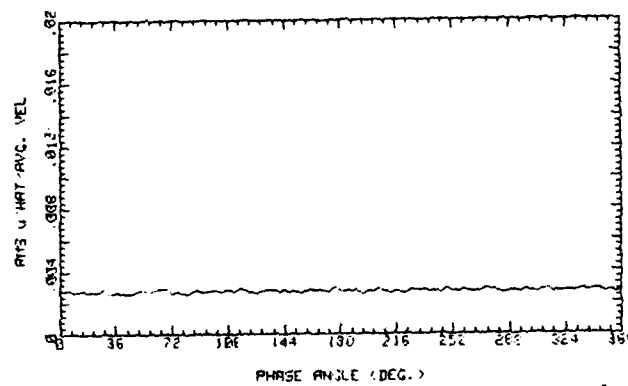
85_1150_0 111090.1557
 AVG. VEL .73m/s RMS VEL .001686m/s
 OSC. FREQ. 0Hz STR. # 0
 BULK VEL. 1.309m/s REY. # 1150

Figure 37. Average and RMS Velocity Traces ($Y/d = 0.85$, $Re = 1100$, 0 Hz)

85_1250_0 122590.1601
 AVG. VEL .9498m/s RMS VEL .002622m/s
 OSC. FREQ. 0Hz STR. # 0
 BULK VEL. 1.485m/s REY. # 1250



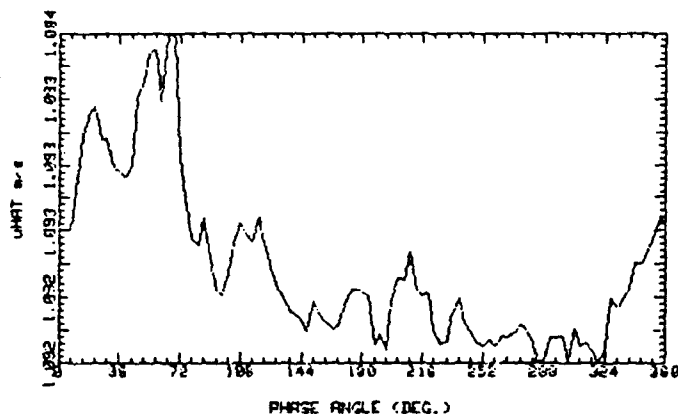
85_1250_0 122590.1601
 AVG. VEL .9498m/s RMS VEL .002622m/s
 OSC. FREQ. 0Hz STR. # 0
 BULK VEL. 1.485m/s REY. # 1250



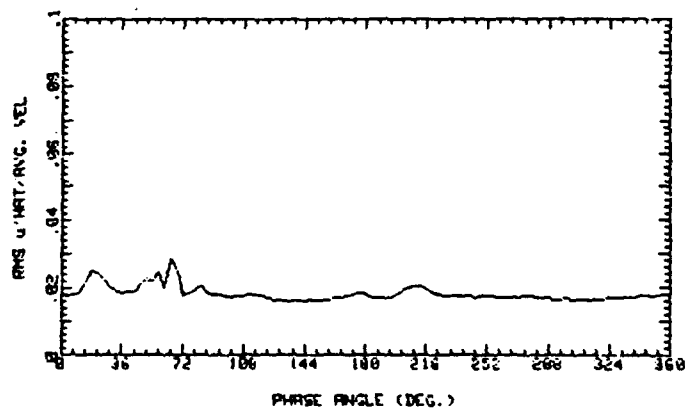
85_1250_0 122590.1601
 AVG. VEL .9498m/s RMS VEL .002622m/s
 OSC. FREQ. 0Hz STR. # 0
 BULK VEL. 1.485m/s REY. # 1250

Figure 38. Average and RMS Velocity Traces ($Y/d = 0.85$, $Re = 1250$, 0 Hz)

85_1350_0 122490.1514
 AVG. VEL 1.092m/s RMS VEL .02022m/s
 OSC. FREQ. 0Hz STR. # 0
 BULK VEL. 1.622m/s REY. # 1350



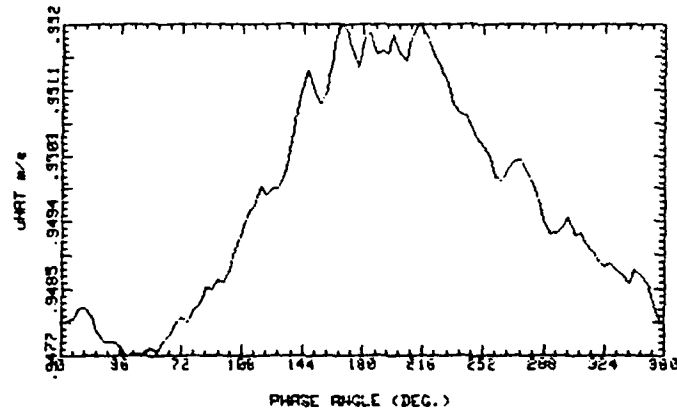
85_1350_0 122490.1514
 AVG. VEL 1.092m/s RMS VEL .02022m/s
 OSC. FREQ. 0Hz STR. # 0
 BULK VEL. 1.622m/s REY. # 1350



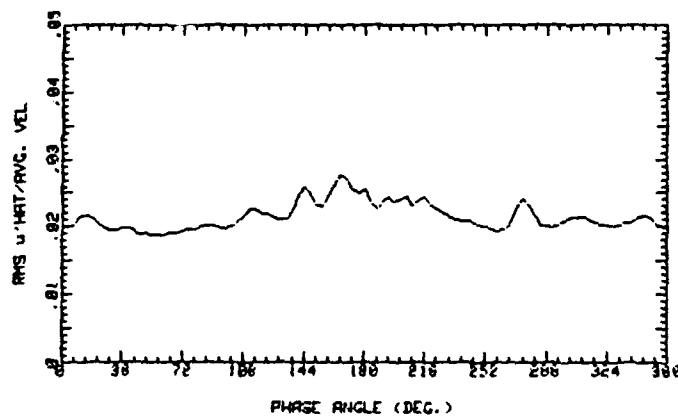
85_1350_0 122490.1514
 AVG. VEL 1.092m/s RMS VEL .02022m/s
 OSC. FREQ. 0Hz STR. # 0
 BULK VEL. 1.622m/s REY. # 1350

Figure 39. Average and RMS Velocity Traces ($Y/d = 0.85$, $Re = 1350$, 0 Hz)

85_1500_0 111390.2247
 AVG. VEL .9497m/s RMS VEL .02052m/s
 OSC. FREQ. 0Hz STR. # 0
 BULK VEL. 1.717m/s REY. # 1500



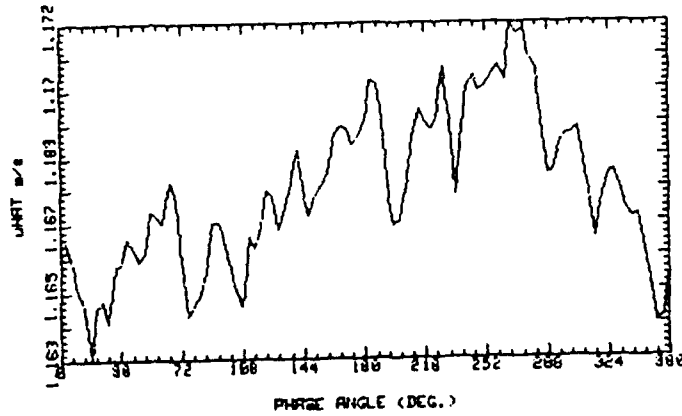
85_1500_0 111390.2247
 AVG. VEL .9497m/s RMS VEL .02052m/s
 OSC. FREQ. 0Hz STR. # 0
 BULK VEL. 1.717m/s REY. # 1500



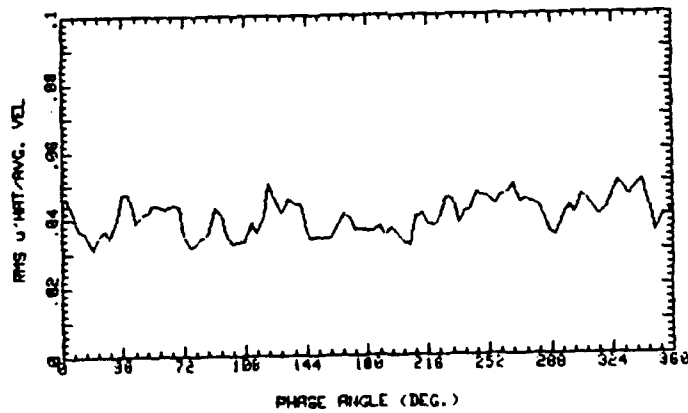
85_1500_0 111390.2247
 AVG. VEL .9497m/s RMS VEL .02052m/s
 OSC. FREQ. 0Hz STR. # 0
 BULK VEL. 1.717m/s REY. # 1500

Figure 40. Average and RMS Velocity Traces ($Y/d = 0.85$, $Re = 1440$, 0 Hz)

05_1550_0 120990.1505
 AVG. VEL 1.168m/s RMS VEL .04766m/s
 OSC. FREQ. 0Hz STR. # 0
 BULK VEL. 1.857m/s REY. # 1550

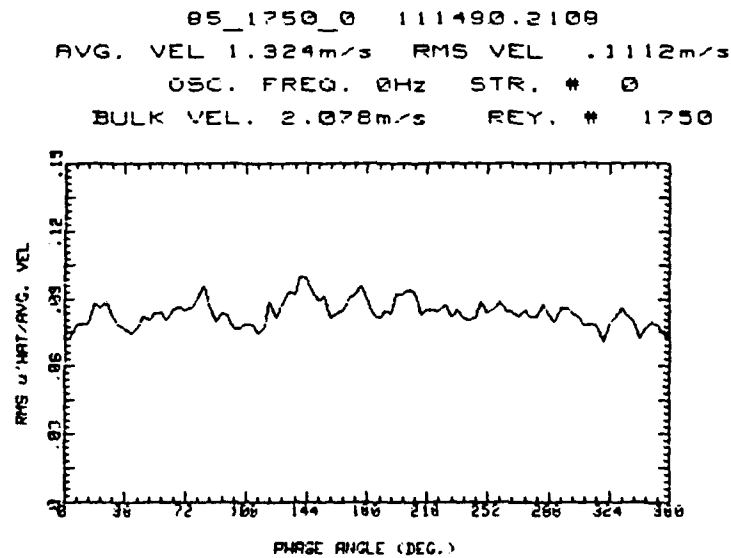
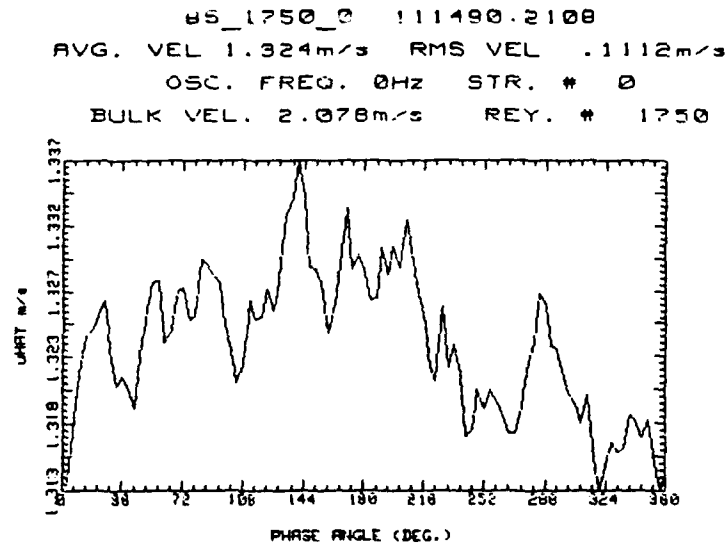


05_1550_0 120990.1505
 AVG. VEL 1.168m/s RMS VEL .04766m/s
 OSC. FREQ. 0Hz STR. # 0
 BULK VEL. 1.857m/s REY. # 1550



05_1550_0 120990.1505
 AVG. VEL 1.168m/s RMS VEL .04766m/s
 OSC. FREQ. 0Hz STR. # 0
 BULK VEL. 1.857m/s REY. # 1550

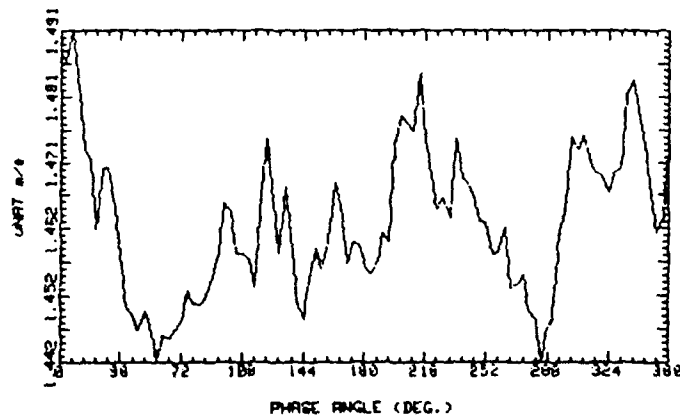
Figure 41. Average and RMS Velocity Traces ($Y/d = 0.85$, $Re = 1550$, 0 Hz)



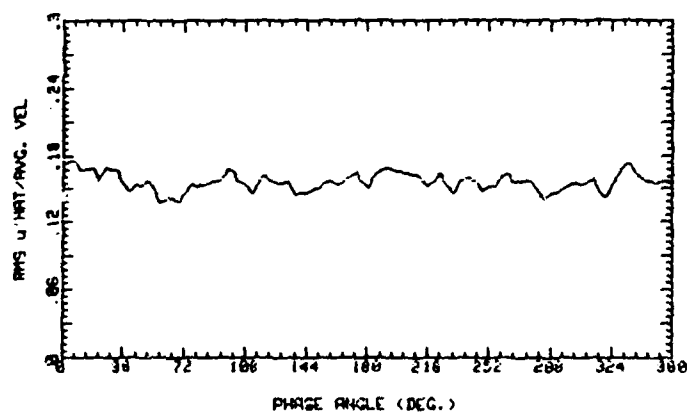
85_1750_0 111490.2108
 AVG. VEL 1.324m/s RMS VEL .1112m/s
 OSC. FREQ. 0Hz STR. # 0
 BULK VEL. 2.078m/s REY. # 1750

Figure 42. Average and RMS Velocity Traces ($Y/d = 0.85$, $Re = 1710$, 0 Hz)

85_1850_0 120890.1503
 AVG. VEL 1.463m/s RMS VEL .2291m/s
 OSC. FREQ. 0Hz STR. # 0
 BULK VEL. 2.211m/s REY. # 1850



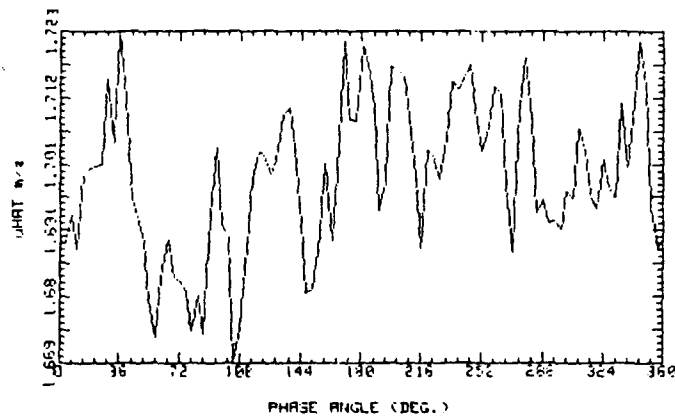
85_1850_0 120890.1503
 AVG. VEL 1.463m/s RMS VEL .2291m/s
 OSC. FREQ. 0Hz STR. # 0
 BULK VEL. 2.211m/s REY. # 1850



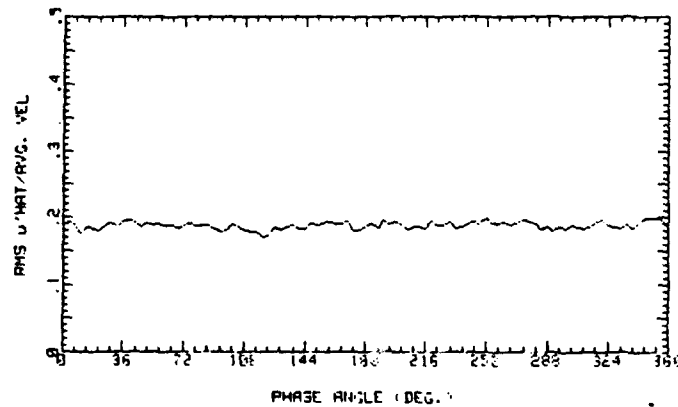
85_1850_0 120890.1503
 AVG. VEL 1.463m/s RMS VEL .2291m/s
 OSC. FREQ. 0Hz STR. # 0
 BULK VEL. 2.211m/s REY. # 1850

Figure 43. Average and RMS Velocity Traces ($Y/d = 0.85$, $Re = 1850$, 0 Hz)

85_2005_0 111090.1951
 AVG. VEL 1.699m/s RMS VEL .3198m/s
 OSC. FREQ. 0Hz STR. # 0
 BULK VEL. 2.289m/s REY. # 2005



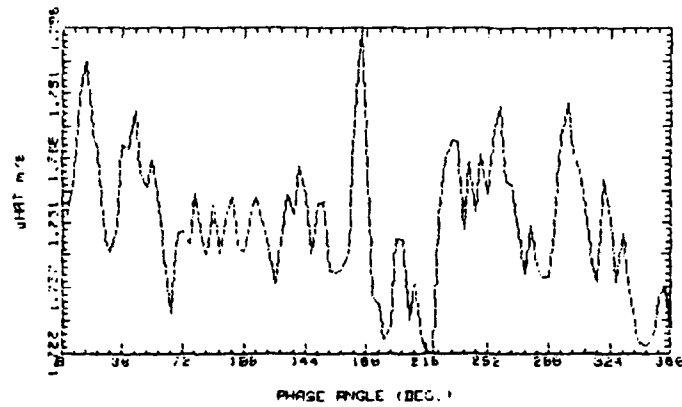
85_2005_0 111090.1951
 AVG. VEL 1.699m/s RMS VEL .3198m/s
 OSC. FREQ. 0Hz STR. # 0
 BULK VEL. 2.289m/s REY. # 2005



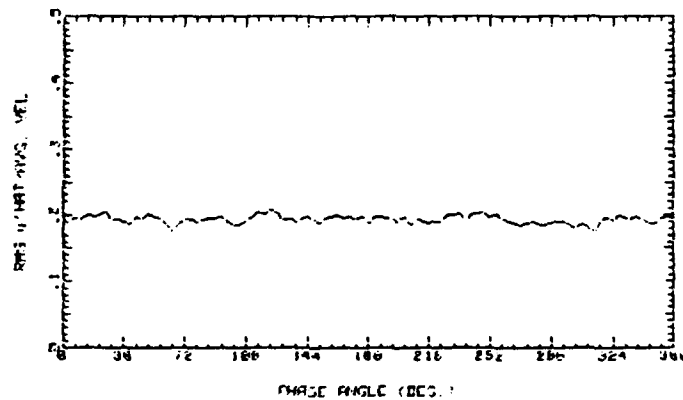
85_2005_0 111090.1951
 AVG. VEL 1.699m/s RMS VEL .3198m/s
 OSC. FREQ. 0Hz STR. # 0
 BULK VEL. 2.289m/s REY. # 2005

Figure 44. Average and RMS Velocity Traces ($Y/d = 0.85$, $Re = 1920$, 0 Hz)

85_2100_0 111090.225
 AVG. VEL 1.751m/s RMS VEL .3378m/s
 OSC. FREQ. 0Hz STR. # 0
 BULK VEL. 2.394m/s REV. # 2100

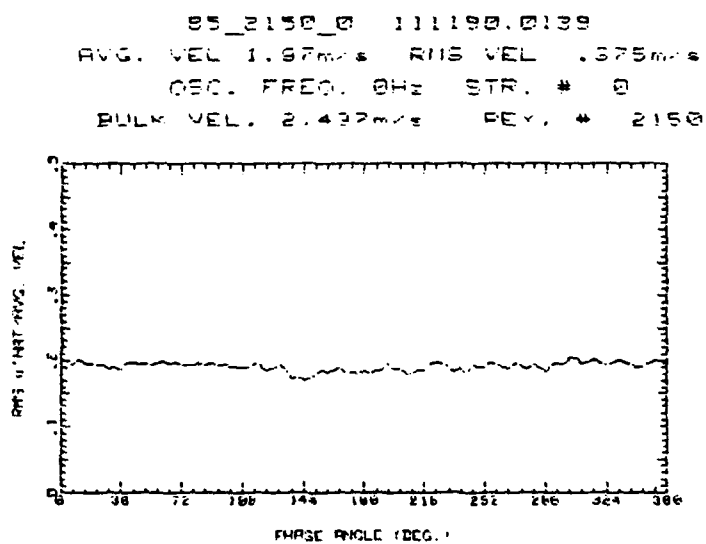
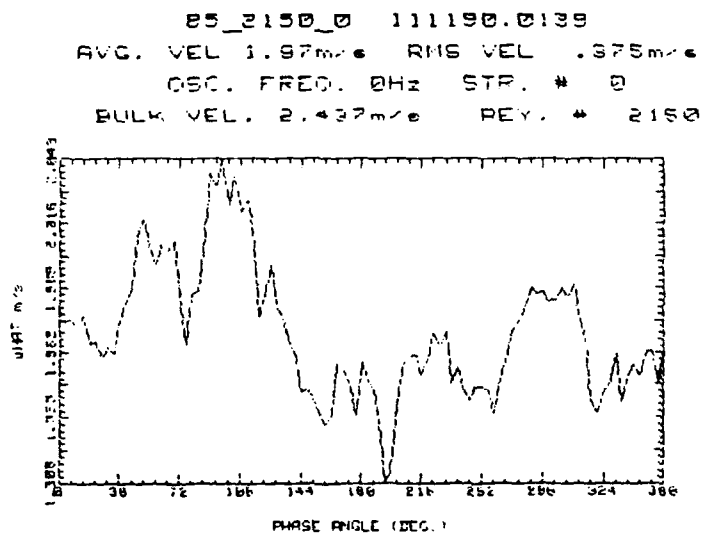


85_2100_0 111090.225
 AVG. VEL 1.751m/s RMS VEL .3378m/s
 OSC. FREQ. 0Hz STR. # 0
 BULK VEL. 2.394m/s REV. # 2100



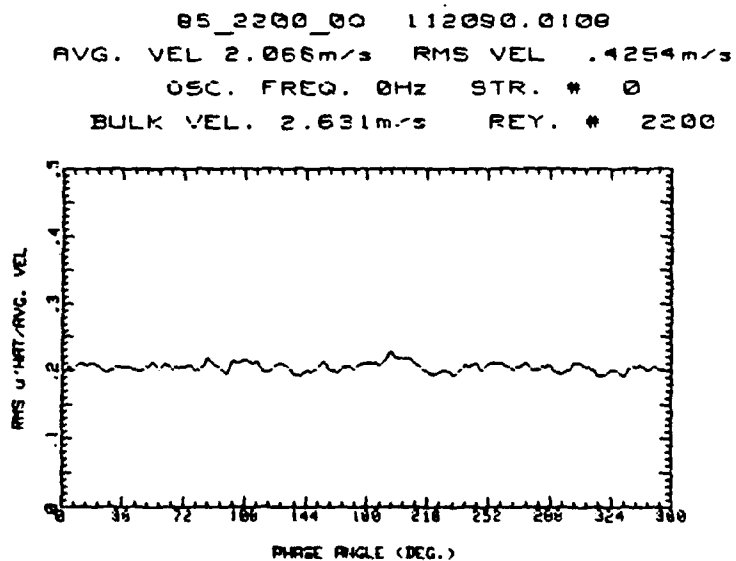
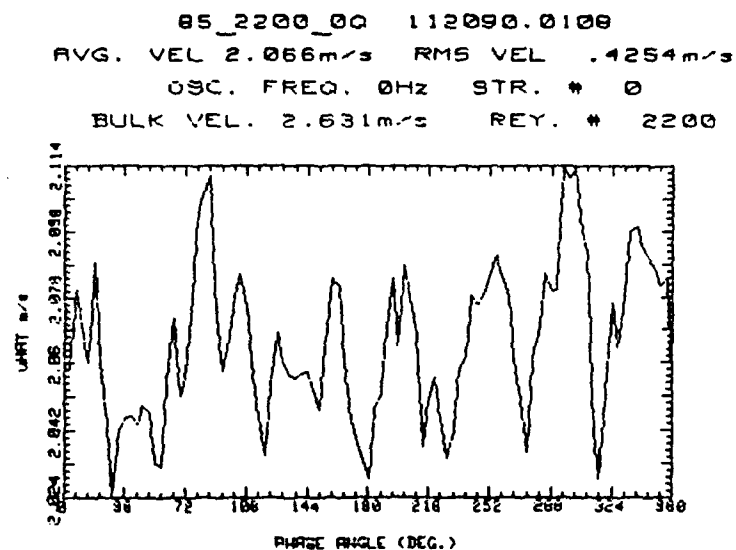
85_2100_0 111090.225
 AVG. VEL 1.751m/s RMS VEL .3378m/s
 OSC. FREQ. 0Hz STR. # 0
 BULK VEL. 2.394m/s REV. # 2100

Figure 45. Average and RMS Velocity Traces ($Y/d \approx 0.85$, $Re = 2000$, 0 Hz)



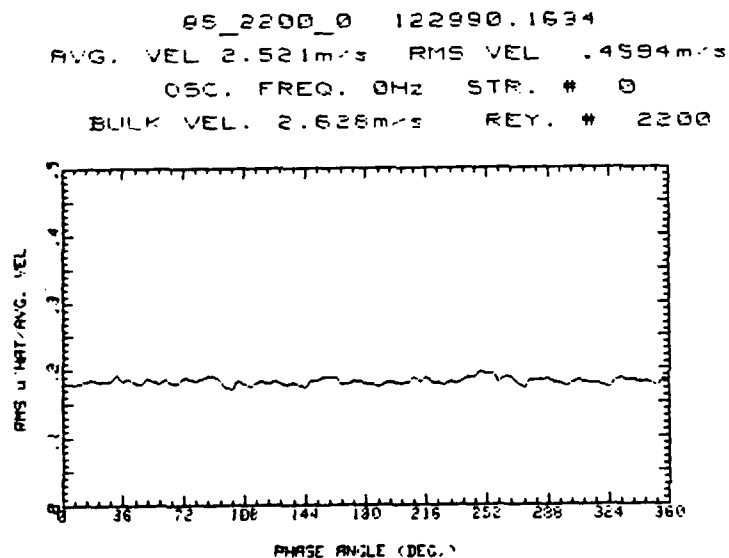
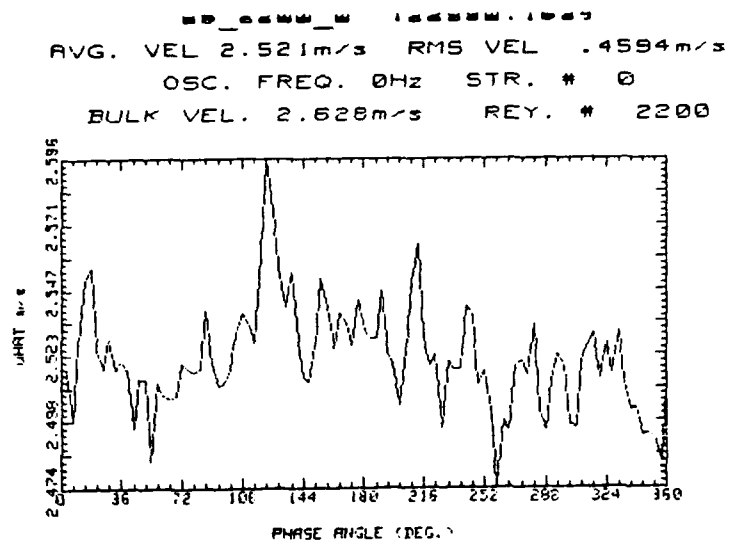
85_2150_0 111190.0139
 AVG. VEL 1.97m/s RMS VEL .375m/s
 OSC. FREQ. 0Hz STR. # 0
 BULK VEL. 2.437m/s REY. # 2150

Figure 46. Average and RMS Velocity Traces ($Y/d=0.85$, $Re=2040$, 0 Hz)



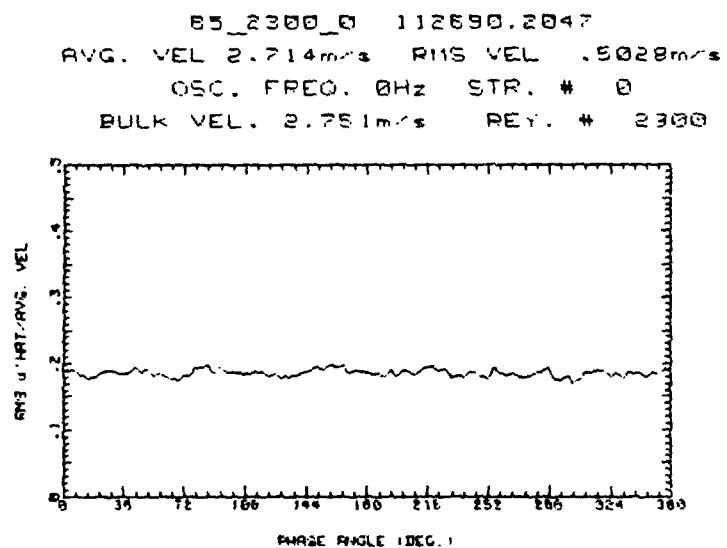
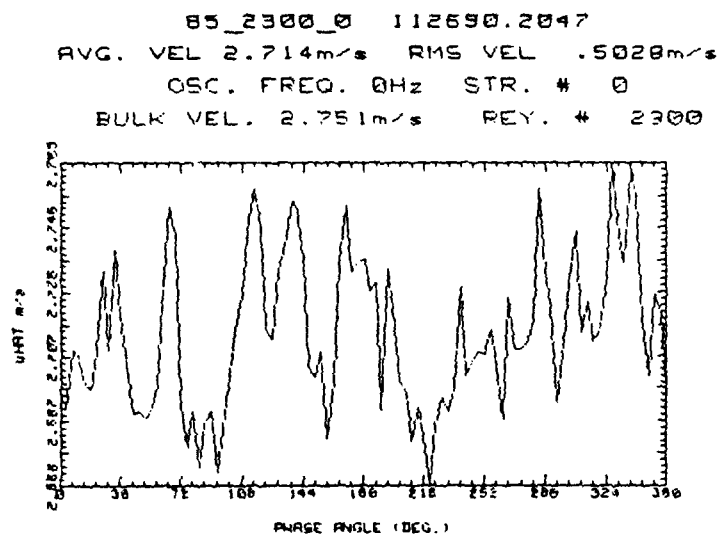
05_2200_00 112090.0100
 AVG. VEL 2.066m/s RMS VEL .4254m/s
 OSC. FREQ. 0Hz STR. # 0
 BULK VEL. 2.631m/s REY. # 2200

Figure 47. Average and RMS Velocity Traces ($Y/d = 0.85$, $Re = 2090$, 0 Hz)



85_2200_0 122990.1634
 AVG. VEL 2.521m/s RMS VEL .4594m/s
 OSC. FREQ. 0Hz STR. # 0
 BULK VEL. 2.628m/s REY. # 2200

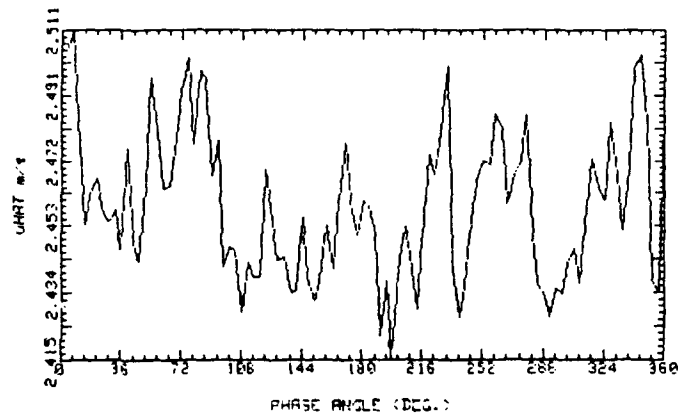
Figure 48. Average and RMS Velocity Traces ($Y/d = 0.85$, $Re = 2200$, 0 Hz)



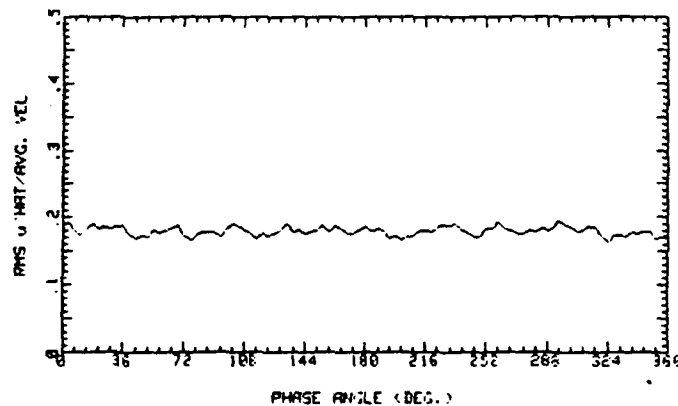
85_2300_0 112690.2047
 AVG. VEL 2.714m/s RMS VEL .5028m/s
 OSC. FREQ. 0Hz STR. # 0
 BULK VEL. 2.751m/s REY. # 2300

Figure 49. Average and RMS Velocity Traces ($Y/d = 0.85$, $Re = 2300$, 0 Hz)

85_2350_0 10391.1156
 AVG. VEL 2.459m/s RMS VEL .4421m/s
 OSC. FREQ. 0Hz STR. # 0
 BULK VEL. 2.81m/s REY. # 2350



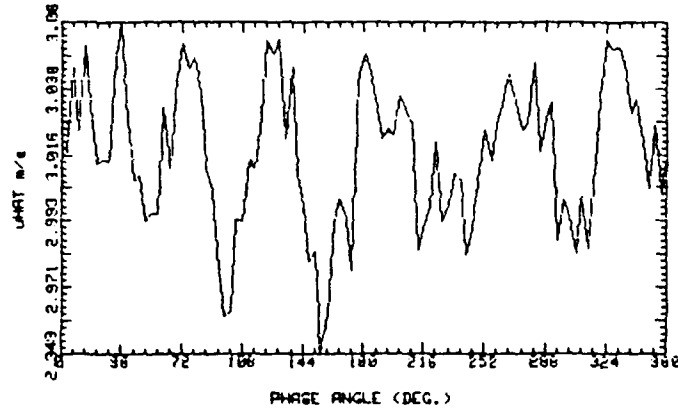
85_2350_0 10391.1156
 AVG. VEL 2.459m/s RMS VEL .4421m/s
 OSC. FREQ. 0Hz STR. # 0
 BULK VEL. 2.81m/s REY. # 2350



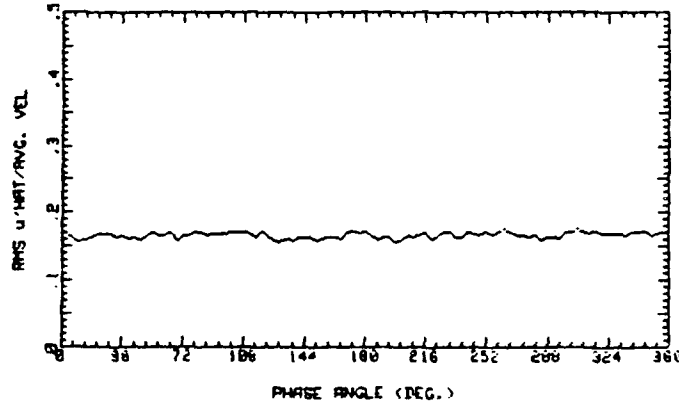
85_2350_0 10391.1156
 AVG. VEL 2.459m/s RMS VEL .4421m/s
 OSC. FREQ. 0Hz STR. # 0
 BULK VEL. 2.81m/s REY. # 2350

Figure 50. Average and RMS Velocity Traces ($Y/d = 0.85$, $Re = 2350$, 0 Hz)

85_2400_0 112790.1951
 AVG. VEL 3.016m/s RMS VEL .5019m/s
 OSC. FREQ. 0Hz STR. # 0
 BULK VEL. 2.872m/s REY. # 2400

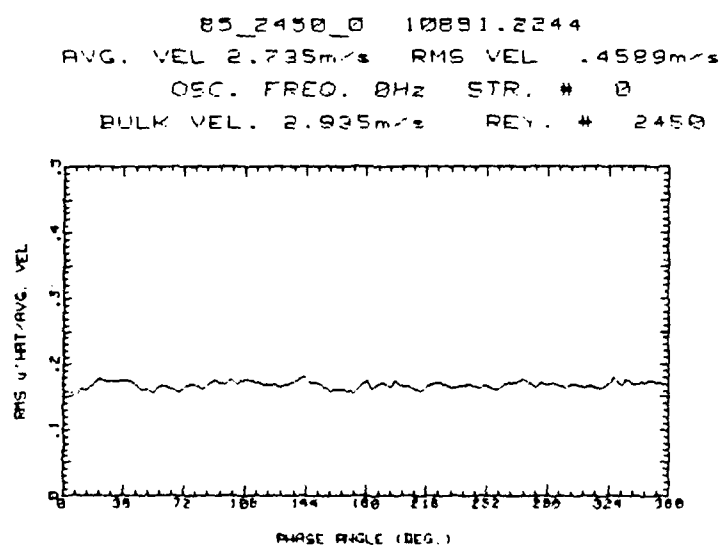
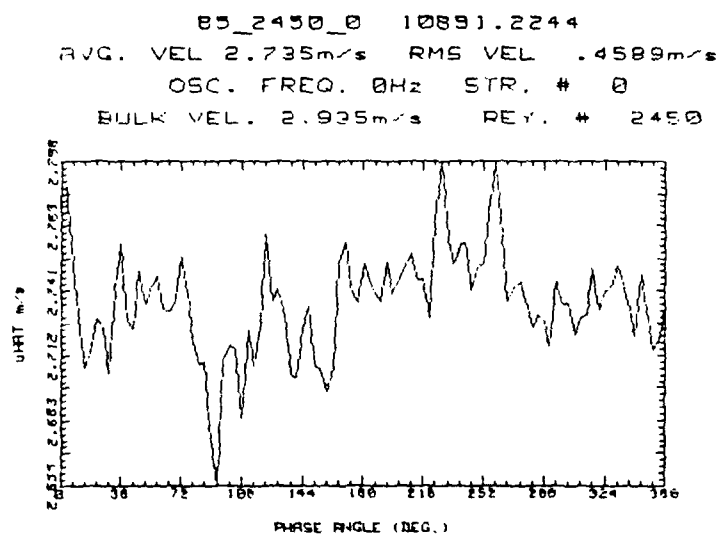


85_2400_0 112790.1951
 AVG. VEL 3.016m/s RMS VEL .5019m/s
 OSC. FREQ. 0Hz STR. # 0
 BULK VEL. 2.872m/s REY. # 2400



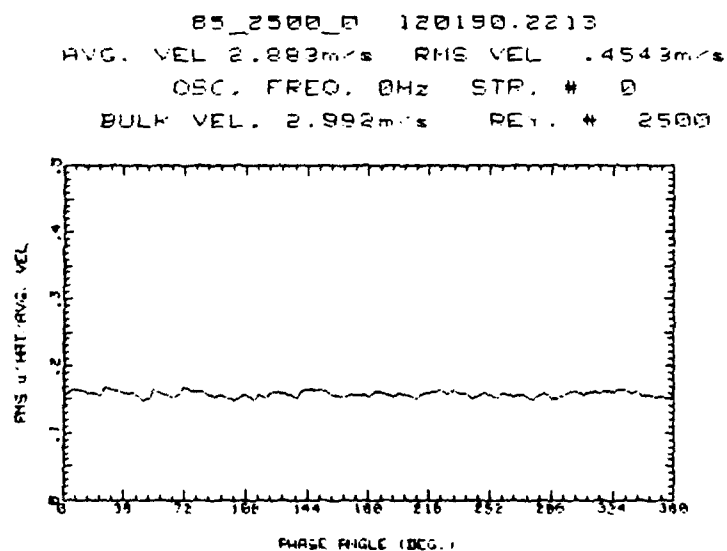
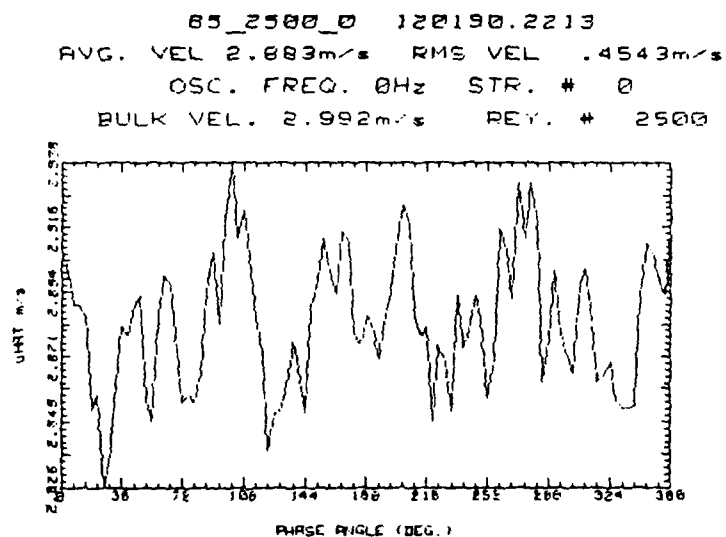
85_2400_0 112790.1951
 AVG. VEL 3.016m/s RMS VEL .5019m/s
 OSC. FREQ. 0Hz STR. # 0
 BULK VEL. 2.872m/s REY. # 2400

Figure 51. Average and RMS Velocity Traces ($Y/d = 0.85$, $Re = 2400$, 0 Hz)



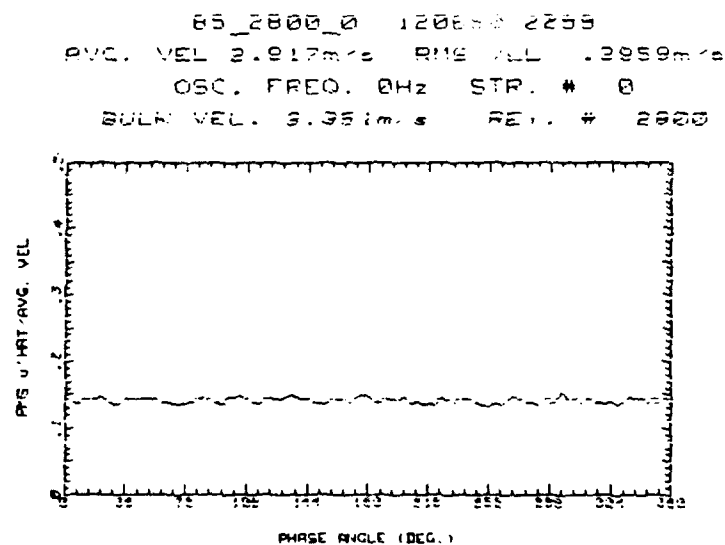
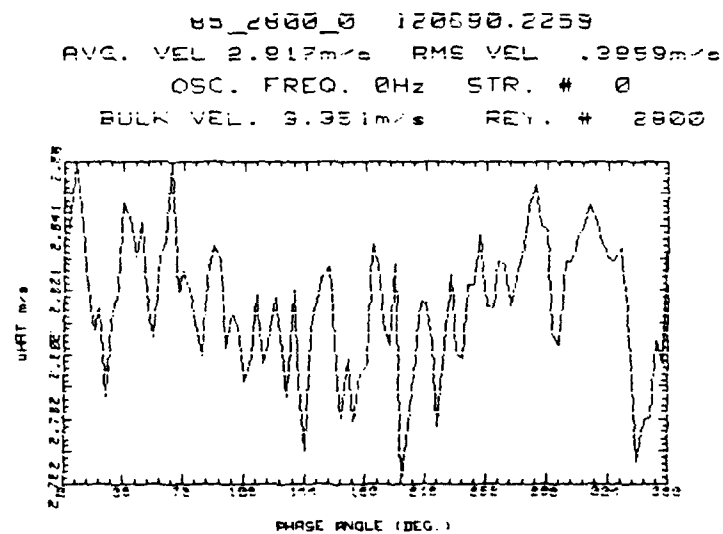
85_2450_0 10891.2244
 AVG. VEL 2.735m/s RMS VEL .4589m/s
 OSC. FREQ. 0Hz STR. # 0
 BULK VEL. 2.935m/s REY. # 2450

Figure 52. Average and RMS Velocity Traces ($Y/d = 0.85$, $Re = 2450$, 0 Hz)



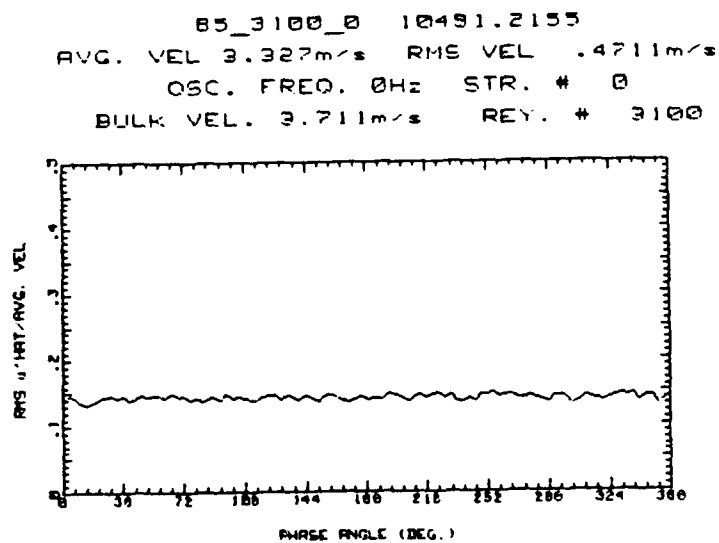
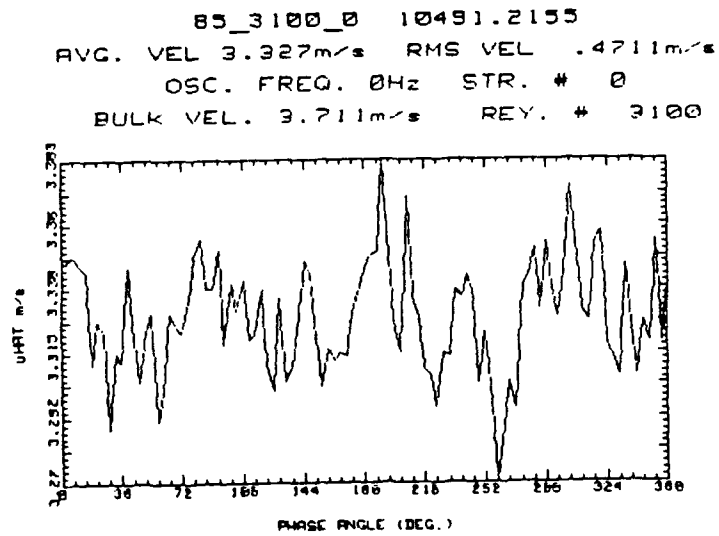
85_2500_0 120190.2213
 AVG. VEL 2.883m/s RMS VEL .4543m/s
 OSC. FREQ. 0Hz STR. # 0
 BULK VEL. 2.992m/s REY. # 2500

Figure 53. Average and RMS Velocity Traces ($Y/d = 0.85$, $Re = 2500$, 0 Hz)



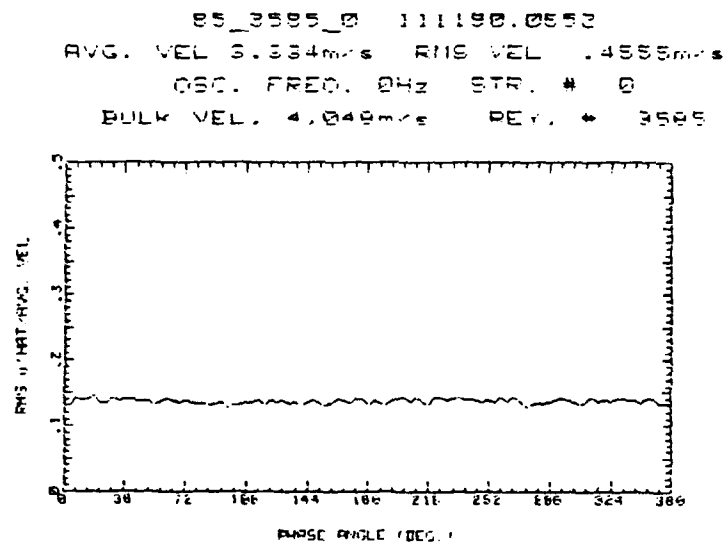
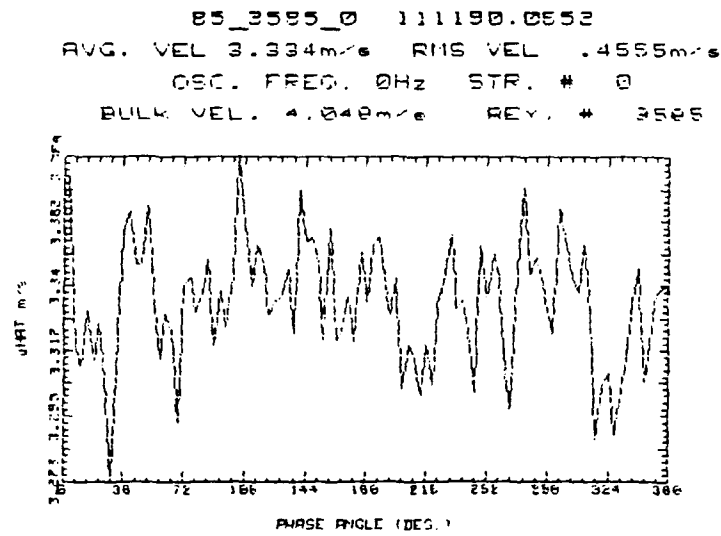
BS_2800_0 120690.2259
 AVG. VEL 2.817m/s RMS VEL .3959m/s
 OSC. FREQ. 0Hz STR. # 0
 BULK VEL. 3.351m/s REY. # 2800

Figure 54. Average and RMS Velocity Traces ($Y/d = 0.85$, $Re = 2800$, 0 Hz)



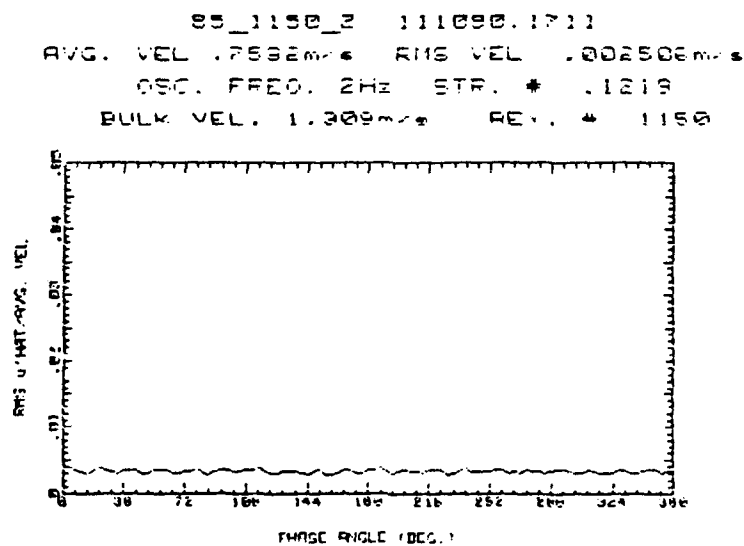
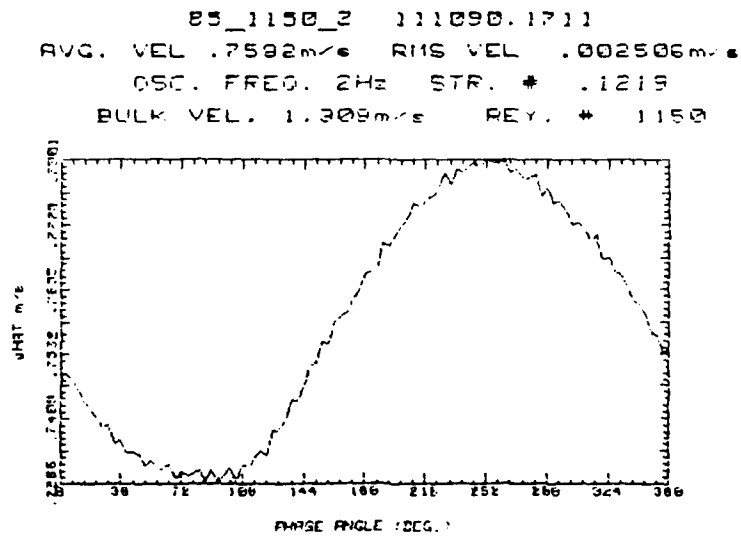
85_3100_0 10491.2155
 AVG. VEL 3.327m/s RMS VEL .4711m/s
 OSC. FREQ. 0Hz STR. # 0
 BULK VEL. 3.711m/s REY. # 3100

Figure 55. Average and RMS Velocity Traces ($Y/d = 0.85$, $Re = 3100$, 0 Hz)



85_3585_0 111190.0852
 AVG. VEL 3.334m/s RMS VEL .4555m/s
 OSC. FREQ. 0Hz STR. # 0
 BULK VEL. 4.049m/s REV. # 3585

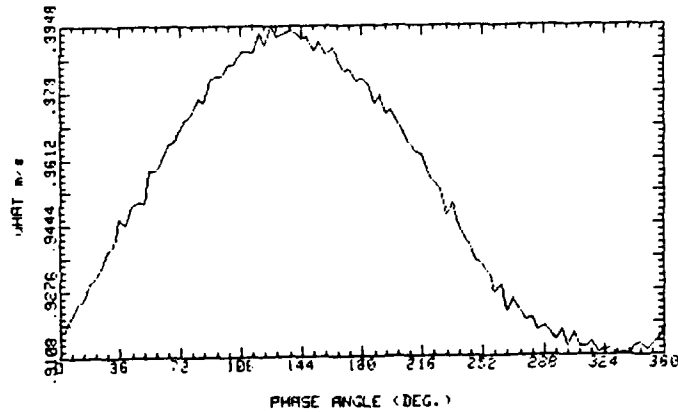
Figure 56. Average and RMS Velocity Traces ($Y/d=0.85$, $Re=3400$, 0 Hz)



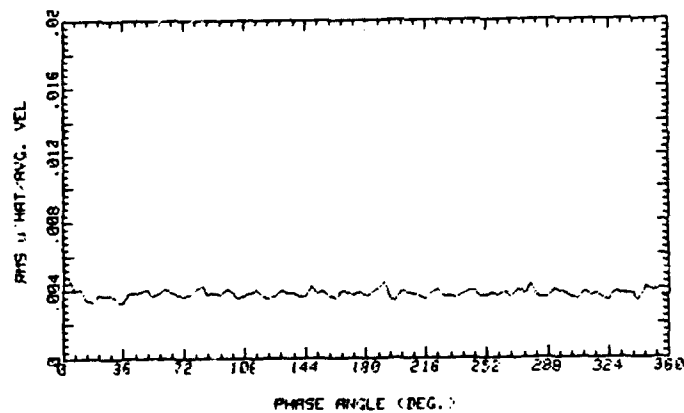
85_1150_2 111090.1711
 AVG. VEL .7592m/s RMS VEL .002506m/s
 OSC. FREQ. 2Hz STR. # .1219
 BULK VEL. 1.309m/s REY. # 1150

Figure 57. Average and RMS Velocity Traces ($Y/d=0.85$, $Re=1100$, 2 Hz)

05_1250_2 122090.1549
 AVG. VEL .9513m/s RMS VEL .003596m/s
 OSC. FREQ. 2Hz STR. # .1071
 BULK VEL. 1.49m/s REY. # 1250



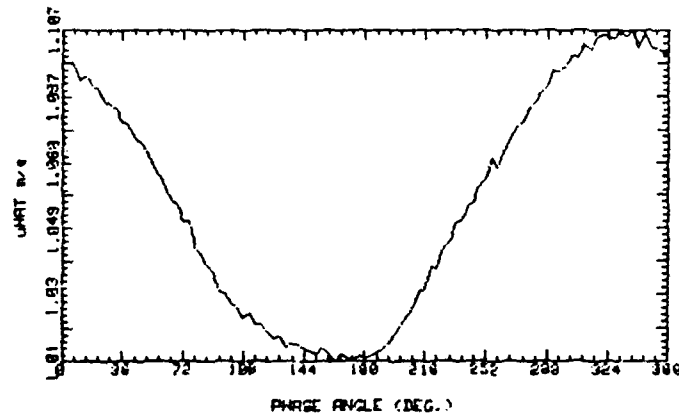
05_1250_2 122090.1549
 AVG. VEL .9513m/s RMS VEL .003596m/s
 OSC. FREQ. 2Hz STR. # .1071
 BULK VEL. 1.49m/s REY. # 1250



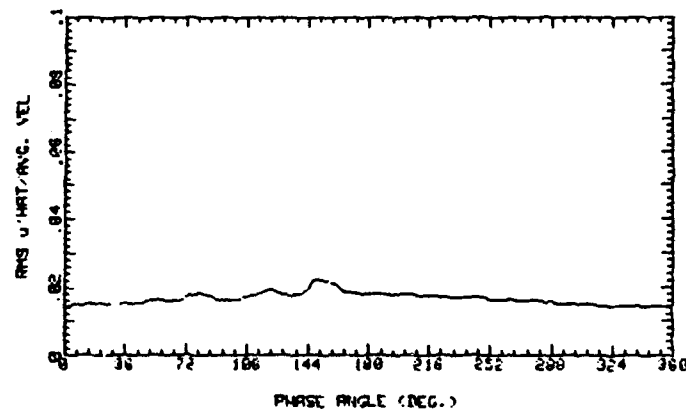
05_1250_2 122090.154
 AVG. VEL .9513m/s RMS VEL .003596m/s
 OSC. FREQ. 2Hz STR. # .1071
 BULK VEL. 1.49m/s REY. # 1250

Figure 58. Average and RMS Velocity Traces ($Y/d = 0.85$, $Re = 1250$, 2 Hz)

85_1350_2 122490.1827
 AVG. VEL 1.057m/s RMS VEL .01787m/s
 OSC. FREQ. 2Hz STR. # .09837
 BULK VEL. 1.622m/s REY. # 1350

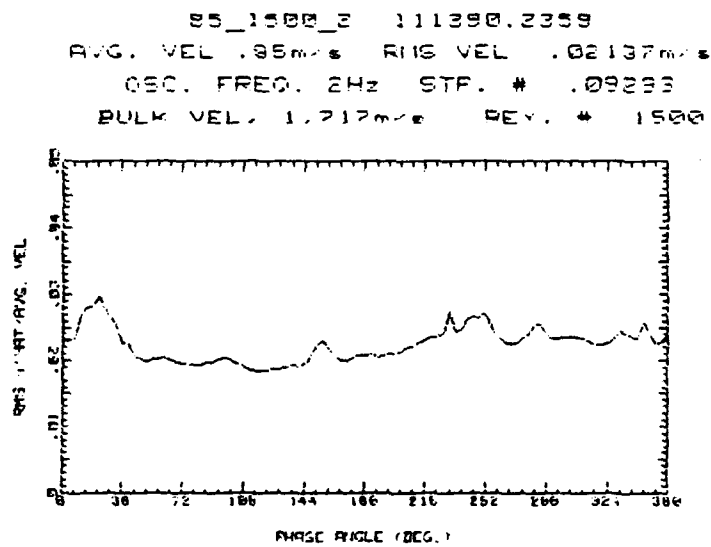
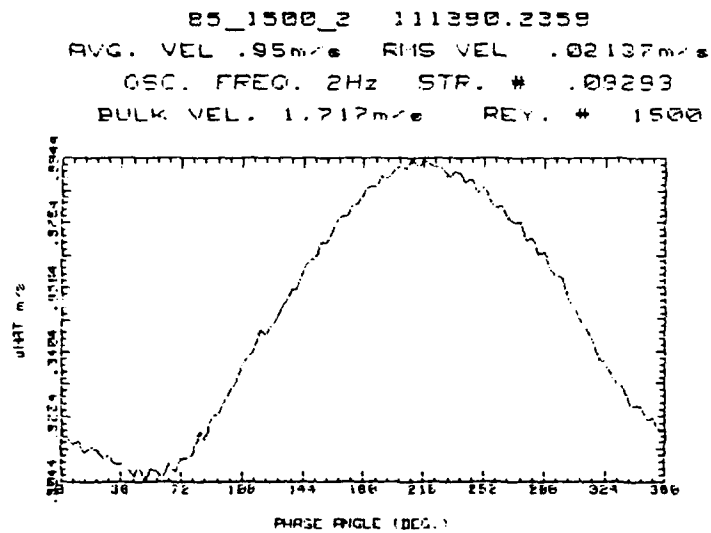


85_1350_2 122490.1827
 AVG. VEL 1.057m/s RMS VEL .01787m/s
 OSC. FREQ. 2Hz STR. # .09837
 BULK VEL. 1.622m/s REY. # 1350



85_1350_2 122490.1827
 AVG. VEL 1.057m/s RMS VEL .01787m/s
 OSC. FREQ. 2Hz STR. # .09837
 BULK VEL. 1.622m/s REY. # 1350

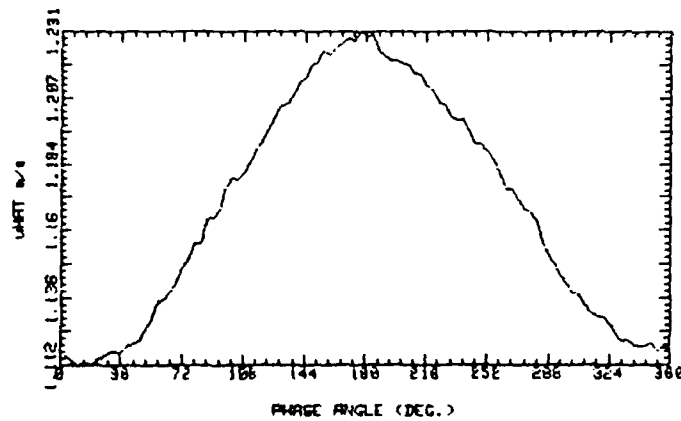
Figure 59. Average and RMS Velocity Traces ($Y/d=0.85$, $Re=1350$, 2 Hz)



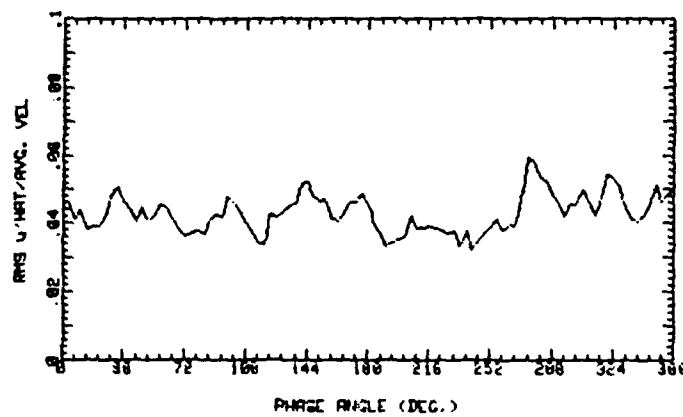
85_1500_2 111390.2359
 AVG. VEL .95m/s RMS VEL .02137m/s
 OSC. FREQ. 2Hz STR. # .09293
 BULK VEL. 1.717m/s REY. # 1500

Figure 60. Average and RMS Velocity Traces ($Y/d = 0.85$, $Re = 1440$, 2 Hz)

05_1550_2 120090.2205
 AVG. VEL 1.168m/s RMS VEL .05067m/s
 OSC. FREQ. 2Hz STR. * .0658
 BULK VEL. 1.86m/s REY. * 1550



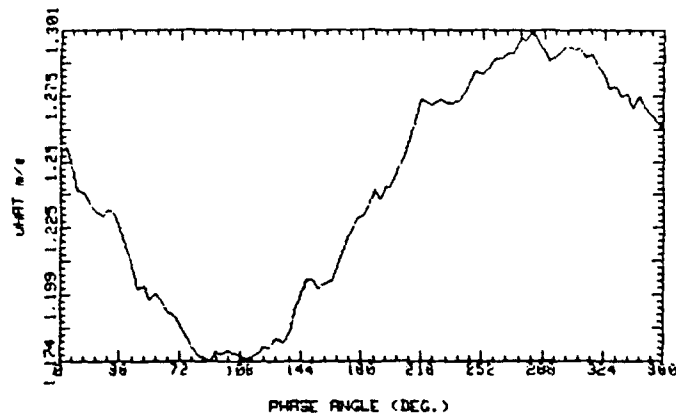
05_1550_2 120090.2205
 AVG. VEL 1.168m/s RMS VEL .05067m/s
 OSC. FREQ. 2Hz STR. * .0658
 BULK VEL. 1.86m/s REY. * 1550



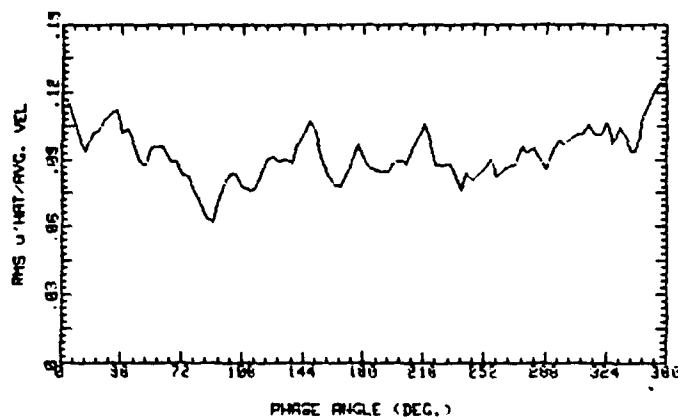
05_1550_2 120090.2205
 AVG. VEL 1.168m/s RMS VEL .05067m/s
 OSC. FREQ. 2Hz STR. * .0658
 BULK VEL. 1.86m/s REY. * 1550

Figure 61. Average and RMS Velocity Traces ($Y/d \approx 0.85$, $Re = 1550$, 2 Hz)

85_1750_2 111590.0109
 AVG. VEL 1.239m/s RMS VEL .1154m/s
 OSC. FREQ. 2Hz STR. # .07679
 BULK VEL. 2.078m/s REY. # 1750



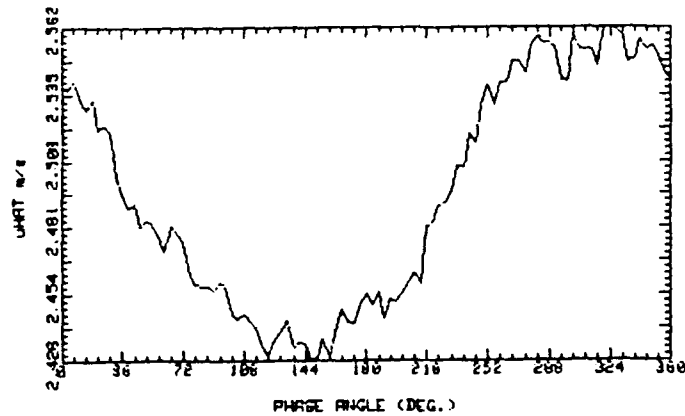
85_1750_2 111590.0.09
 AVG. VEL 1.239m/s RMS VEL .1154m/s
 OSC. FREQ. 2Hz STR. # .07679
 BULK VEL. 2.078m/s REY. # 1750



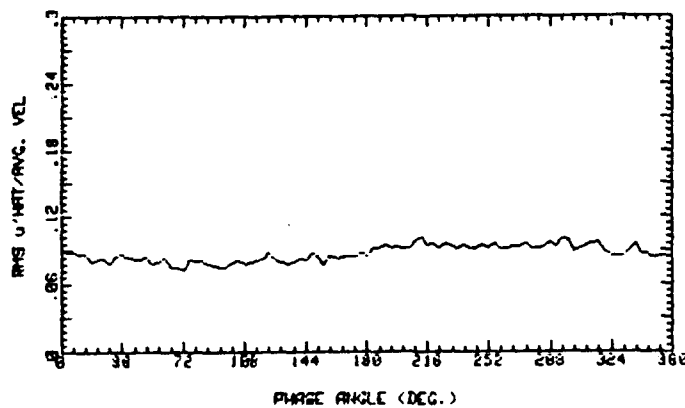
85_1750_2 111590.0109
 AVG. VEL 1.239m/s RMS VEL .1154m/s
 OSC. FREQ. 2Hz STR. # .07679
 BULK VEL. 2.078m/s REY. # 1750

Figure 62. Average and RMS Velocity Traces ($Y/d = 0.85$, $Re = 1710$, 2 Hz)

65_1850_2 120890.1813
 AVG. VEL 2.495m/s RMS VEL .2191m/s
 OSC. FREQ. 2Hz STR. # .07217
 BULK VEL. 2.211m/s REY. # 1850



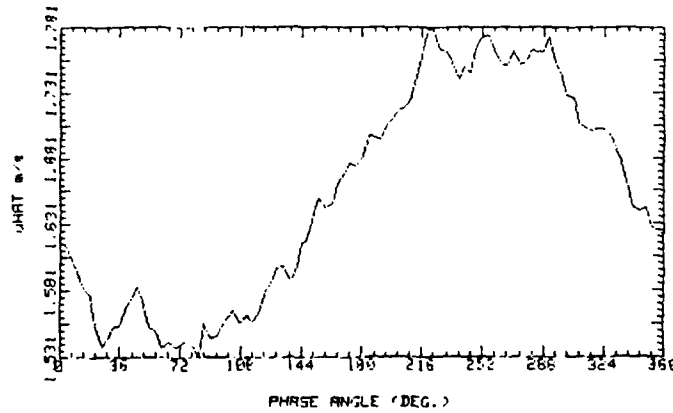
65_1850_2 120890.1813
 AVG. VEL 2.495m/s RMS VEL .2191m/s
 OSC. FREQ. 2Hz STR. # .07217
 BULK VEL. 2.211m/s REY. # 1850



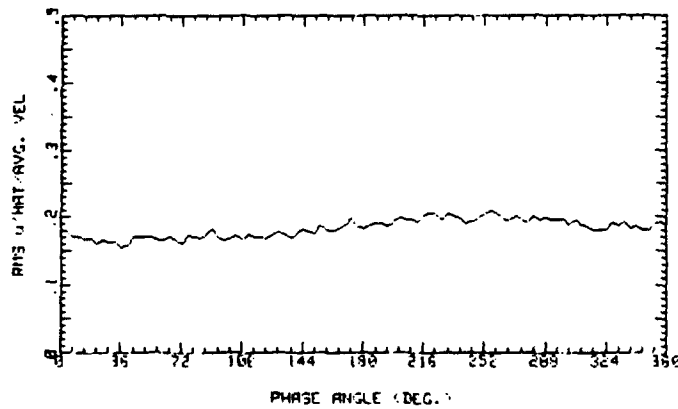
65_1850_2 120890.1813
 AVG. VEL 2.495m/s RMS VEL .2191m/s
 OSC. FREQ. 2Hz STR. # .07217
 BULK VEL. 2.211m/s REY. # 1850

Figure 63. Average and RMS Velocity Traces ($Y/d = 0.85$, $Re = 1850$, 2 Hz)

85_2005_2 111090.2107
 AVG. VEL 1.653m/s RMS VEL .3039m/s
 OSC. FREQ. 2Hz STR. # .06971
 BULK VEL. 2.289m/s REY. # 2005

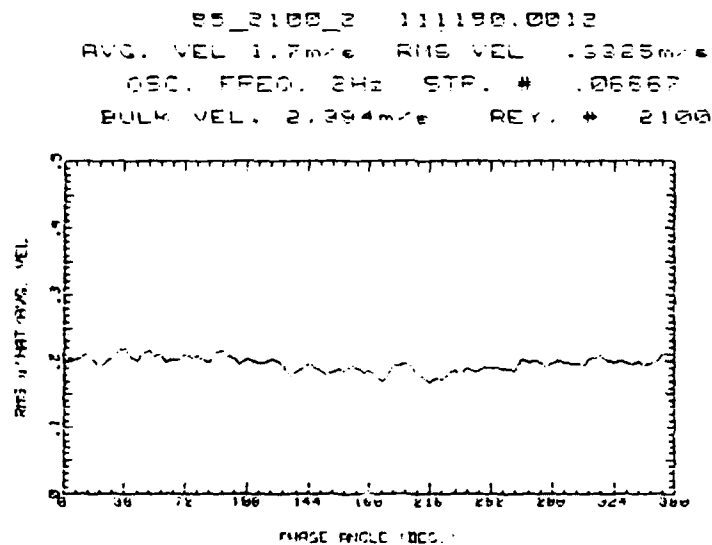
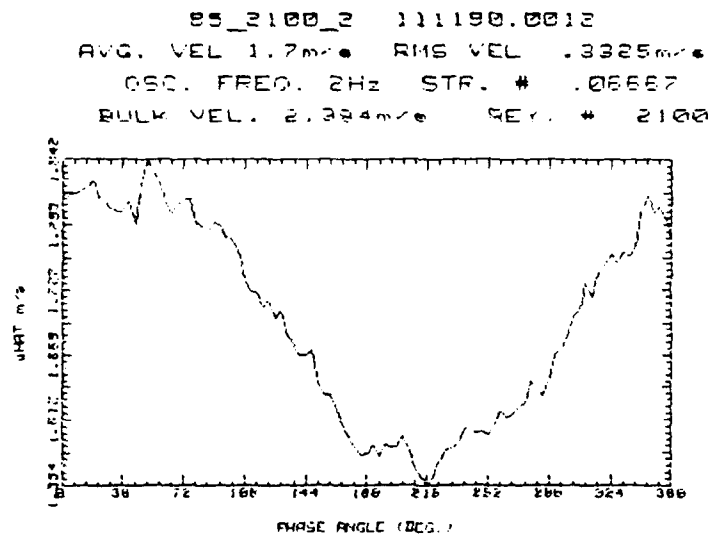


85_2005_2 111090.2107
 AVG. VEL 1.653m/s RMS VEL .3039m/s
 OSC. FREQ. 2Hz STR. # .06971
 BULK VEL. 2.289m/s REY. # 2005



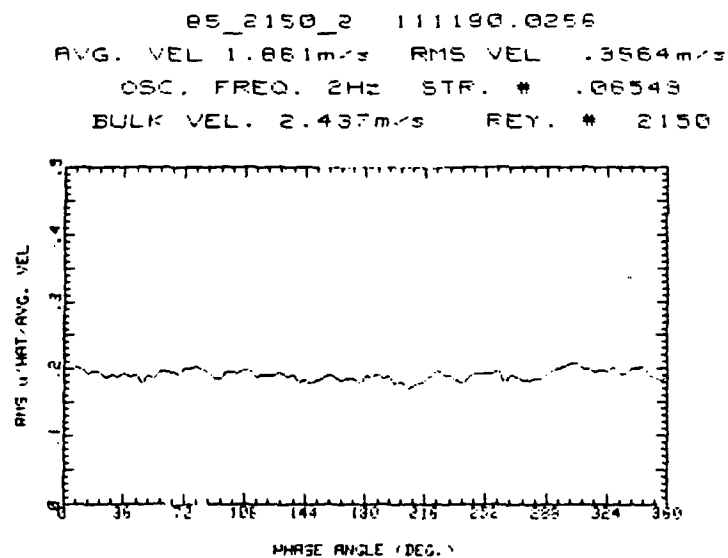
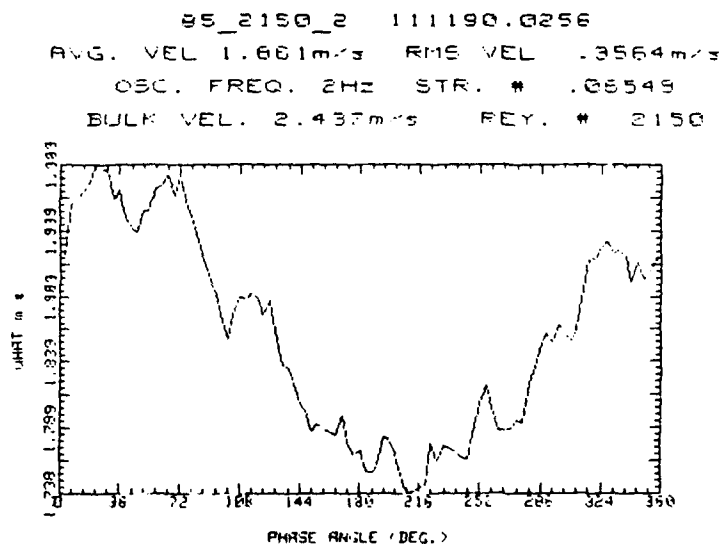
85_2005_2 111090.2107
 AVG. VEL 1.653m/s RMS VEL .3039m/s
 OSC. FREQ. 2Hz STR. # .06971
 BULK VEL. 2.289m/s REY. # 2005

Figure 64. Average and RMS Velocity Traces ($Y/d = 0.85$, $Re = 1920$, 2 Hz)



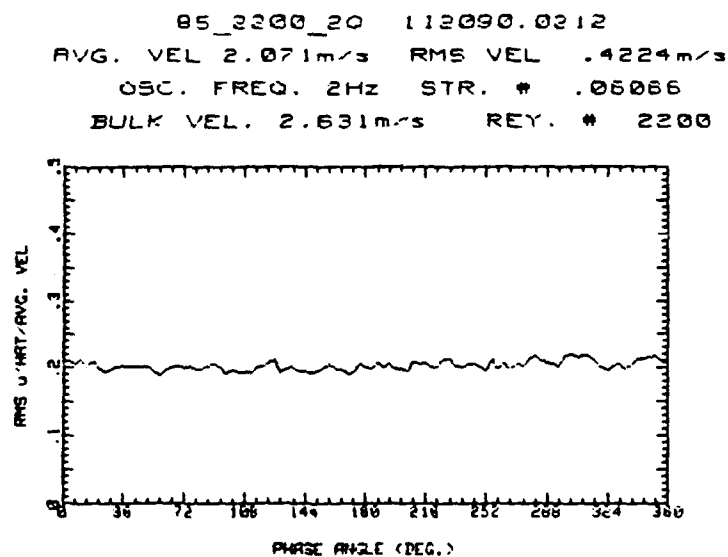
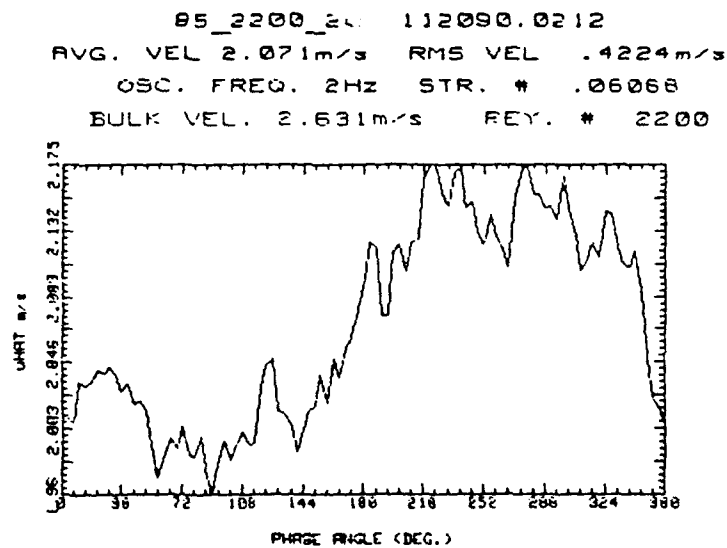
85_2100_2 111190.0012
 AVG. VEL 1.7m/s RMS VEL .3325m/s
 OSC. FREQ. 2Hz STR. # .06667
 BULK VEL. 2.394m/s REY. # 2100

Figure 65. Average and RMS Velocity Traces ($Y/d = 0.85$, $Re = 2000$, 2 Hz)



85_2150_2 111190.0256
 AVG. VEL 1.661m/s RMS VEL .3564m/s
 OSC. FREQ. 2Hz STR. # .06549
 BULK VEL. 2.437m/s REY. # 2150

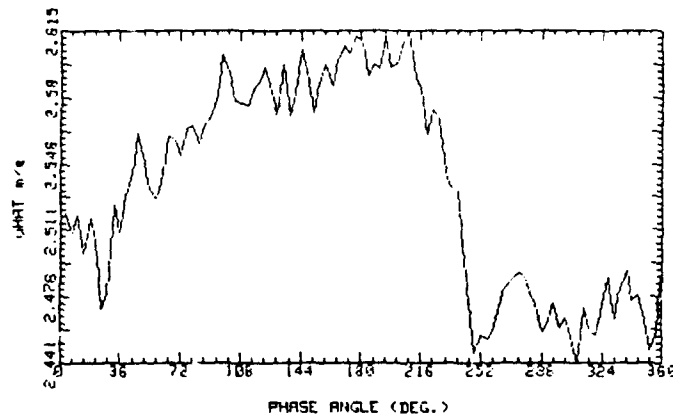
Figure 66. Average and RMS Velocity Traces ($Y/d = 0.85$, $Re = 2040$, 2 Hz)



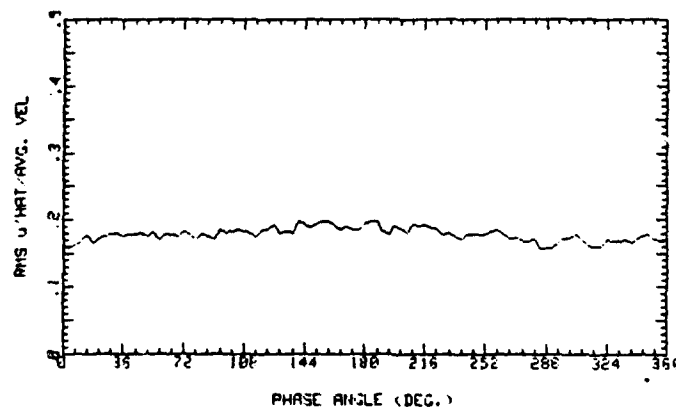
85_2200_20 112090.0212
 AVG. VEL 2.071m/s RMS VEL .4224m/s
 OSC. FREQ. 2Hz STR. # .06066
 BULK VEL. 2.631m/s REY. # 2200

Figure 67. Average and RMS Velocity Traces ($Y/d=0.85$, $Re=2090$, 2 Hz)

05_2200_2 123090.1605
 AVG. VEL 2.533m/s RMS VEL .4538m/s
 OSC. FREQ. 2Hz STR. # .06054
 BULK VEL. 2.636m/s REY. # 2200



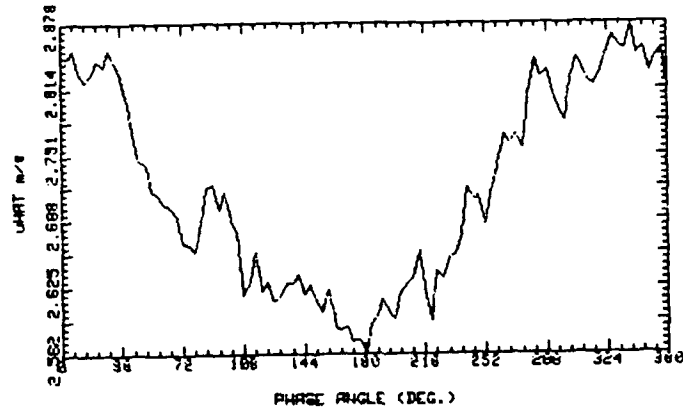
05_2200_2 123090.1605
 AVG. VEL 2.533m/s RMS VEL .4538m/s
 OSC. FREQ. 2Hz STR. # .06054
 BULK VEL. 2.636m/s REY. # 2200



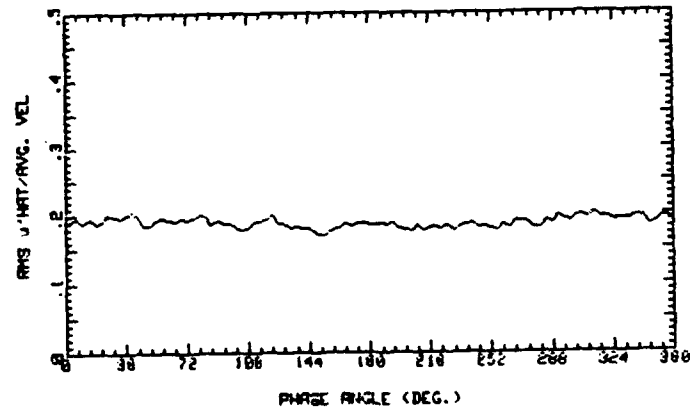
05_2200_2 123090.1605
 AVG. VEL 2.533m/s RMS VEL .4538m/s
 OSC. FREQ. 2Hz STR. # .06054
 BULK VEL. 2.636m/s REY. # 2200

Figure 68. Average and RMS Velocity Traces ($Y/d = 0.85$, $Re = 2200$, 2 Hz)

85_2300_2 112690.2211
 AVG. VEL 2.72m/s RMS VEL .5143m/s
 OSC. FREQ. 2Hz STR. # .05801
 BULK VEL. 2.751m/s REY. # 2300



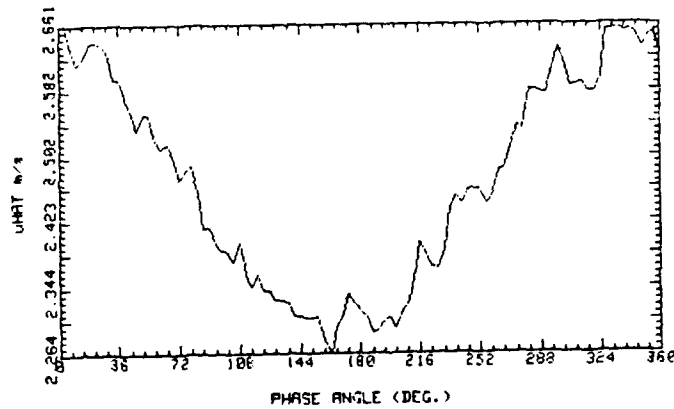
85_2300_2 112690.2211
 AVG. VEL 2.72m/s RMS VEL .5143m/s
 OSC. FREQ. 2Hz STR. # .05801
 BULK VEL. 2.751m/s REY. # 2300



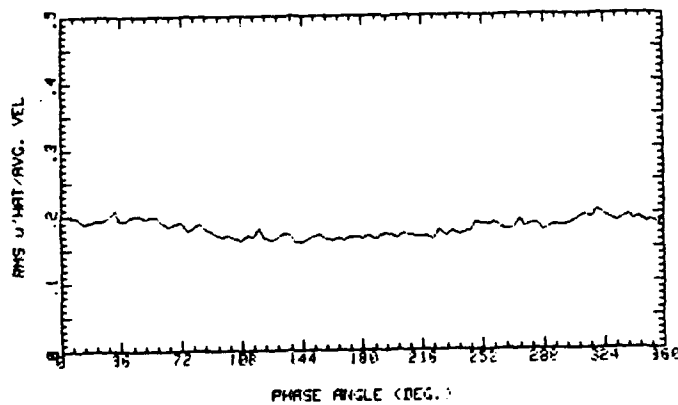
85_2300_2 112690.2211
 AVG. VEL 2.72m/s RMS VEL .5143m/s
 OSC. FREQ. 2Hz STR. # .05801
 BULK VEL. 2.751m/s REY. # 2300

Figure 69. Average and RMS Velocity Traces ($Y/d = 0.85$, $Re = 2300$, 2 Hz)

05_2350_2 10391.1619
 AVG. VEL 2.472m/s RMS VEL .4488m/s
 OSC. FREQ. 2Hz STR. # .05679
 BULK VEL. 2.81m/s REY. # 2350

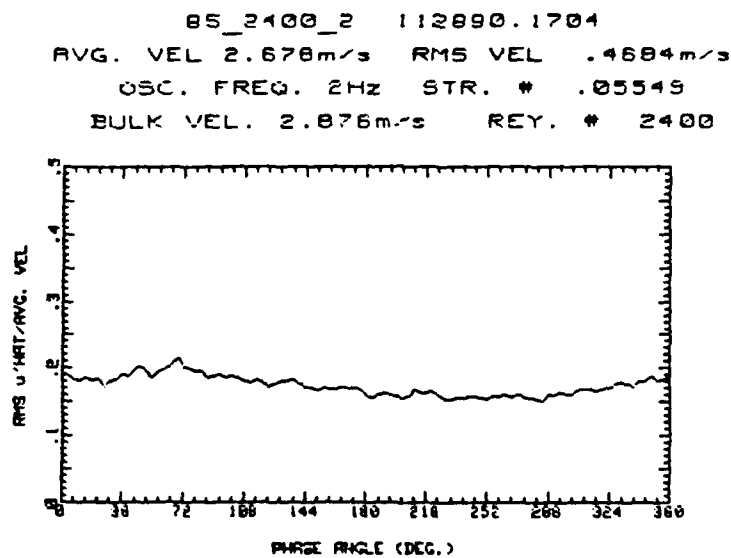
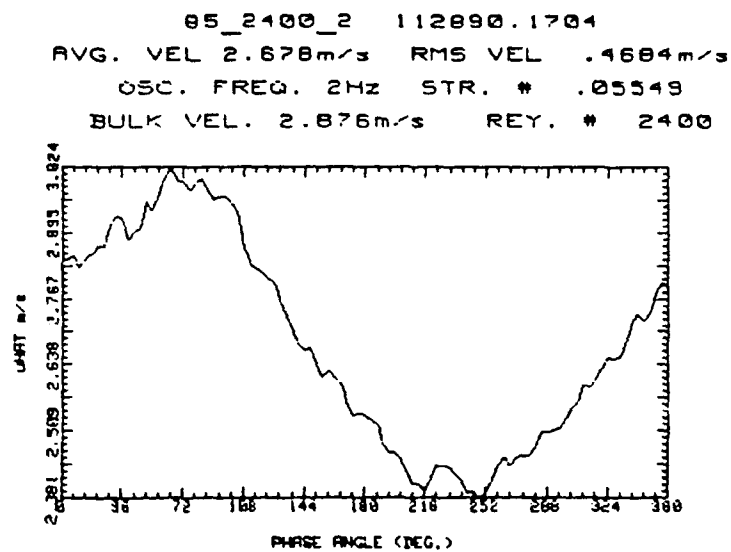


05_2350_2 10391.1619
 AVG. VEL 2.472m/s RMS VEL .4488m/s
 OSC. FREQ. 2Hz STR. # .05679
 BULK VEL. 2.81m/s REY. # 2350



05_2350_2 10391.1619
 AVG. VEL 2.472m/s RMS VEL .4488m/s
 OSC. FREQ. 2Hz STR. # .05679
 BULK VEL. 2.81m/s REY. # 2350

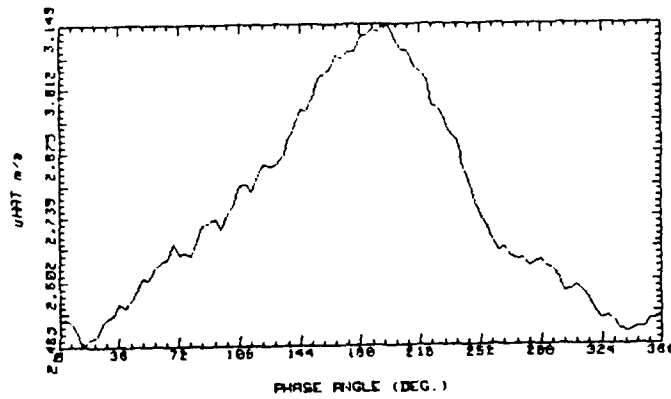
Figure 70. Average and RMS Velocity Traces ($Y/d = 0.85$, $Re = 2350$, 2 Hz)



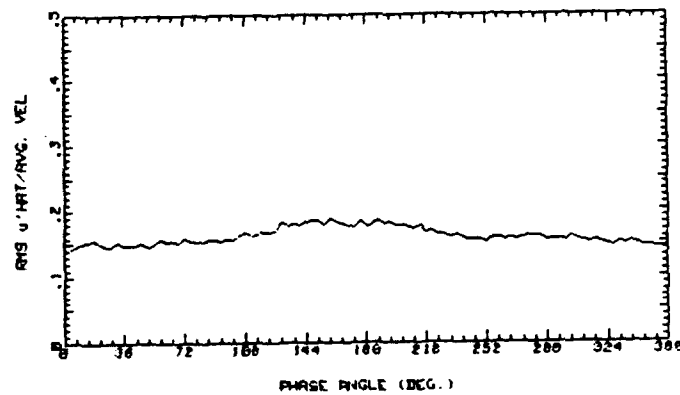
85_2400_2 112890.1704
 AVG. VEL 2.678m/s RMS VEL .4684m/s
 OSC. FREQ. 2Hz STR. # .05549
 BULK VEL. 2.876m/s REY. # 2400

Figure 71. Average and RMS Velocity Traces ($Y/d = 0.85$, $Re = 2400$, 2 Hz)

85_2450_2 10891.2352
 AVG. VEL 2.751m/s RMS VEL .4431m/s
 OSC. FREQ. 2Hz STR. # .05438
 BULK VEL. 2.935m/s REY. # 2450



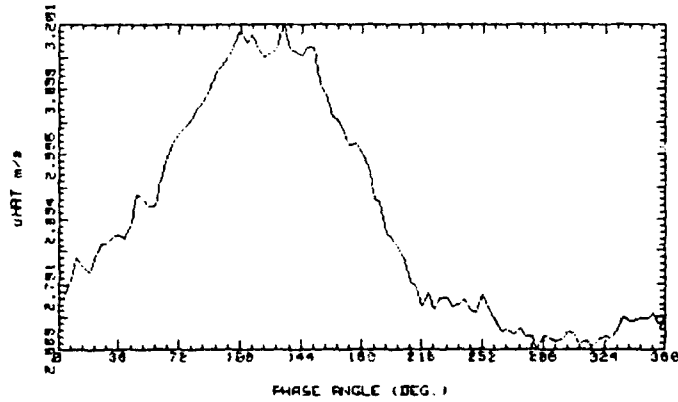
85_2450_2 10891.2352
 AVG. VEL 2.751m/s RMS VEL .4431m/s
 OSC. FREQ. 2Hz STR. # .05438
 BULK VEL. 2.935m/s REY. # 2450



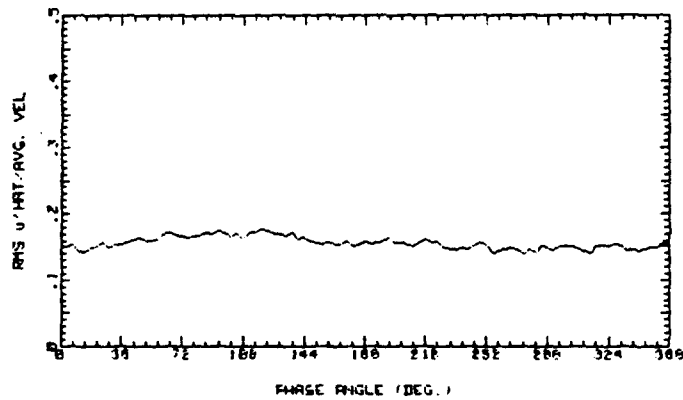
85_2450_2 10891.2352
 AVG. VEL 2.751m/s RMS VEL .4431m/s
 OSC. FREQ. 2Hz STR. # .05438
 BULK VEL. 2.935m/s REY. # 2450

Figure 72. Average and RMS Velocity Traces ($Y/d=0.85$, $Re=2450$, 2 Hz)

85_2500_2 120190.2316
 AVG. VEL 2.889m/s RMS VEL .4502m/s
 OSC. FREQ. 2Hz STR. # .05334
 BULK VEL. 2.992m/s REY. # 2500

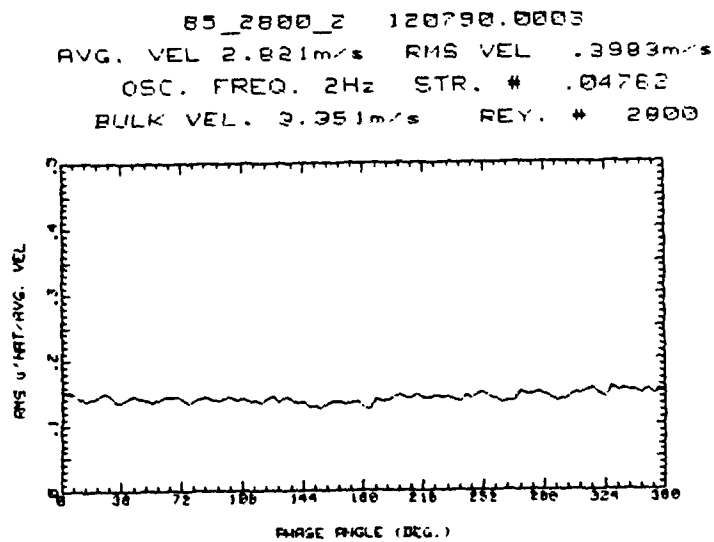
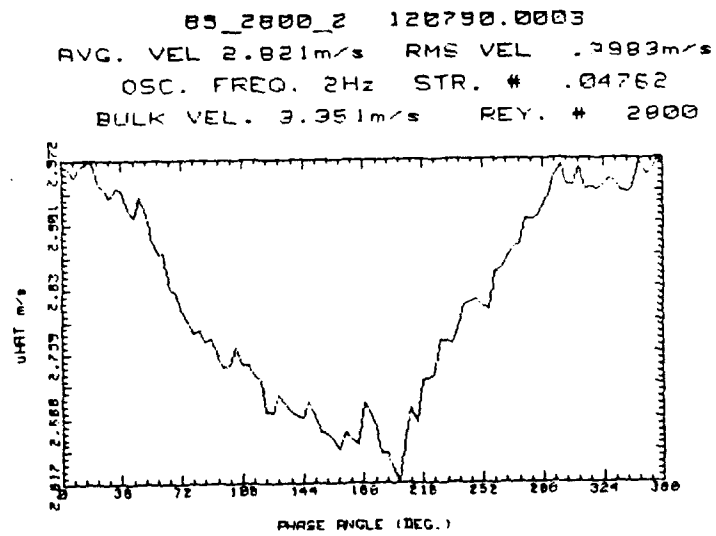


85_2500_2 120190.2316
 AVG. VEL 2.889m/s RMS VEL .4502m/s
 OSC. FREQ. 2Hz STR. # .05334
 BULK VEL. 2.992m/s REY. # 2500



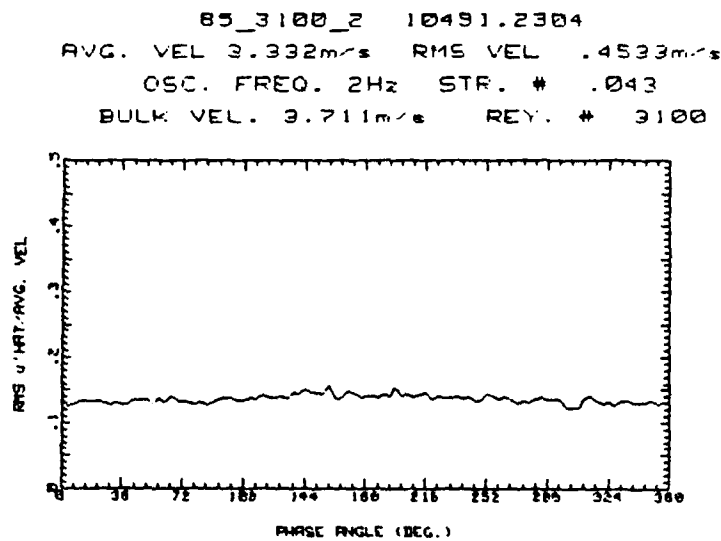
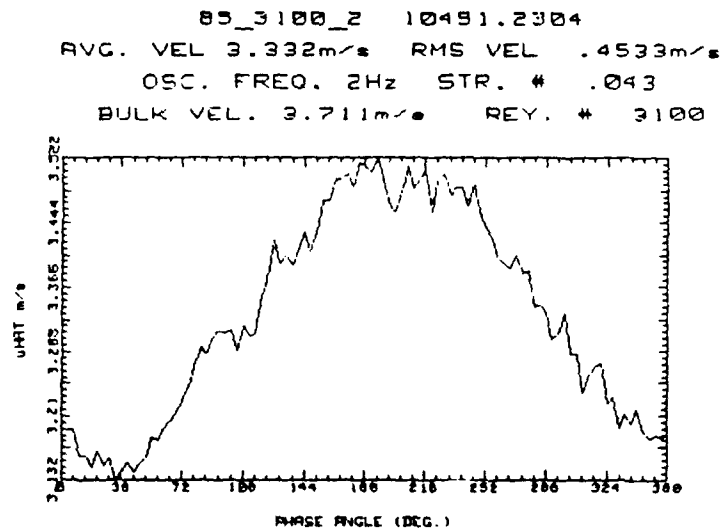
85_2500_2 120190.2316
 AVG. VEL 2.889m/s RMS VEL .4502m/s
 OSC. FREQ. 2Hz STR. # .05334
 BULK VEL. 2.992m/s REY. # 2500

Figure 73. Average and RMS Velocity Traces ($Y/d = 0.85$, $Re = 2500$, 2 Hz)



85_2800_2 120790.0003
 AVG. VEL 2.821m/s RMS VEL .3983m/s
 OSC. FREQ. 2Hz STR. # .04762
 BULK VEL. 3.351m/s REY. # 2800

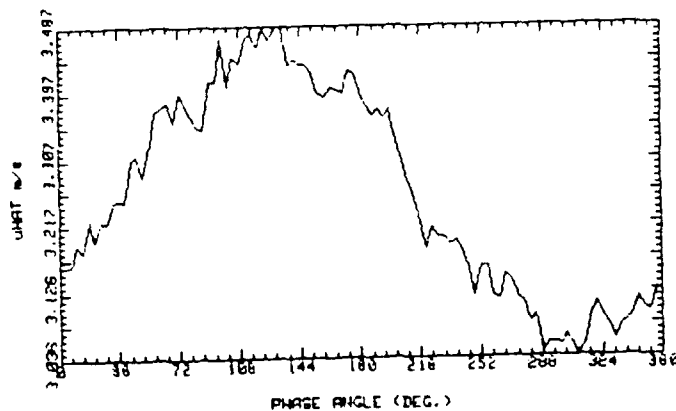
Figure 74. Average and RMS Velocity Traces ($Y/d = 0.85$, $Re = 2800$, 2 Hz)



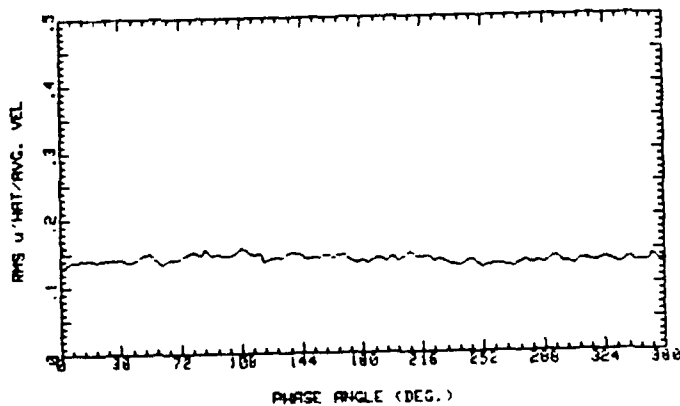
85_3100_2 10491.2304
 AVG. VEL 3.332m/s RMS VEL .4533m/s
 OSC. FREQ. 2Hz STR. # .043
 BULK VEL. 3.711m/s REY. # 3100

Figure 75. Average and RMS Velocity Traces ($Y/d = 0.85$, $Re = 3100$, 2 Hz)

85_3585_2 111190.0807
 AVG. VEL 3.26m/s RMS VEL .4549m/s
 OSC. FREQ. 2Hz STR. # .03943
 BULK VEL. 4.048m/s REY. # 3585



85_3585_2 111190.0807
 AVG. VEL 3.26m/s RMS VEL .4549m/s
 OSC. FREQ. 2Hz STR. # .03943
 BULK VEL. 4.048m/s REY. # 3585



85_3585_2 111190.0807
 AVG. VEL 3.26m/s RMS VEL .4549m/s
 OSC. FREQ. 2Hz STR. # .03943
 BULK VEL. 4.048m/s REY. # 3585

Figure 76. Average and RMS Velocity Traces ($Y/d = 0.95$, $Re = 3400$, 2 Hz)

LIST OF REFERENCES

1. Shemer, L., "Laminar-Turbulent Transition in a Slowly Pulsating Pipe Flow", *Phys. Fluids*, 28, pp.3506-3509, 1985.
2. Tu, S. W. and Ramaprian, B. R., "Fully Developed Periodic Turbulent Pipe Flow. Part I. Main Experimental Results and Comparisons with Predictions," *J. Fluid Mech*, 137, pp. 31-58, 1983.
3. Ramaprian, B. R. and Tu, S. W., "An Experimental Study of Oscillatory Pipe Flow At Transitional Reynolds Numbers," *J. Fluid Mech*, 100, pp. 513-544, 1980.
4. Stettler, J. C. and Hussain, A. K. M. F., "On Transition of the Pulsatile Pipe Flow," *J. Fluid Mech*, 170, pp. 169-197, 1986.
5. Merkli, P. and Thomann, H., "Transition to Turbulence in Oscillating Pipe Flow," *J. Fluid Mech.*, 68, pp. 567-575, 1975.
6. Sergeev, S. I., "Fluid Oscillations in Pipes at Moderate Reynolds Numbers," *Fluid Dyn.*, Mekh 2H" 1, pp. 21-22, 1966.
7. Hino, M. and Sawamoto, M., "Linear Stability Analysis of an Oscillator Flow Between Parallel Plates," *Proc. 7th Symposium on Turbulence*, H. Sato and M. Ohji, Eds., pp. 1-7. Inst. of Space & Aeronautics, Univ. of Tokyo, 1975.
8. Hino, M., Sawamoto, M. and Takasu, S., "Experiments on Transition to Turbulence in an Oscillatory Pipe Flow," *J. Fluid Mech.*, 75, pp. 193-207, 1976.
9. Gerrard, J. H., "An Experimental Investigation of the Pulsating Turbulent Water Flow in a Tube," *J. Fluid Mech.*, 46, pp. 43-64, 1971.

10. Gilbrech, D. A. and Combs, G. D., "Critical Reynolds Numbers for Incompressible Pulsating Flow in Tubes," in *Developments in Theoretical and Applied Mechanics*, Plenum Press, New York, 1963.
11. Sarpkaya, T., "Experimental Determination of the Critical Reynolds Number for Pulsating Poiseuille Flow," *Trans. A. S. M. E. D. J. Basic Engrg.*, 88, pp. 589-598, 1966.
12. Simpson, R. L., Sallas, J. J. and Nasburg, R. E., "Tailoring the Wave Form of a Periodic Flow with a Programmable Damper," *J. Fluids Engrg.*, 100, pp. 287-290, 1978.
13. Grosch, C. E. and Salwen, H., "The Stability Of Steady and Time-Dependent Plane Poiseuille Flow," *J. Fluid Mech.*, 34, pp. 177-205, 1968.
14. Herbert, D. M., "The Energy Balance in Plane Poiseuille Flow," *J. Fluid Mech.*, 56, pp. 73-80, 1972.
15. Hall, P., "The Stability of Plane Poiseuille Flow Modulated at High Frequency," *Proc R. Soc. Lond. A.*, 344, pp. 453-464, 1975.
16. von Kerczek, C. H., "The Instability of Oscillatory Plane Poiseuille Flow," *J. Fluid Mech.*, 116, pp. 91-114, 1982.
17. Singer, B., Ferziger, J. H. and Reed, H., *Numerical Simulation of Laminar-Turbulent Transition in the Plane Channel*, Report TF-31, Thermosciences Division, Department of Mechanical Engineering, Stanford University, Stanford, May, 1987.
18. Singer, B., Ferziger, J. H. and Reed, H., "Numerical Simulation of Transition in Oscillatory Plane Channel Flow," *J. Fluid Mech.*, 208, pp. 45-66, 1989.
19. Tozzi, J. T., Ph. D. Thesis, Catholic University, 1982.
20. Davies, S., "Stability of Time Periodic Flows," *Ann. Rev. Fluid Mech.*, 8, pp. 57-74, 1976.

21. Morrow, D. S., *Transition Phenomena in a Straight Channel With a 40 to 1 Aspect Ratio With and Without Imposed Pulsations, Part I: Near-Wall and Central Region Profiles*, Master's Thesis, Naval Postgraduate School, Monterey, CA, March, 1991.
22. Koth, H. E., *Effects of Imposed Bulk Flow Oscillations At 1, 2, 3 and 4 Hz on Transition in a Straight Channel With 40 to 1 Aspect Ratio*, Master's Thesis, Naval Postgraduate School, Monterey, CA, June, 1990.
23. Coumes, T. M., *The Effects of 1 Hz Imposed Unsteadiness on Laminar/Turbulent Transition in a Straight Channel Flow*, Master's Thesis, Naval Postgraduate School, Monterey, CA, December, 1989.
24. Longest, J., *Flow Visualization Studies in (1) a Curved Rectangular Channel With 40 to 1 Aspect Ratio and (2) a Straight Channel With Bulk Flow Unsteadiness*, Master's Thesis, Naval Postgraduate School, Monterey, CA, June 1989.
25. Ligrani, P. M., Subramanian, C. S., Coumes, T. M., Greco, F. J., Koth, H., and Longest, J. M., "Study of the Imposition of Bulk Flow Pulsations on Plane Channel Flow at Moderate Stokes Numbers, submitted to *Int'l J. of Experimental Thermal and Fluid Sciences* in February, 1991.
26. Han, L. S., "Hydrodynamic Entrance Lengths for Incompressible Laminar Flow in Rectangular Ducts," *J. of Appl. Mech*, 27, pp. 403-410, 1960.
27. Schlichting, H., *Boundary Layer Theory*, Seventh Edition, McGraw-Hill Book Company, New York, 1979.
28. Zang, T. A. and Krist, S. E., "Numerical Experiments on Stability and Transition in Plane Channel Flow," *Theoretical and Computational Fluid Dynamics*, 1, pp. 41-64, 1989.